

Challenges in Computational Electromagnetics: Analysis and Optimization of Planar Multilayered Structures

THÈSE N° 5122 (2011)

PRÉSENTÉE LE 30 SEPTEMBRE 2011

À LA FACULTÉ SCIENCES ET TECHNIQUES DE L'INGÉNIEUR
LABORATOIRE D'ÉLECTROMAGNÉTISME ET ACOUSTIQUE
PROGRAMME DOCTORAL EN GÉNIE ÉLECTRIQUE

ÉCOLE POLYTECHNIQUE FÉDÉRALE DE LAUSANNE

POUR L'OBTENTION DU GRADE DE DOCTEUR ÈS SCIENCES

PAR

Ružica GOLUBOVIĆ

acceptée sur proposition du jury:

Prof. P. Vandergheynst, président du jury
Prof. J. R. Mosig, directeur de thèse
Prof. D. Atienza Alonso, rapporteur
Prof. A. Djordjevic, rapporteur
Prof. G. Vandenbosch, rapporteur



ÉCOLE POLYTECHNIQUE
FÉDÉRALE DE LAUSANNE

Suisse
2011

To my family

Abstract

To meet strict requirements of the information society technologies, antennas and circuit elements are becoming increasingly complex. Frequently, their electromagnetic (EM) properties cannot be anymore expressed in closed-form analytical expressions mainly because of the multitude of irregular geometries found in actual devices. Therefore, accurate and efficient (in terms of computational time and memory) electromagnetic models coupled with the robust optimization techniques, are needed in order to be able to predict and optimize the behavior of the innovative antennas in complex environments.

The contribution of this thesis consists in the development and improvement of accurate electromagnetic modeling and optimization algorithms for an ubiquitous class of antennas, the planar printed antennas. The approach most commonly used to model and analyze this type of structures is the Integral Equation (IE) technique numerically solved using the Method of Moments (MoM). From the computational point of view, the main challenge is to develop techniques for efficient numerical evaluation of spatial-domain Green's functions, which are commonly expressed in terms of the well-known Sommerfeld integrals (SIs), i.e., semi-infinite range integrals with Bessel function kernels. Generally, the analytical solution of the SIs is not available, and their numerical evaluation is notoriously difficult and time-consuming because the integrands are both oscillatory and slowly decaying, and might possess singularities on and/or near the integration path. Due to the key role that SIs play in many EM problems, the development of fast and accurate techniques for their evaluation is of paramount relevance. This problem is studied in detail and several efficient methods are developed. Finally, the applicability of one of these methods, namely the Weighted Averages (WA) technique, is extended to the challenging case appearing in many practical EM problems: the evaluation of semi-infinite integrals involving products of Bessel functions.

However, the development of effective analysis codes is only one aspect. At least equally important is the availability of reliable optimization techniques for an adequate design of antennas. For that purpose, the Particle Swarm Optimization (PSO) algorithm is introduced in the context of our analysis codes. Moreover, the innovative hybrid version of the PSO algorithm, called the Tournament Selection PSO, has been proposed with the aim of even further improving convergence performances of the classical PSO algorithm. Detailed theoretical description of this socially inspired evolutionary algorithms is given in the thesis. Finally, the characteristics of both algorithms are compared throughout several EM optimization problems.

Keywords: Computational Electromagnetics (CEM), convergence accelerators, Double-Exponential (DE) quadrature formulas, extrapolation techniques, Green's functions (GFs), Integral Equations (IE), multilayered substrates, Particle Swarm Optimization (PSO) algorithm, planar stratified media, Sommerfeld integrals (SIs), Weighted Averages (WA) method.

Résumé

Pour répondre aux exigences strictes des technologies de l'information, les antennes et les éléments de circuit deviennent de plus en plus complexes. Leurs propriétés électromagnétiques (EM) ne peuvent souvent pas être exprimées sous forme de formules explicites, principalement en raison de la multitude de géométries irrégulières que l'on trouve dans les dispositifs réels. Par conséquent, afin d'être en mesure de prévoir et d'optimiser le comportement d'antennes innovantes en environnement complexe, des modèles électromagnétiques précis et efficaces (en termes de temps de calcul et d'utilisation de la mémoire), couplés avec des techniques d'optimisation robustes, sont nécessaires.

La contribution de cette thèse consiste au développement et à l'amélioration de technique de modélisation électromagnétique précises et d'algorithmes d'optimisation destinés à une classe d'antennes omniprésentes : les antennes imprimées planaires. L'approche la plus couramment utilisée pour modéliser et analyser ce type de structures est la technique des Equations Intégrales ("Integral Equations", or IE) résolues numériquement grâce à la méthode des moments ("Method of Moments", or MoM). Du point de vue du calcul par ordinateur, le principal défi consiste à développer des techniques permettant une évaluation numérique efficace des fonctions de Green dans le domaine spatial, qui sont généralement exprimées en termes d'intégrales de Sommerfeld (IS), soit des intégrales à domaine semi-infini dont le noyau est une fonction de Bessel. En général, la solution analytique des ISs n'est pas disponible, et leur évaluation numérique est notoirement difficile et de longue haleine car les intégrandes sont à la fois oscillatoires et lentement décroissants, et peuvent présenter des singularités à proximité du contour d'intégration. En raison du rôle clé que jouent les ISs dans de nombreux problèmes EM, le développement de techniques rapides et précises permettant leur évaluation est d'une importance primordiale. Ce problème est étudié en détail et plusieurs méthodes efficaces sont élaborées. Finalement, l'applicabilité de l'une de ces méthodes, à savoir la nouvelle technique des moyennes pondérées ("Weighted Averages", or WA), est étendue au cas difficile apparaissant dans de nombreux problèmes EM pratiques : l'évaluation des intégrales à domaine semi-infini impliquant des produits de fonctions de Bessel.

Cependant, le développement de logiciels d'analyse efficaces n'est qu'un aspect. Au moins d'égale importance est la disponibilité de techniques d'optimisation fiables pour l'optimisation et la conception d'antennes. À cette fin, l'algorithme d'optimisation par essaim de particules ("Particle Swarm Optimization", or PSO) est présenté dans le cadre de nos programmes d'analyse. En outre, la version hybride de l'algorithme PSO, appelée "Tournoi de Sélection PSO", a été proposée dans le but d'améliorer encore les performances de convergence de l'algorithme PSO Classique. Une description théorique détaillée de cet algorithme inspiré de l'évolution sociale est proposée dans la thèse. Finalement, les caractéristiques des deux algorithmes sont comparées à travers plusieurs problèmes d'optimisation EM.

Mots-clés: électromagnétisme numérique (CEM), accélérateurs de convergence, formules quadratiques à double-exponentielle (DE), techniques d'extrapolation, fonctions de Green (GFs), équations intégrales (IE), substrats multicouches, algorithme d'optimisation par essaim de particules (PSO), milieux stratifiés planaires, intégrales de Sommerfeld (SIs), méthode des moyennes pondérées (WA).

Acknowledgements

I would like to thank all the people that have been supporting and encouraging me during my thesis, and by being part of my life made it very beautiful experience. First of all, to my thesis advisor, Prof. Juan R. Mosig, for giving me the opportunity of joining LEMA and doing this work. Juan, I am deeply thankful for your good advices, constant support, inspiring scientific discussions, many brilliant ideas, and most importantly for taking really good care of us. *Muchas gracias por todo!*

My appreciation goes to the committee members: Prof. Antonije Djordjevic, from University of Belgrade, Prof. Guy Vandebosch, from Katholieke Universiteit Leuven and Prof. David Atienza Alonso from EPFL, for having accepted to examine this work, and for their valuable insights that have contributed to the improvement of the quality of this thesis. Dear Tony, I can not express my gratitude to you, not only for being in my committee, but for introducing me to the world of electromagnetism and being excellent example to follow. Thank you very much for all your support and for believing in me. I would also like to thank to Prof. Vandebosch, for welcoming me in TELEMIC, and for very nice collaboration and interesting discussions we have had during the COST Project. I also thank Prof. Pierre Vandergheynst for charing this jury.

Huge thanks goes to Dragan Olcan, my very good friend and “mom prvom mentoru”. Thank you enormously for inspiring and encouraging me to do PhD, for many discussions, advices and memorable moments we spent in conferences and outside work.

Very special thanks to my best man Ivica Stevanovic, for always being there for me. I can not express my gratitude for making Lausanne feel much more like home. Thank you very much for your firm commitment, constant support, kindness, patience and for always having time to listen and encourage me.

I would like to thank my colleagues and friends from LEMA, for making the lab being great place to be and to work. Michael, my warmest thanks for all the time you have generously shared with me, for your patience and for all your good advices. Vielen dank! My sincere appreciation to Prof. Anja Skrivervik and J.-F. Zürcher for many shared coffee breaks and persistent encouragement to improve my French. Eulalia, *muchas gracias* for your permanent help. Gabriela, Laleh, Maddalena, thank you for spending cheerful girls moments and laughs. Thanos, *ευχαριστώ πολύ* for all the discussions and support, sound advices, for sharing your time, good ideas and expertise. *Gracie mille* to my thesis mate Francesco and *merci beaucoup* to Benji, for all the laughs and encouragements during the not easy thesis writing period. Roberto, *muchas gracias* for all the talks we shared and for all your kind helps in administrative procedures at my arrival to LEMA. Fred, thanks for being good and sincere friend, and for your precious help in preparing the French version of the thesis abstract.

Eden, thank you so much for your outstanding human qualities, for being great friend and taking care of me in numerous occasions. Ioannis and Apostolos, thank you a lot for your contaminating enthusiasm and optimism. I would also like to extend my gratitude to Marko, Gabriele, Nuno and Jovance for their generous company.

A very special thanks to my Serbian friends. Nevena Vratonjic, thank you for walks and talks we closely shared, for wonderful lunch breaks and much more. Natasa Vuckovic, Nevena Krsmanovic, and Maja Matic thanks for staying so close and good friends regardless the distance.

My boundless gratitude goes to my family, for always being with me despite the distance. Mama, tata, puno, puno, puno hvala for your unconditional love, continuous support, endless understanding, and for always inspiring me to find the strength for new challenges in my life. Vejo, huge thanks and big hug for being my best friend and my inspiration. To my brother in law, Srdja for always being ready to listen and advise me, and my nephew Marko for cheering me up. To all of you with all my heart I dedicate this thesis!

Ružica

Table of Contents

1	Introduction	1
1.1	Numerical modeling	2
1.1.1	Planar structures	3
1.1.2	Green's functions and Sommerfeld integrals	3
1.2	Optimization techniques	3
1.3	Objectives	4
1.4	Outline	5
2	Efficient computation of Sommerfeld integrals	11
2.1	Introduction	11
2.2	Sommerfeld integral	14
2.3	Evaluation of the Sommerfeld integrals	19
2.4	The first part of the SI	20
2.4.1	Half-sine contour integration	21
2.4.2	Real-axis integration	22
2.4.2.1	Pole extraction	23
2.4.2.2	Treatment of branch-point singularities	24
2.4.3	Numerical results	28
2.4.3.1	Example with analytical solution	29
2.4.3.2	Examples without analytical solution	32
2.5	Sommerfeld integral tail	42
2.5.1	Weighted averages method	43
2.5.2	New weighted averages method	46
2.5.3	Double exponential-type quadrature formulas	51
2.5.4	Numerical results	54
2.6	Conclusion	69
3	Numerical evaluation of the integrals involving products of Bessel functions of arbitrary order	77

3.1	Introduction	77
3.2	Integrals with products of Bessel functions	78
3.3	Algorithm description	83
3.4	Numerical results	86
3.5	Generalization of the algorithm	89
3.5.1	Products of more than two oscillating functions	90
3.5.2	Test cases for the generalized algorithm	91
3.6	Conclusion	94
4	Particle Swarm Optimization Algorithm	99
4.1	Introduction	99
4.2	Classical PSO algorithm	101
4.2.1	PSO language	101
4.2.2	Algorithm description	102
4.2.3	Algorithm implementation	106
4.2.4	Swarm convergence	108
4.3	Tournament selection PSO	112
4.4	Optimization Examples	113
4.4.1	First optimization problem: microstrip antenna	114
4.4.2	Second optimization problem: SSFIP antenna	116
4.4.3	Third optimization problem: Broadside coupled filter	119
4.5	Conclusion	122
5	Conclusion	127
5.1	Thesis assessment	127
5.2	Perspectives	130
	List of Acronyms	137
	List of Figures	143
	List of Tables	145

1 Introduction

Antennas are a key constituent of all terrestrial, airborne and space based wireless multimedia, communications and sensor systems. Their functions are fast evolving, driven by the demanding needs of the Information Society Technologies. There is still a lot of research and innovation to accomplish in traditional antenna areas, like base stations and satellite antennas for telecom and remote sensing. But also, there are new challenging problems appearing. Antennas are deeply integrated into complex systems. They are used as biological sensors (Body Area Networks, BAN) and as identification tags (Radio Frequency Identifications, RFID). They are essential for navigation (Global Positioning Systems, GPS) and monitoring of Earth resources and natural disasters. They must cope with increasing demands in bandwidth/bit rate (Ultra Wide Band antennas, UWB) and channel capacity (multiple input/multiple output, MIMO). They use the electromagnetic properties of new materials (metamaterials, plasmonics) and the most advanced technologies (Radio Frequency Micro Electro Mechanical Systems, RF-MEMS). And, of course, they must keep pace with fast developments in the area of wireless telecommunications (Wi-Fi, WiMax systems).

Nowadays, applications are calling for more and more performant antennas and circuits. In order to meet strict requirements, antennas and circuit elements are becoming increasingly complex. At the most fundamental level, antennas are characterized by their electromagnetic properties. It is the electromagnetic (EM) analysis of the antenna that yields the basic parameters (input impedance, radiation pattern, etc) which will in turn allow the definition of the antenna properties at the subsystem and system levels. Today, EM analysis is greatly facilitated by the ever-increasing resources of computers and it has led to the discipline of computational electromagnetics (CEM) to which this thesis belongs.

The most advanced commercial computer aided design (CAD) tools available today on the market, in conjunction with powerful computers, allow analysis of complicated electromagnetic structures with a relatively long computational time for a single simulation. Therefore, these tools are not convenient for handling optimization of large and/or complicated environments. Taking into account a trend towards the use of higher and higher frequencies, it is clear that the need for efficient numerical tools cannot be addressed by relying only on the increase of computer speed and memory. In this context, the development of accurate and fast electromagnetic models coupled with the efficient optimization techniques is a must, providing substantial reductions in overall computational time and allowing a much welcome flexibility to the designer. The goal of this thesis is to face some of these theoretical challenges and to develop some numerically efficient algorithms, that should contribute towards the accurate modeling and optimization of complex multilayered antennas, thus avoiding the iterative

design cycle with costly and time-consuming experimental prototypes.

1.1 Numerical modeling

All electrodynamic phenomena at a macroscopic level are described by Maxwell's equations already established in the 19th century. Although in principle this set of equations provides the whole field of electrical engineering with a concise and complete mathematical foundation, a majority of the structures used today are complex enough to prevent their analytical resolution. Therefore, the existence of powerful and robust CAD tools, providing on the one hand very accurate and reliable final results, and being on the other hand, efficient in terms of computational time and memory, becomes essential. The proper trade-off between these two antagonistic features is a key attribute of a good CAD tool, and can be achieved only by optimally combining the advantages of numerical and analytical techniques.

Before the appearance of high-speed personal computers (PCs), it was mandatory to manipulate analytical solutions into forms that required minimal numerical effort. While in former times a lot of effort was invested in analytical manipulations with the aim of minimizing the numerical effort, nowadays, computer time is commonly used to reduce analytical efforts. The constantly growing power of PCs makes practicable methods of solution too repetitious for hand calculations [1]. A significant portion of research today is numerically oriented, to the extent that one could believe that analytical techniques have become of secondary importance. However, without analysis, numerical methods are at a significant risk of degenerating into brute force methods with low accuracy and robustness. It is clear that analysis will continue to play important role, although with a different emphasis. Since it is no longer necessary to seek solutions that are easy to compute, new analytical methods should be motivated and governed by the need of stable numerical evaluation. Moreover, future progress in our capability to solve problems of increasing scale size and complexity depends critically on the development of appropriate analytical tools and on the insight into underlying physical phenomena that analysis brings about [2].

The numerical solution of Maxwell's equations for electromagnetic fields for a given structure and specified environment (boundary conditions) is called computational electromagnetic simulation. The field computations can be performed either in time or in frequency domain. While the frequency domain approach is appropriate when all the media are linear, in the case that the structure to be simulated contains nonlinear active devices, time domain analysis must be used. Recently, the development of pulse-based communication systems has led to the increasing practical relevance of time-domain techniques. Among them, the most commonly used approach is finite-difference time-domain (FDTD) method. A well known commercial FDTD tool is SEMCAD [3]. Another well-known software based on time-domain approach, but using Finite Integration Technique, is CST Microwave Studio [4]. The typical examples of frequency domain techniques are differential-equation based Finite Element Method (FEM) and full wave solution of integral equations by Method of Moments (IE-MoM). The former is used for general three-dimensional structures, while the latter one is specially well-suited for

analysis of structures with homogeneous or piecewise homogeneous dielectrics, as for example planar microwave and millimeter wave circuits and antennas. Well known commercial softwares based on those approaches are ANSOFT DESIGNER and HFSS [5] (FEM), WiPL-D [6], MAGMAS [7], FEKO [8] and ADS-Momentum [9] (IE-MoM), among others.

1.1.1 Planar structures

Planar technologies, in which thin metallizations are embedded within stratified dielectric media, are one of the most popular and successful approaches to build circuits and antennas in microwaves and millimeter waves with a good performance-to-price ratio. In the modeling of printed circuit elements, such as microstrip interconnects terminated by complex loads, patch antennas and printed dipoles, it is generally accepted that algorithms based on IE, using MoM discretization procedure, are the most efficient and rigorous for the analysis of multilayered structures. Any integral equation formulation starts by setting up the boundary conditions that must be satisfied by electromagnetic field [10]. Depending on the type of boundary conditions used, the obtained formulation is an electric field integral equation (EFIE), a magnetic field integral equation (MFIE), or a combined field integral equation (CFIE). The EFIE can be solved either in spectral domain, or in space domain, where it is usually transformed into a mixed potential integral equations (MPIE). For multilayered structures, MPIE formulation is generally considered to be the best choice, since it combines the efficiency of integral operators for open planar stratified geometries with weakly singular kernels [10–13].

1.1.2 Green's functions and Sommerfeld integrals

The key step in any IE formulation is the construction and evaluation of the associated Green's function (GF), defined as the field or potential created by unit source embedded in layered media and playing the role of the mathematical kernel in the integral equation. In the case of stratified structures, the space-domain Green's functions required in the process of filling the MoM matrix, are commonly expressed in terms of well-known Sommerfeld integrals (SIs) [14]. Generally the analytical solution of the SIs is not available, and their numerical evaluation, even with the state-of-the-art techniques, is very time-consuming. Thus, the development of fast and accurate techniques for their evaluation is of paramount importance.

1.2 Optimization techniques

The latest advances in mathematical theory and the availability of fast computers have given great relevance to global optimization techniques, and more specially to those called evolutionary techniques, as an alternative to traditional gradient-based local-search optimization methods [15, 16]. The well established global optimization techniques are Simulated Annealing (SA) [17], Genetic algorithm (GA) [18–21], Ant colony optimization [22], and more recently developed Particle Swarm Optimization algorithm [23–25], among others. These optimization techniques belong to the class of heuristic methods, i.e., the strict mathematical proof of their

convergence after finite number of iterations does not exist. Moreover, since they involve stochastic elements, they do not necessarily produce the same solution each time. Nevertheless, they have been showing plenty of promise in various fields ranging from engineering and computer science to finance, due to their ability to handle nonlinear, multidimensional problems. Furthermore, they are particularly suitable for real-life optimization problems, for which no *a priori* information is available, as they do not make any assumptions about the optimization problem. Basically, these stochastic methods attempt to simulate natural, biological, or even cultural evolution, depending on the nature of the process they mimic.

PSO algorithm, based on an analogy with the social behavior of the swarm of bees, has emerged during the last years as an attractive alternative to other heuristic optimization methods. It has been continuously gaining popularity since it was introduced by Kennedy and Eberhart in 1995 [23], particularly because of its implementation simplicity and its relatively fast convergence. The method was first used by the antenna community in 2004 [24] and it was shown to be very efficient for electromagnetic problems [25]. In this thesis, we introduce the PSO algorithm in the context of optimization of multilayered printed antennas. In order to even further improve its overall performance, a novel hybrid Tournament Selection PSO (TS-PSO) algorithm is suggested.

1.3 Objectives

The work presented within this manuscript has been developed in the frame of European COST action IC0603 ASSIST (2008-2011) [26], in which many European research groups and universities have been involved. The generic research goal was the development of not redundant and numerically efficient algorithms, allowing accurate modeling and optimization of complex electromagnetic structures.

The first objective of this thesis was to develop specific numerical techniques for efficient calculation of Sommerfeld integrals (SIs), ubiquitous in the analysis of problems involving antennas and scatterers embedded in multilayered media. It is well-known that calculation of SIs is a cumbersome and time-consuming task. The problem of the efficient evaluation of the SIs, although nowadays a classic one, it still attracts a lot of attention, which is witnessed by numerous publications on this topic [11, 27–43]. Having in mind that SIs need to be repeatedly evaluated in the process of filling the MoM matrix, it is clear that, in the case of objects placed in multilayered media, filling the MoM matrix might take a sizeable part of the computational load involved in the solution of the MPIE via MoM. Therefore, efficient and fast computation of SIs is of paramount relevance. Several methods for efficient evaluation of SIs are currently available [11, 27–43]. However, due to the key role that SIs play in many EM problems possible improvements are always worth being investigated, and any improved algorithm is always welcome.

The second objective of this thesis is related to the development of efficient optimization techniques for EM applications. In particular, since in the design process of an EM structure an EM simulator must be run for many times in order to obtain the structure with the specified

characteristics, the development of efficient analysis codes is only one aspect. At least equally important is the availability of reliable optimization techniques. Assuming the availability of efficient analysis tools, the most relevant challenge is probably that of developing optimization approaches that are robust against the occurrence of false, non optimal solution. For that purpose, the PSO algorithm has been introduced and studied in detail. Moreover, since the EM simulation is frequently the most time-consuming part of the optimization process, designers need efficient optimization algorithms, in terms of the total number of EM solver calls. In this context, in order to further improve convergence of the PSO algorithm, a binary tournament selection strategy successfully used in GA is introduced to the classical PSO algorithm, leading to a new hybrid algorithm, called Tournament Selection PSO.

1.4 Outline

This section summarizes the contents of the chapters in the thesis. Each chapter contains selective literature review substantial for the material presented in it.

Chapter 2 presents several newly developed techniques for efficient numerical evaluation of SIs, arising in the formulation of Green's functions for planar multilayered problems. The SIs are known to be very difficult to evaluate because of the oscillating and slowly converging nature of their kernels, as well as the possible occurrence of surface-wave poles and branch-point singularities in the integrand. First, in order to be able to separately treat these two problems, the semi-infinite integration interval is split into two parts. Then, a new method, based on the double exponential transformation, is proposed for the real-axis integration of the first part of the integral. For the computation of the remaining SI tail, two new techniques are developed: a new version of the Weighted Averages (WA) algorithm and a specially tailored Double Exponential (DE) quadrature formula. Superior performance of the newly developed techniques, in terms of computational cost, is demonstrated throughout a series of representative numerical experiments.

Chapter 3 extends the applicability of the new WA method to the evaluation of semi-infinite integrals involving products of Bessel functions. This type of integrals can be found in numerous problems in electromagnetics [44–46], as well as in the other fields [47–49]. First, the case of product of two Bessel functions of the first kind and of an arbitrary order is describes in detail. The method makes use of extrapolation of sequence of partial sums, and requires rewriting the product of Bessel functions as a sum of two well-behaved (asymptotically simply oscillating) functions. The superior performance of the proposed method is demonstrated throughout numerical experiments. Furthermore, by following the same philosophy, i.e., by representing the irregular oscillatory behavior of the integrand as a linear combination of functions with asymptotically simple oscillating behavior, the method is generalized to the product of an arbitrary number of Bessel functions of the first and/or second kind and/or sine/cosine functions. The correctness

of the generalized method is demonstrated through an example of an integral containing a product of three Bessel functions of the first kind. The solution to the additional complications arising in the case when the integrand involves a Bessel function of the second kind (caused by its singular behavior at the origin), is also suggested.

Chapter 4 introduces the basic concepts of Particle Swarm Optimization algorithm. The binary tournament selection strategy is then introduced to the classical PSO algorithm, in order to further improve its performances. Finally, both the classical PSO and this hybrid version of PSO, called Tournament Selection PSO algorithm, are applied to several layered media problems, in order to compare convergence performances of these algorithms. The obtained results demonstrate that the tournament selection significantly speeds-up the convergence of the PSO algorithm.

Chapter 5 summarizes the thesis and highlights the original contributions. It discusses also the possible future work directions that might be followed, inspired by this thesis.

Bibliography

- [1] R. F. Harrington, *Field computation by moment method*. New York: IEEE Press, 1993.
- [2] R. E. Collin, “The role of analysis in an age of computers: view from the analytical side,” *Antennas and Propagation Society International Symposium, 1990. AP-S. Merging Technologies for the 90’s. Digest*, vol. 4, pp. 1480–1483, May 1990.
- [3] SEMCAD X. <http://www.speag.com/products/semcad/solutions/>.
- [4] Sonnet Software. CST Microwave Studio - Full 3-D Electromagnetic Analysis Software. <http://www.sonnetusa.com/products/cst/index.asp>.
- [5] Ansoft Corporation. (2011) <http://www.ansoft.com/products/>.
- [6] WIPL-D. Electromagnetic modeling of composite metallic and dielectric structures. <http://www.wipl-d.com/>.
- [7] MAGMAS. The TELEMIC antenna modeling software. <http://www.esat.kuleuven.be/telemic/antennas/magmas/>.
- [8] FEKO. Comprehensive electromagnetic simulation software. <http://www.feko.info/>.
- [9] Agilent Technologies. Advanced Design System Momentum Simulator. <http://home.agilent.com/>.
- [10] J. R. Mosig, “Integral-equation techniques for three-dimensional microstrip structures,” in *Review of Radio Science*, R. Stone, Ed. Oxford: URSI-Oxford Science Publications, 1992, ch. 6, pp. 127–152.
- [11] —, “Integral equation techniques,” in *Numerical Techniques for Microwave and Millimeter-Wave Passive Structures*, T. Itoh, Ed. New York: Wiley, 1989, ch. 3, pp. 133–213.
- [12] J. R. Mosig and F. E. Gardiol, “General integral equation formulation for microstrip antennas and scatterers,” *IEE Proceedings, Part H - Microwaves, Optics and Antennas*, vol. 132, no. 7, pp. 424–432, Dec. 1985.
- [13] G. A. E. Vandenbosch and A. R. V. de Capelle, “Mixed-potential integral expression formulation of the electric field in a stratified dielectric medium: Application to the case of a probe current source,” *IEEE Trans. Antennas Propag.*, vol. 40, no. 7, pp. 806–817, July 1992.

-
- [14] K. A. Michalski and J. R. Mosig, "Multilayered media Green's functions in integral equation formulations," *IEEE Trans. Antennas Propag.*, vol. 45, no. 3, pp. 508–519, Mar. 1997.
- [15] B. D. Popovic, M. B. Dragovic, and A. R. Djordjevic, *Analysis and Synthesis of Wire Antennas*. John Wiley & Sons, 1982.
- [16] B. M. Kolundzija and D. I. Olcan, "Multiminima heuristic methods for antenna optimization," *IEEE Trans. Antennas Propag.*, vol. 54, no. 5, pp. 1405–1415, May 2006.
- [17] S. Kirkpatrick, C. D. Gelatt, Jr., and M. P. Vecchi, "Optimization by simulated annealing," *Science*, vol. 220, no. 4598, pp. 671–680, May 1983.
- [18] R. L. Haupt, "An introduction to genetic algorithms for electromagnetics," *IEEE Antennas and Propagation Magazine*, vol. 37, no. 2, pp. 7–15, Apr. 1995.
- [19] D. S. Weile and E. Michielssen, "Genetic algorithm optimization applied to electromagnetics: a review," *IEEE Trans. Antennas Propag.*, vol. 45, no. 3, pp. 343–353, Mar. 1997.
- [20] J. M. Johnson and Y. Rahmat-Samii, "Genetic algorithms in engineering electromagnetics," *IEEE Antennas and Propagation Magazine*, vol. 39, no. 4, pp. 7–21, Aug. 1997.
- [21] Y. Rahmat-Samii and E. Michielssen, *Electromagnetic optimization by genetic algorithm*. New York: John Wiley & Sons, INC, 1999.
- [22] M. Dorigo, M. Birattari, and T. Stutzle, "Ant colony optimization," *IEEE Computational Intelligence Magazine*, vol. 1, no. 4, pp. 28–39, Nov. 2006.
- [23] J. Kennedy and R. Eberhart, "Particle swarm optimization," in *IEEE Int. Conf. Neural Networks*, Perth, WA, Australia, Nov. 17 – Dec. 1, 1995, pp. 1942–1948.
- [24] J. Robinson and Y. Rahmat-Samii, "Particle swarm optimization in electromagnetics," *IEEE Trans. Antennas Propag.*, vol. 52, no. 2, pp. 397–407, Feb. 2004.
- [25] N. Jin and Y. Rahmat-Samii, "Advances in particle swarm optimization for antenna designs: real-number, binary, single-objective and multiobjective implementations," *IEEE Trans. Antennas Propag.*, vol. 55, no. 3, pp. 556–567, Mar. 2007.
- [26] COST action IC0603 ASSIST. Antenna System & Sensors for Information Society Technologies. <http://www.cost-ic0603.org/>.
- [27] M. I. Aksun and G. Dural, "Clarification of issues on the closed-form Green's functions in stratified media," *IEEE Trans. Antennas Propag.*, vol. 53, no. 11, pp. 3644–3653, Nov. 2005.

-
- [28] M. Yuan, T. K. Sarkar, and M. Salazar-Palma, "A direct discrete complex image method from the closed-form Green's functions in multilayered media," *IEEE Trans. Microw. Theory Tech.*, vol. 54, no. 3, pp. 1025–1032, Mar. 2006.
- [29] V. N. Kourkoulos and A. C. Cangellaris, "Accurate approximation of Green's functions in planar stratified media in terms of a finite sum of spherical and cylindrical waves," *IEEE Trans. Antennas Propag.*, vol. 54, no. 5, pp. 1568–1576, May 2006.
- [30] R. R. Boix, F. Mesa, and F. Medina, "Application of total least squares to the derivation of closed-form Green's functions for planar layered media," *IEEE Trans. Microw. Theory Tech.*, vol. 55, no. 2, pp. 268–280, Feb. 2007.
- [31] A. G. Polimeridis, T. V. Yioultis, and T. D. Tsiboukis, "A robust method for the computation of Green's functions in stratified media," *IEEE Trans. Antennas Propag.*, vol. 55, no. 7, pp. 1963–1969, July 2007.
- [32] —, "Fast numerical computation of Green's functions for unbounded planar stratified media with a finite-difference technique and Gaussian spectral rules," *IEEE Trans. Microw. Theory Tech.*, vol. 55, no. 1, pp. 100–107, Jan. 2007.
- [33] A. G. Polimeridis and T. V. Yioultis, "On the efficient computation of closed-form Green's functions in planar stratified media," *Int. J. RF Microw. Computer Aided Eng.*, vol. 18, no. 2, pp. 118–126, Mar. 2008.
- [34] K. A. Michalski, "Application of the complex image method to electromagnetic field computation in planar uniaxial multilayers," in *I Workshop on Integral Techniques for Electromagnetics (INTELECT)*, Lausanne, Switzerland, July 2007.
- [35] F. J. Demuynck, G. A. E. Vandebosch, and A. R. V. de Capelle, "Analytical treatment of the Green's function singularities in a stratified dielectric medium," in *Proc. European Microwave Conference*, Madrid, Spain, Sept. 6–10, 1993, pp. 1000–1001.
- [36] F. J. Demuynck and G. A. E. Vandebosch, "The expansion wave concept - part I: efficient calculation of spatial Green's functions in a stratified dielectric medium," *IEEE Trans. Antennas Propag.*, vol. 46, no. 3, pp. 397–406, Mar. 1998.
- [37] N. Kinayman and M. I. Aksun, "Comparative study of acceleration techniques for integrals and series in electromagnetic problems," *Radio Science*, vol. 30, no. 6, pp. 1713–1722, Nov.–Dec. 1995.
- [38] K. A. Michalski, "Extrapolation methods for Sommerfeld integral tails," *IEEE Trans. Antennas Propag.*, vol. 46, no. 10, pp. 1405–1418, Oct. 1998.
- [39] T. Hasegawa and A. Sidi, "An automatic integration procedure for infinite range integrals involving oscillatory kernels," *Numerical Algorithms*, vol. 13, no. 1, pp. 1–19, Mar. 1996.

-
- [40] T. Ooura, "A continuous Euler transformation and its application to the Fourier transforms of a slowly decaying functions," *J. Comput. Appl. Math.*, vol. 130, no. 1–2, pp. 259–270, May 2001.
- [41] S. Singh and R. Singh, "Computation of Sommerfeld integrals using tanh transformation," *MOTL*, vol. 37, no. 3, pp. 177–180, Mar. 2003.
- [42] T. Ooura, "A generalization of the continuous Euler transformation and its application to numerical quadrature," *J. Comput. Appl. Math.*, vol. 157, no. 2, pp. 251–259, 2003.
- [43] M. Yuan and T. K. Sarkar, "Computation of the Sommerfeld integral tails using the matrix pencil method," *IEEE Trans. Antennas Propag.*, vol. 54, no. 4, pp. 1358–1362, Apr. 2006.
- [44] M. Ikonomou, P. Köhler, and A. F. Jacob, "Computation of integrals over the half-line involving products of Bessel functions, with application to microwave transmission lines," *ZAMM -J. of Appl. Math. and Mech./ Zeitschrift für Angewandte Mathematik und Mechanik*, vol. 75, no. 11, pp. 917–926, Nov. 1995.
- [45] N. P. Singh and T. Mogi, "Electromagnetic response of a large circular loop source on a layered earth: a new computation method," *Pure App. Geophys.*, vol. 162, no. 1, pp. 181–200, 2005.
- [46] N. N. Lebedev, I. P. Skalskaya, and Y. S. Uflyand, *Worked problems in applied mathematics*. New York: Dover publications, 1965.
- [47] A. M. J. Davis, "Drag modifications for a sphere in a rotational motion at small non-zero Reynolds and Taylor numbers: wake interference and possible Coriolis effects," *J. Fluid Mech*, vol. 237, pp. 13–22, 1992.
- [48] H. A. Stone and H. M. McConnell, "Hydrodynamics of quantized shape transitions of lipid domains," *Proc. Math. and Phys. Sci.*, vol. 448, no. 1932, pp. 97–111, Jan. 1995.
- [49] P. M. Morse and H. Feshbach, *Methods of theoretical physics: part II*. Minneapolis: Feshbach publishing, LLC, 1981.

2 Efficient computation of Sommerfeld integrals

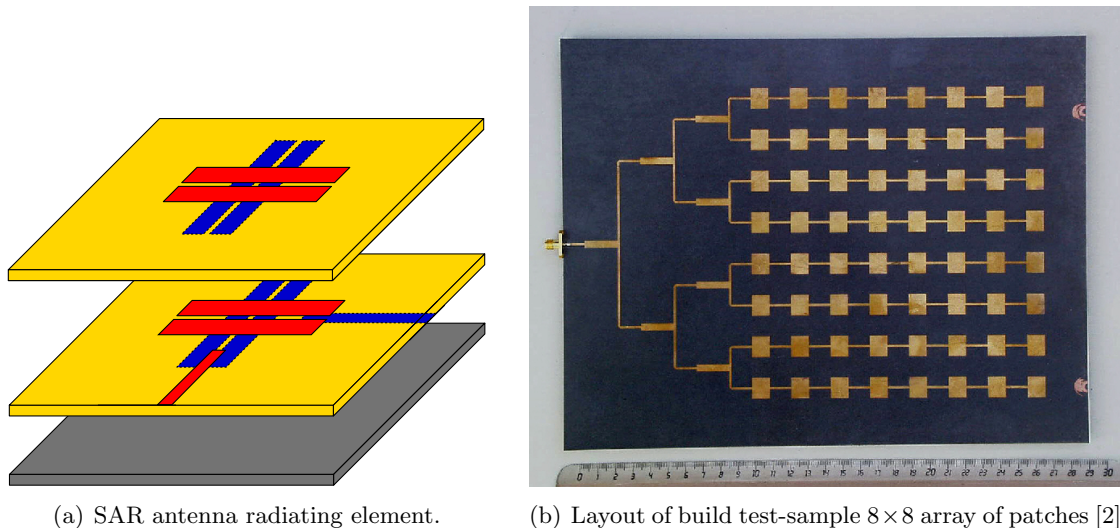
2.1 Introduction

The early development of planar printed circuits for the microwave applications was mainly driven by the need of low-cost microwave circuits, and their use for radiating purposes was not immediately evident. First, the microstrip line was developed as a normal evolution of the two wire and coaxial transmission lines. Despite the radiation losses due to their open nature, the use of microstrip lines was rapidly expanding particularly because of their easy integration with other microwave circuits and very easy manufacturing process. Although already in 1953 Deschamps introduced the microstrip antenna concept, when studying radiation loss of planar printed circuits, it was only in early 1970s that the antenna community started considering the possibility of using microstrip structures for radiation purposes. Nowadays, planar technologies, in which thin metallizations are embedded within stratified dielectric media, are considered as one of the most popular and successful approaches to build circuits and antennas in microwaves and millimeter waves with a good performance-to-price ratio, like the dual polarized eight element subarray SAR antenna [1] whose radiating element is depicted in Fig. 2.1(a) and 8×8 corporate-fed array of patches [2] shown in Fig. 2.1(b).

The need to satisfy all sorts of requirements, ranging from electromagnetic to thermal and mechanical behavior of the system elements, especially in space applications, in many cases can be fulfilled only by using very complex multilayered structures. Although the experimental characterization of all parts of such a complicated system is possible, it would be unacceptably time-consuming and expensive. Therefore, we need fast and accurate software tools for the electromagnetic analysis of these structures, which allow efficient computer-aided design of the different parts of satellite systems.

One of the most proven mathematical models to analyze multilayered structures is based on the integral equation formulations, combined with a Galerkin Method of Moments (MoM) approach for the numerical solution [3–5]. Among several possible variants, the Mixed Potential Integral Equation (MPIE) formulation is generally considered to be more efficient for numerical modeling of arbitrarily shaped printed circuits, because its kernel is only weakly singular. Indeed, the kernel singularities in MPIE correspond to the $1/R$ singularities of EM potentials, while other formulations like EFIE and MFIE show in their kernels the singularity of the EM field ($1/R^2$ or $1/R^3$).

When the integral equation model is applied to a multilayered substrate, the preliminary



(a) SAR antenna radiating element.

(b) Layout of build test-sample 8×8 array of patches [2]**Figure 2.1:** Real-life multilayered working setups.

step is the accurate determination of its kernel, which corresponds to Green's functions (GFs) associated with the layered medium. Green's function is defined as the field or potential created by unit source (electric or magnetic dipole) embedded in layered media. Therefore, in the engineering terminology, GF is nothing else but the impulse response of a system. Since the system is linear, the superposition principle applies: the potentials/fields resulting from any finite source can be determined by dividing this source into an infinite number of elementary dipoles, and by adding (integrating) the contributions of all the sources [6].

The theoretical foundations for the computation of fields and potentials in multilayered structure were developed in [7], where it was established that the Green's functions can be most easily determined in the Fourier transform domain (also called spectral domain), reducing the original problem to that of solving an equivalent transmission line network. It is shown, that by considering two dual networks (for TE and TM waves), all the components of the spectral-domain GFs associated with arbitrary excitations (electric or magnetic, oriented along x , y or z axis) can be represented in closed-form expressions in terms of electric parameters (currents and voltages) [8–10].

Once the spectral-domain GFs have been determined, they have to be transformed back in the space domain, using inverse Fourier transform. In the case of multilayered structures, it is well known that this Fourier-Bessel transformation reduces to an one-dimensional integral of the complex spectral variable k_ρ over a semiinfinite interval, usually known as the Sommerfeld integral (SI) [11].

Sommerfeld integrals are very complex and time consuming to evaluate, because of the oscillatory and slowly decaying nature of the integrand, as well as the presence of singularities on and/or near the integration path in the complex spectral k_ρ -plane. Over the last 30 years,

researchers have intensively worked on efficient methods for the evaluation of SIs, that are valid for all distances between field and source points. Generally, several methods have been proposed in order to tackle this problem, which can be roughly categorized into two main families. First, we mention the closed-form Green's functions methods (see [12–18] among others), where no numerical integration is needed. Instead, the integrand (spectral-domain Green's function) is approximated via a finite sum of special functions, such that their SIs admit analytical evaluation. Although via the aforementioned methods, GFs need to be evaluated only once for all transverse distances, the lack of a robust a priori error control still remains a critical challenge for the future.

As an alternative, the second family consists of all methods that are based on the numerical integration of the SIs. There are mainly two difficulties arising when numerically evaluating SIs. The first one is related to the presence of an oscillating integrand which converges slowly, or even diverges, and which has to be considered over an infinite interval. The second difficulty is due to the possible existence of the singularities in the integrand. However, by adequately dividing the integration interval, those problems can be always treated separately. Since the integrand of SI is defined in the complex plane, numerous integration paths can be selected for its evaluation (see for example [19]). Among them we should mention the real-axis integration deformed into the first quadrant of the complex plane, to avoid surface-wave poles and branch-point singularities of Green's functions, using rectangular [20], elliptic [21] or alternatively half-sine [22] integration paths (see Fig. 2.2), which is considered by many authors as the most convenient choice, since it obviates the need of locating the poles. Integration along the real axis combined with the pole extraction techniques is also widely used [23, 24]. Choosing either of those approaches calls for the special treatment of the SI tails, like the so-called integration-then-summation procedure combined with one of the numerous extrapolation techniques for the convergence acceleration. Among them, the weighted averages (WA) method is proven to be one of the most efficient [25, 26].

Alternatively, one could also choose the direct integration of the SIs, based on Euler and double-exponential (DE) transformations, as suggested in [27–30]. Finally, a somewhat hybrid approach was introduced in [31], where the integrand of the SI tail is fitted by a sum of finite complex exponentials, similar to the philosophy of closed-form Green's functions methods, leaving a remainder to be numerically evaluated.

In this chapter, we address the problem of numerical evaluation of the SIs. Even with the state-of-the-art techniques, the evaluation of the space-domain GFs from their spectral-domain counterparts may take the dominant part of the overall computation effort involved in the solution of MPIE. Therefore, the problem of the efficient numerical evaluation of the SIs, both in terms of accuracy and computational cost, is of paramount relevance.

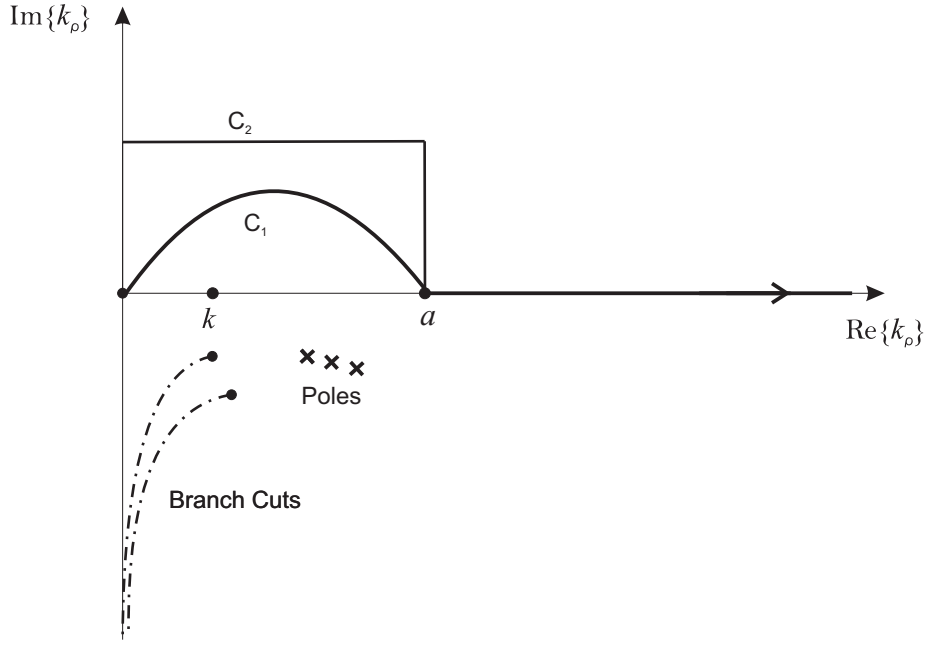


Figure 2.2: Possible integration paths for the computation of Sommerfeld integrals (choice $a = k(\sqrt{(\varepsilon_{r_i}\mu_{r_i})_{\max}} + 1)$ assures that there are no singularities for $k_\rho > a$).

2.2 Sommerfeld integral

With reference to the generic layered media of Fig. 2.3, the Sommerfeld-type integrals can be written as follows [23, 26]:

$$S_n\{\tilde{G}(k_\rho; z|z')\} = \frac{1}{4\pi} \int_{-\infty}^{+\infty} \tilde{G}(k_\rho; z|z') H_n^{(2)}(k_\rho \rho) k_\rho dk_\rho \quad (2.1)$$

or,

$$S_n\{\tilde{G}(k_\rho; z|z')\} = \frac{1}{2\pi} \int_0^\infty \tilde{G}(k_\rho; z|z') J_n(k_\rho \rho) k_\rho dk_\rho \quad (2.2)$$

where \tilde{G} is the spectral-domain Green's function of the layered media, J_n is the Bessel function of the first kind of order n , $H_n^{(2)}$ is the Hankel function of the second kind of order n , ρ is the horizontal distance between the field and source points, and z, z' are the vertical coordinates of those points, respectively. Notice that the passage from (2.1) to the traditional form (2.2) is done using the symmetry properties of Hankel function [32], and the fact that the function $\tilde{G}(k_\rho; z|z')$ is always an even (odd) function in k_ρ for even (odd) n [8–10].

It is well known that the evaluation of SIs is very delicate, because of the following reasons:

1. The integration domain extends to infinity;
2. The integrand exhibits oscillatory behavior due to the Bessel function;

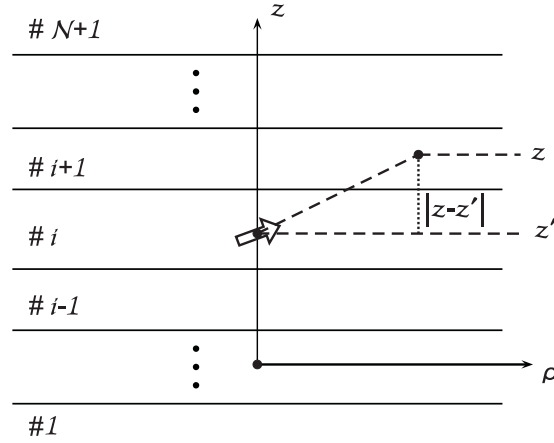


Figure 2.3: Generic stratified media showing a point source (level z') and a field observation point (level z) separated by a radial distance ρ . The medium can be terminated on the top and/or on the bottom by a perfect electric conductor (PEC), perfect magnetic conductor (PMC) and impedance plane.

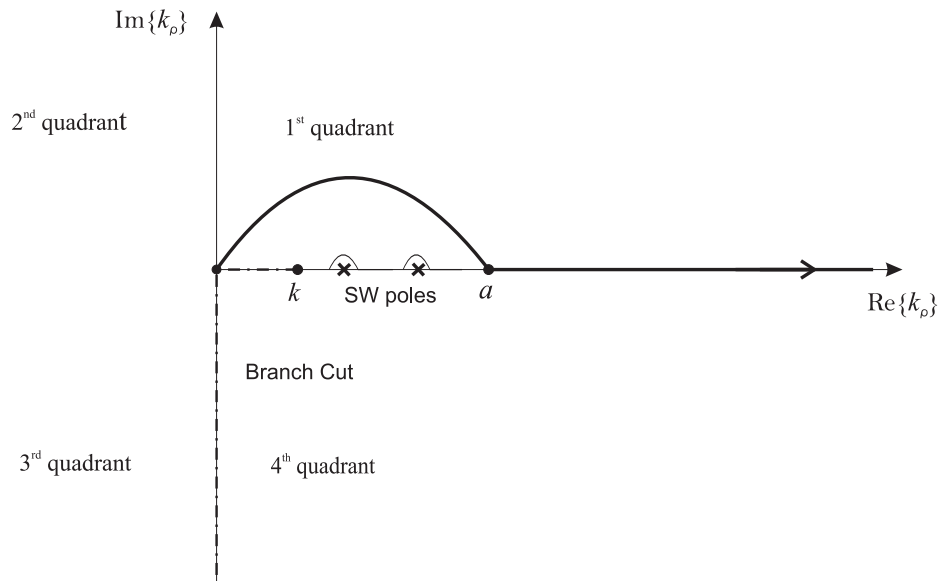
3. The integrand's envelope is slowly converging or even diverging;
4. The spectral-domain function $\tilde{G}(k_\rho; z|z')$ presents in general surface-wave poles and branch-point singularities on and/or near the integration path.

Since the numerical techniques to be used for evaluation of the Sommerfeld integrals are closely dependent on the behavior of the integrand, we should first proceed with the precise discussion of the properties of the Bessel and spectral-domain Green's functions in the complex k_ρ -plane. Special attention must be paid to the particular topology of the complex spectral k_ρ -plane due to the existence of the surface-wave poles, branch points, branch cuts and associated Riemann sheets.

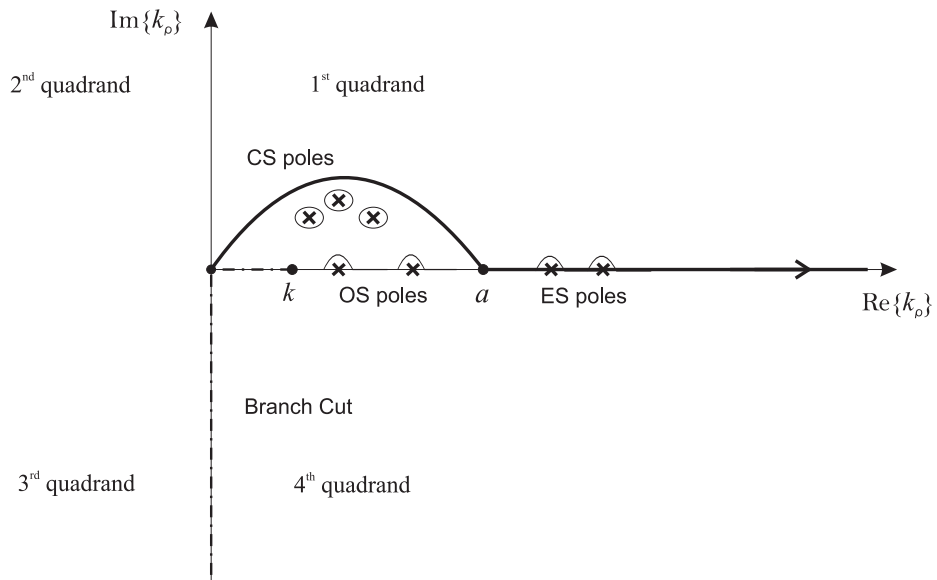
Surface-wave poles

Spectral-domain Green's function poles are located on the real axis of the complex k_ρ -plane, if the structure is considered without losses. If, moreover, the structure is bounded by a lower ground plane and radiates into the open half space, the surface-wave poles are located within the $[k, k\sqrt{(\varepsilon_{r_i}\mu_{r_i})_{\max}}]$ interval, where $k = 2\pi f\sqrt{\varepsilon_0\mu_0}$, and ε_{r_i} and μ_{r_i} are the relative permittivities and permeabilities of different layers [33], and ε_0 and μ_0 are vacuum permittivity and permeability. If the structure is closed by an upper ground plane, the GFs may exhibit poles also in the $[0, k]$ region, which correspond to the waveguide modes. In the case of lossy media, poles migrate from the real axis to the fourth quadrant of complex k_ρ -plane [34].

The previous paragraph discusses conventional layered media consisting of double positive (DPM) or right-handed materials (RHMs), which is the problem we are focussing on throughout this manuscript. However, because of the increasing interest of our community in



(a) Grounded slab made of RHMs.



(b) Grounded slab made of MTMs.

Figure 2.4: Poles and branch point in complex k_ρ -plane for lossless grounded slab ($a = k\sqrt{(\epsilon_{r_i}\mu_{r_i})_{\max}}$).

Table 2.1: Spectral properties of complex modes on lossless DNG, ENG, MNG and DPS grounded slabs.

	TE	TM
double-negative	proper	proper
μ -negative	proper	improper
ε -negative	improper	proper
double-positive	improper	improper

materials with negative magnetic permeability ($\mu < 0$) and/or negative dielectric permittivity ($\varepsilon < 0$), a word must be said about the peculiar features of EM wave propagation when such materials are involved in multilayered geometry. Usually, these materials are called left-handed materials (LHMs), or negative (refractive) index materials (NIMs), or, even more general metamaterials (MTMs), and they include: double negative materials (DNM, $\varepsilon, \mu < 0$) and single negative materials (SNM), which can be either μ -negative (MNG) or ε -negative (ENM).

Modal properties of multilayered media with MTMs have been studied by several groups, and they mainly focus on a lossless grounded slab made of MTMs (see [35–38], among others). For this type of geometry there are three different types of poles. First, similarly to the case of DPMs, poles located within the region $[k, k\sqrt{(\varepsilon_{r_i}\mu_{r_i})_{\max}}]$ can be found in the case of grounded metamaterial slab. They correspond to ordinary surface (OS) modes, which are transversely attenuating only on the air side. Besides them, one has to also consider real poles in the region $k_\rho > k\sqrt{(\varepsilon_{r_i}\mu_{r_i})_{\max}}$, which correspond to evanescent surface (ES) modes, transversally attenuating on both sides of the air-slab interface. Finally, in addition to real modes, complex surface (CS) modes may also exist on a grounded metamaterial slab. In isotropic structures, the corresponding GF's poles in the complex k_ρ -plane form always groups of four (lying on the proper Riemann sheet), symmetrically placed with respect to the real and imaginary axes [35, 36]. They have high cutoff frequency, which means they only exist when the frequency is lower than their respective cutoff frequency. This property implies two facts: an infinite number of complex surface modes exist at any frequency and they cannot be suppressed. However, the investigation on the Poynting vectors shows that their integrals along the longitudinal directions are zero, i.e., they don't transport any energy [37]. Nevertheless, this by no means implies that they are unimportant. Although these complex poles will not directly contribute to the SI of the mixed-potential GFs if the integration is performed along the real axis, they have to be taken into account when the integration contour is deformed in the first quadrant of the complex k_ρ -plane, since there is a possibility of capturing a finite number of these poles [38]. Then, the calculation of residues at captured poles is needed. The spectral properties of the CS modes for different kinds of lossless grounded slabs are outlined in Table 2.1.

Finally, the above discussion is summarized in Fig. 2.4 depicting the allowed regions for the

existence of all the operating modes, and the possible integration path for evaluation of SI, for the case of a lossless grounded slab. For the sake of illustration, only one of the four CS mode groups (in the first quadrant of the complex k_ρ -plane) is depicted in Fig. 2.4(b) for the slab made of MTMs.

Branch-point singularities

For half-opened structures, a second type of singularities occurs at the branch point $k_\rho = \pm k$, where k is the wavenumber of the opened half space. The branch cuts are associated with the vertical wavenumber

$$k_z = \sqrt{k^2 - k_\rho^2} \quad (2.3)$$

which is a double-valued function of k_ρ . In order to satisfy the radiation condition at infinity, k_z has to be taken with negative imaginary part, which is referred to as the proper Riemann sheet. For the multilayered media under consideration, there are vertical wavenumbers associated with each layer, but only the sign of the imaginary parts of those related to the unbounded regions will be relevant for the evaluation of the space-domain Green's functions [7], which can be intuitively understood from the propagation point of view. Since in bounded layers the waves are traveling in both directions, the choice of the sign of the wavenumber is irrelevant. Nevertheless, since in the unbounded layers the waves are traveling away from the source only, the sign of the wavenumber must be selected accordingly [39]. Finally, double-opened structures have two branch points: one associated with the first layer (layer #1), and the second one associated with the last layer (layer #($N + 1$)), see Fig. 2.3).

Asymptotic behavior of the integrand

As the integral (2.2) extends to infinity, it is important to understand the behavior of the integrand for the large values of k_ρ . The spectral-domain GFs arising in the layered media have the asymptotic form:

$$\tilde{G}(k_\rho; z|z') \sim \frac{e^{-k_\rho|z-z'|}}{k_\rho^\mu} (C + O(k_\rho^{-1})) \quad (2.4)$$

where C is a constant, and the exponent μ can be easily determined by inspection of the relevant expressions for spectral-domain GFs [8, 22]. The asymptotic behavior of the Bessel function is given by [32]:

$$J_n(k_\rho \rho) \sim \sqrt{\frac{2}{\pi k_\rho \rho}} \cos\left(k_\rho \rho - \frac{n\pi}{2} - \frac{\pi}{4}\right). \quad (2.5)$$

2.3 Evaluation of the Sommerfeld integrals

Since the integrand in the SI (2.2) is defined in the complex domain, various paths of the integration can be selected [19]. The common approach is to split the generic SI (2.2) into two parts, $(0, \xi_0)$ and (ξ_0, ∞) , as shown in Fig. 2.5:

$$S_n = \frac{1}{2\pi}(I_n + T_n). \quad (2.6)$$

The integration path for I_n joins the origin to a point $\xi_0 > a$ on the real axis, chosen so to guarantee that there are no singularities for $\text{Re}(k_\rho) > a$. When evaluating this integral, special attention has to be paid to the presence of the singularities in the integrand, which can be treated in several ways. First, the integration path can be deformed into the first quadrant of the complex k_ρ -plane to avoid pole and branch-point singularities, which is usually considered to be the most convenient approach in the case of multilayered media [8, 22], since it obviates the need to extract the poles. In the case that one selects to perform the integration of I_n along the real-axis path, the surface-wave poles have to be extracted and the residue theorem has to be applied. An infinite derivative of the integrand at a branch point must be eliminated by using a change of variable [23], or by extracting its contribution in the spectral-domain and adding it back analytically in the space domain [24].

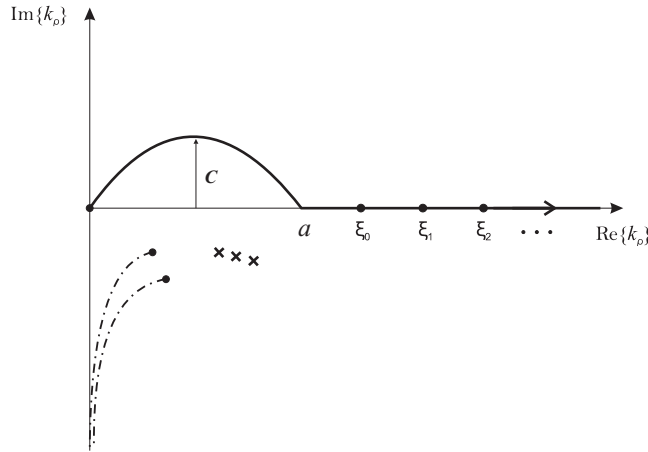


Figure 2.5: Deformed integration path for the computation of Sommerfeld integrals.

The remaining integral T_n is the so-called SI tail. It is defined as a singularity-free semi-infinite integral on the real axis, that needs a special treatment because of its oscillating and slowly decaying or even diverging integrand. The most common strategy is to calculate the SI tail with the help of the integration-then-summation procedure, which transforms the original integration problem into the problem of evaluating an infinite sum of partial integrals over finite intervals. Since the so-obtained sum converges very slowly, the direct summation and truncation is out of question, because it would require an unacceptably high number of

partial integrals. This deficiency is circumvented by applying one of the numerous extrapolation techniques that accelerate the convergence of the sum. Those techniques can mainly be categorized into linear and nonlinear ones. As a typical example of linear transformation, we mention the Euler method [40, 41], which is applicable only to alternating series, and the more general-purpose weighted-averages (or generalized Euler) method [42–45]. On the other hand, the Shanks transformation [46] and the generalized Levin transformation [47] stand as two of the most representative members of the nonlinear methods. In practical problems, the Shanks transformation is efficiently implemented via a recursive scheme, i.e., the Wynn’s ϵ algorithm [48], while in the Levin transformation, structural information of the sequence is explicitly incorporated into the overall procedure, resulting in some of the most powerful and most versatile sequence acceleration methods that are currently known [49]. A more complete history of the previous work relevant to the extrapolation methods can be found in the excellent monograph [50]. The performance of those methods when applied to SI tails is studied in detail in [26], where the weighted averages method [6, 23, 26, 51], also referred in the literature as Mosig-Michalski transformation [52], was shown to be the best choice for the SI type of problems.

The above described numerical techniques, traditionally used in the evaluation of the Sommerfeld integrals, are very efficient for small to moderate source-observer distances ρ , but become computationally heavy for large values of ρ . For numerical evaluation of the spatial domain Green’s functions in the case of medium and large source-observer distances, a new choice of the integration contour closed through the imaginary axis of the spectral k_ρ -plane has been suggested in [51, 53]. This technique is not recommended for very small values of ρ , because of possible numerical instabilities.

Another very interesting approach for the numerical evaluation of the SIs has been suggested in [24], where the surface-wave poles, branch-point singularities and the asymptote of the spectral-domain Green’s function are annihilated in the spectral domain. Their contributions are evaluated analytically and added back in the spatial domain. The integral of the remaining smooth function is numerically evaluated. The main advantage of this technique is the possibility to express the spatial domain GFs evaluated not too close to the source as a sum of simple analytic functions with a well-known physical meaning: surface waves and the dominant part of the space wave.

2.4 The first part of the SI

The first part of the SI can be written as:

$$I_n = \int_0^{\xi_0} \tilde{G}(k_\rho; z|z') J_n(k_\rho \rho) k_\rho dk_\rho \quad (2.7)$$

where the upper limit of the integrand is chosen in a way that guarantees that there are no singularities for $k_\rho > \xi_0$. First, we recall the two most popular techniques for the evaluation of the above integral: half-sine contour path integration [22] and the real-axis integration combined with the pole extraction technique and variable transformation for treating the branch-point singularity [23]. Then, we propose a general, accurate and efficient method for integration of (2.7) along the real axis, that is valid and computationally inexpensive for both small and large values of source-observer distances. The method uses a very robust automatic algorithm for pole extraction, based on the sine transformation [54]. The problematic behavior of the integrand at the branch point is taken care of by using the double exponential transformation [55].

2.4.1 Half-sine contour integration

In this section we discuss the calculation of the first part of the SI along the path partially indented into the upper halfspace of the complex spectral k_ρ -plane. Here, we follow the approach from [22] and express the integral (2.7) as:

$$I_n = I_{n_a} + I_{n_b} \quad (2.8)$$

where the right-hand terms are defined as follows: I_{n_a} is the integral along the path deformed into the first quadrant of the complex k_ρ -plane in order to avoid surface-wave pole and branch-point singularities:

$$I_{n_a} = \int_0^a \tilde{G}(k_\rho; z|z') J_n(k_\rho \rho) k_\rho dk_\rho. \quad (2.9)$$

Its exact shape is not critical as far as the singularities are circled around. Conventionally, a half-sine shape is employed, because of its convenient parametrization, namely:

$$k_\rho(t) = a \cdot (1 + \cos(\frac{\pi}{2}(1-t))) + j \cdot c \cdot \sin(\frac{\pi}{2}(1-t)) \quad (2.10)$$

where a and c are the major and minor semi-axis of the half-sine (see Fig. 2.5). With this parametric change of variable, I_{n_a} is transformed into the integral extended over a finite interval of a function presenting no singularities in the integration path:

$$I_{n_a} = \int_{-1}^1 \tilde{G}(k_\rho(t); z|z') J_n(k_\rho(t) \rho) k_\rho(t) \frac{dk_\rho(t)}{dt} \quad (2.11)$$

which can be easily evaluated using an adaptive quadrature based on Patterson's formulas [56]. The half-sine width

$$a = k(\sqrt{(\varepsilon_{r_i} \mu_{r_i})_{\max}} + 1) \quad (2.12)$$

is determined by the possible location of the poles. The following choice of the maximal sine height c , recommended in [22],

$$\frac{c}{k} = \begin{cases} \min\left(1, \frac{1}{k\rho}\right), & \text{if } \rho > \operatorname{Re}|z - z'|, \\ 1, & \text{otherwise.} \end{cases} \quad (2.13)$$

is governed by the exponential growth of the Bessel function when k_ρ departs from the real axis [32]. The problem is as follows. For large values of the horizontal source-observer distance ρ , the argument of the Bessel function becomes large, leading to an unacceptable numerical error associated with the evaluation of the Bessel function. A possible remedy to this problem is to decrease the value of the maximal height c of the half-sine as ρ increases, bounding the argument of the Bessel function in the non-numerical error region. However, the maximal height of the half-sine cannot be made arbitrarily small, since then the integration path would pass very close to the singularities related to the spectral-domain GF poles, resulting again in numerical inaccuracies. As good trade-off, the choice (2.13) for the half-sine height c has been proposed. This somewhat arbitrary choice is experimentally proven to give very good results.

The integral I_b is the real-path integral from a to the first break point ξ_0 exceeding a , and is defined as:

$$I_{n_b} = \int_a^{\xi_0} \tilde{G}(k_\rho; z|z') J_n(k_\rho \rho) k_\rho dk_\rho. \quad (2.14)$$

Possible choices for the breakpoints ξ_i include the asymptotic half-periods, exact zero crossings and extrema of the Bessel functions [26]. This integral is well-behaved and can be efficiently evaluated by an adaptive quadrature based on Patterson's formulas [56].

2.4.2 Real-axis integration

There are mainly two problems arising in the real-axis integration of the first part of the Sommerfeld integral (2.7). The first one is related to the singular behavior of the integrand due to the presence of the surface-wave poles on and/or near the integration path. The solution to this problem consists of subtracting a well-chosen analytic function showing the behavior needed to eliminate the difficulty in question and re-adding the same function after analytical inverse Fourier transformation, i.e., first subtracting the surface-wave poles in spectral domain and then adding their contribution in the spacial domain analytically. For the extraction of the surface-wave poles of multilayered spectral-domain Green's function, the efficient automatic algorithm proposed in [54] is used. The second difficulty is due to an infinite derivative of the integrand at the branch point k , related with the open half-space of the structure. As a solution, we propose to split the integration interval of (2.7) into two parts: $(0, k)$ and (k, ξ_0) , and evaluate each of them with the help of the double exponential quadrature

formula [55], which has been shown to be very efficient for the integrals with integrable endpoint singularities.

2.4.2.1 Pole extraction

The problematic singular behavior of the spectral-domain Green's function can be annihilated by subtracting the spectral function [24]:

$$f_{\text{sing}} = \sum_{i=1}^{N_p} f_{\text{sing}}^{P_i} = \sum_{i=1}^{N_p} \frac{4P_i^3 R_i}{k_\rho^4 - P_i^4} \quad (2.15)$$

where P_i is the position of the i -th pole, R_i is its residue and N_p is number of poles. The corresponding spatial function can be calculated analytically as:

$$F_{\text{sing}} = \sum_{i=1}^{N_p} F_{\text{sing}}^{P_i} = \sum_{i=1}^{N_p} 2P_i R_i \left(-j \frac{\pi}{2} H_0^{(2)}(P_i \rho) - K_0(P_i \rho) \right) \quad (2.16)$$

where $H_0^{(2)}$ is the Hankel function and K_0 is the modified Bessel function, both of the 2nd kind and order 0. Although this procedure looks very easy, locating the spectral-domain GFs' surface-wave poles can be a very demanding task, especially in the case when those poles lie close to the branch point. Actually, this difficulty is one of the main reasons why the real-axis integration has not been more exploited.

For simple geometries, such as single-layered structures, the modified Newton-Raphson algorithm is commonly used for locating the poles. However, this method is limited to simple structures, since in the case of more complicated geometries, finding suitable starting points for the Newton-Raphson algorithm is often extremely difficult. In [57] a method for automatic extraction of the poles was proposed, but the existence of the branch points prevented finding the poles located very close to k . This deficiency is successfully solved in [54], by embedding in [57] a proper sine transformation:

$$k_\rho = k \sin w \quad (2.17)$$

which removes the branch cut of the Green's function. In the transformed w -plane, the branch point becomes a regular point, and therefore in the w -plane all the poles can be efficiently located, regardless how close to the branch point they were in the original k_ρ -plane. The merits of this algorithm are numerous. Not only it works for general multilayered media, whether shielded or opened, lossy or lossless, but it can be embedded in the routines for numerical evaluation of SIs in a fully automatic way. Moreover, in the case of complicated geometries at high frequencies, when the number of poles can be large, the computational time is only slightly increased.

2.4.2.2 Treatment of branch-point singularities

Once the poles are extracted, the remaining spectral-domain GF to be integrated shows a very smooth behavior, except at the branch point k , where it exhibits a removable singularity due to the presence of the term $\sqrt{k^2 - k_\rho^2}$. Therefore, by extracting the poles and splitting the integral (2.7) into two parts, $(0, k)$ and (k, ξ_0) , the original problem boils down to the one of evaluating integrals with endpoint singularities.

These integrals cannot be efficiently evaluated using standard interpolatory quadrature rules, like for example Gauss-Legendre formulas, since those are only suitable for the integrals that are regular at the endpoints of integration interval. One possibility to tackle this problem, is to apply the variable transformation that eliminates the infinite derivative at k , as suggested in [23]. For the integral over the interval $(0, k)$ the variable transformation is given as:

$$k_\rho = k \cos(t) \quad (2.18)$$

and for the integral over (k, ξ_0) as:

$$k_\rho = k \cosh(t). \quad (2.19)$$

After the variable transformation, one obtains a very smooth integrand, which can be integrated by an adaptive quadrature based on Patterson's formulas.

The alternative we propose is a new method using the double exponential (DE) quadrature formulas to evaluate integrals over $(0, k)$ and (k, ξ_0) . The DE quadrature was first proposed by Takasaki and Mori in 1974 [55], as a result of intensive research on numerical methods for efficient numerical evaluation of integrals with endpoint singularities, which arise in many practical problems. Since the DE quadrature is based on the appropriate tanh-sinh transformation, it represents a general purpose quadrature, which is generally so efficient as to be used as one of the members in the mathematical subroutine library [55]. DE formulas are already incorporated into the well known mathematical software, such as Maple and Mathematica. In this section we aim to introduce the DE quadrature formulas in the context of SIs.

Double exponential transformation

We will confine ourself to the following integral:

$$I = \int_{-1}^1 f(x) dx \quad (2.20)$$

without loss of generality, since the discussion can be easily generalized to the integral $\int_a^b f(\xi) d\xi$ by applying the change of variables $\xi = (b - a)x/2 + (b + a)/2$. Since Takahasi and Mori in [58] had already proven the optimality of the trapezoidal formula with equal mesh size for integrals of analytic function over $(-\infty, \infty)$, it was quite natural that they focused on the variable transformation which maps the interval $(-1, 1)$ into $(-\infty, \infty)$. Therefore, the

following transformation

$$x = \phi(t) \tag{2.21}$$

which we assume is analytic over $(-\infty < t < \infty)$ and satisfies

$$\phi(-\infty) = -1, \quad \phi(+\infty) = 1 \tag{2.22}$$

transforms the original integral (2.20) into the following one:

$$I = \int_{-\infty}^{\infty} f(\phi(t))\phi'(t)dt \tag{2.23}$$

which can be efficiently solved with the help of the trapezoidal formula:

$$I_h = h \sum_{k=-\infty}^{\infty} f(\phi(kh))\phi'(kh)dt. \tag{2.24}$$

The remaining point is now the optimal selection of the change of variable $x = \phi(t)$. The main idea is based on the Euler-Maclaurin formula [59]: if the selected transformation is such that all its derivatives tend sufficiently rapidly to zero as $t \rightarrow \infty$, then even if the function $f(x)$ or its derivatives have an integrable algebraic singularity at the endpoints, they will disappear within the smooth and fast convergence of the new integrand $f(\phi(t))\phi'(t)$ at infinity. In these cases, according to the Euler-Maclaurin argument, the quadrature error should decrease faster than any power of h .

Among numerous transformations that fulfill the Euler-Maclaurin argument, Takahasi and Mori aimed to find the optimal one, which gives the highest accuracy with the minimal number of function evaluations. So, in order to pursue the optimal transformation, they continued with the following analysis. Basically, when approximating the integral (2.20) with the infinite sum (2.24), the discretization error is introduced. Then, in order to evaluate this sum, we must truncate it, introducing the second type of error: truncation error. Suppose now, that we choose the transformation $x = \phi(t)$ which makes the decay of the integrand in (2.23) too fast as $t \rightarrow \infty$ and we keep h at a moderate value. If now the double infinite summation is truncated at the moderate value of $k = \pm n$, the truncation error becomes small. However, the mesh size h becomes relatively large compared with the variation of the integrand $f(\phi(t))\phi'(t)$, making the discretization error very large. On the contrary, a transformation that makes the decay of the integrand $f(\phi(t))\phi'(t)$ insufficiently fast, leads to a small discretization error, since now the mesh size h becomes relatively small compared with the variation of $f(\phi(t))\phi'(t)$. However, if we truncate the summation at the same $k = \pm n$, the truncation error becomes large, since the terms we are neglecting are not yet small enough. Therefore, we have to choose the transformation with the optimal decay of the integrand, leading to a good trade-off between the truncation and discretization errors.

Based on this reasoning, the following transformation was proposed by Takahasi and Mori [55]:

$$x = \phi(t) = \tanh \left(h \cdot \left(\frac{\pi}{2} \sinh(t) \right) \right). \quad (2.25)$$

It is called double exponential transformation because of the double exponential (DE) decay of $\phi'(t)$ as $t \rightarrow \infty$:

$$\phi'(t) = \frac{\frac{\pi}{2} \cosh(t)}{\cosh^2 \left(\frac{\pi}{2} \sinh(t) \right)} \approx O \left(\exp \left(-\frac{\pi}{2} \exp(|t|) \right) \right). \quad (2.26)$$

In the literature it is also referred to as the “tanh-sinh” technique. The above discussion, on which the discovery of the transformation (3.30) is based, is quite intuitive, and the rigorous mathematical proof of the optimality of the selected transformation can be found in [60].

The final DE formula is obtained by truncating the double infinite sum in (2.24):

$$I_h^{(N)} = h \sum_{k=-n}^n f \left(\tanh \left(\frac{\pi}{2} \sinh(kh) \right) \right) \frac{\frac{\pi}{2} \cosh(kh)}{\cosh^2 \left(\frac{\pi}{2} \sinh(kh) \right)}, \quad (2.27)$$

where $N = 2n + 1$ is the number of the points in quadrature rule. The key feature of the superior performance of the DE formulas, when compared to other quadrature rules designed to handle endpoint singularities, lies in the fact that via the DE transformation one can approach the endpoint singularity as close as one wants, because of the infinite number of points of the DE rule in the neighborhood of the endpoints [61].

Remarks on the implementation of the DE transformation

In order to efficiently use the DE transformation, special attention must be paid to the coding. According to [62], careless coding might be one of the main reasons that prevented faster spread of the DE formula.

There are basically two problems arising in the implementation of the DE formulas. The first and most severe problem is the loss of significant digits. If the function $f(x)$ has endpoint singularity like $(1+x)^{-1+\mu}$ or $(1-x)^{-1+\mu}$, where μ is a small positive constant, a large error due to the loss of significant digits at x very close to -1 or 1 is often encountered. One possible remedy for the aforementioned problem is to compute and store the following values:

$$\Xi = 1 + x = \frac{\exp\left(\frac{\pi}{2} \sinh t\right)}{\cosh\left(\frac{\pi}{2} \sinh t\right)} \quad (2.28)$$

$$H = 1 - x = \frac{\exp\left(-\frac{\pi}{2} \sinh t\right)}{\cosh\left(\frac{\pi}{2} \sinh t\right)} \quad (2.29)$$

for $t = kh$, beforehand in addition to the values of the abscissas $\phi(kh)$ and weights $\phi'(kh)$ of the quadrature. This, of course, requires the a priori identification of the binomials (2.28)-(2.29) in the integrand, reducing in many cases the generality of the DE scheme.

The second problem is related to the numerical underflow and overflow due to the denominator of the weights in (2.27), as well as in binomials (2.28)-(2.29). Constraints imposed in order to avoid the numerical underflow and overflow, when working in the double precision format, lead to the following parametrization [63]:

$$n = 6 \cdot 2^M, \quad (2.30)$$

$$h = \frac{1}{2^M} \quad (2.31)$$

where $M = 1, 2, 3, \dots$ is so-called level of the quadrature.

Two strategies of programming the DE quadrature are suggested in [63]. The first one is the general purpose scheme. It is based on truncating the series of weights and abscissas at the point x_k ($k > 0$), for which the following inequality holds: $1 - x_k < \text{eps}$, ensuring that $1 - x$ and $1 + x$ are never equal to zero. Here $\text{eps} = 2^{-52}$ is the machine precision accuracy in double-precision arithmetics. The final truncated number of points is equal to $N = 2k + 1$. The second strategy calls for a priori identification of the binomials Ξ and H , which, as already commented above, reduces the generality of such a scheme. However, in the class of problems where it is easy to identify these binomials (as in the case of the branch-point singularity problem for SIs), this scheme guarantees a much higher accuracy. In addition to the weights, the binomials Ξ and H have to be precomputed and stored. We do not truncate the series, and therefore the actual number of the integration points is $N = 2n + 1 = 2 \cdot (6 \cdot 2^M) + 1$.

Application of the DE transformation for the first part of the Sommerfeld integrals

As already discussed in this chapter, if we want to perform the integration of the Sommerfeld integral along the real axis, the singularities must be first extracted. Then, the first part of the Sommerfeld integral (2.7) can be written as:

$$I_n = \int_0^a (\tilde{G}(k_\rho; z|z') - f_{\text{sing}}) J_n(k_\rho \rho) k_\rho dk_\rho \quad (2.32)$$

where f_{sing} defined in (2.15) is a function used to annihilate the singular behavior of the spectral-domain Green's function in the proximity of the surface-wave poles.

After the removal of the pole singularities, the remaining spectral function $\tilde{G}(k_\rho; z|z') - f_{\text{sing}}$ exhibits a smooth behavior, except at the branch point $k_\rho = k$, where it poses an infinite derivative. This is due to the presence of the following term:

$$\sqrt{k^2 - k_\rho^2} \quad (2.33)$$

in the spectral-domain Green's function. Since this problematic behavior is related to the wavenumber of the open half-space of the structure under consideration k , we suggest to decompose the integral (2.32) into two parts:

$$I_n = I_{n,1} + I_{n,2} = \int_0^k (\tilde{G}(k_\rho; z|z') - f_{\text{sing}}) J_n(k_\rho \rho) k_\rho dk_\rho + \int_k^a (\tilde{G}(k_\rho; z|z') - f_{\text{sing}}) J_n(k_\rho \rho) k_\rho dk_\rho. \quad (2.34)$$

Since the integrals $I_{n,1}$ and $I_{n,2}$ possess the endpoint singularities, they can be efficiently evaluated using the double exponential quadrature formulas. Moreover, the singularity is due to the term (2.33), which can be written in a more suitable form:

$$\sqrt{k^2 - k_\rho^2} = \sqrt{(k - k_\rho) \cdot (k + k_\rho)} = k \cdot \sqrt{\left(1 - \frac{k_\rho}{k}\right) \left(1 + \frac{k_\rho}{k}\right)} \stackrel{x = \frac{k_\rho}{k}}{=} k \cdot \underbrace{\sqrt{(1-x)(1+x)}}_{H \quad \Xi} \quad (2.35)$$

allowing easy identification of the binomials Ξ and H . Therefore, as our target is to evaluate the integrals $I_{n,1}$ and $I_{n,2}$ with the highest possible precision, the second implementation strategy of the DE quadrature should be used.

2.4.3 Numerical results

Here we present various numerical results, in order to demonstrate the validity and efficiency of the above described approach for the evaluation of the first part of the Sommerfeld integral along the real axis using the pole extraction [54] and DE transformation methods.

2.4.3.1 Example with analytical solution

First we consider the integral obtained from the well-known Sommerfeld identity and for which an analytic solution exists. The Sommerfeld identity is given as:

$$\int_0^\infty \frac{e^{-jk_z|z|}}{jk_z} J_0(k_\rho \rho) k_\rho dk_\rho = \frac{e^{-jkr}}{r} \quad (2.36)$$

where $r = \sqrt{\rho^2 + z^2}$ and $k_z = \sqrt{k^2 - k_\rho^2}$. The square root defining k_z is to be taken with negative imaginary part, in order to satisfy the radiation condition. In the case $z = 0$, the integrand in (2.36) is purely imaginary for $k_\rho < k$, and purely real for $k_\rho > k$. Therefore, the value of the integral over the interval $(0, k)$ corresponds to the imaginary part of the right-hand side term in (2.36), i.e.,:

$$\int_0^k \frac{1}{\sqrt{k^2 - k_\rho^2}} J_0(k_\rho \rho) k_\rho dk_\rho = \frac{\sin(k\rho)}{\rho}. \quad (2.37)$$

The integrand in (2.37) does not possess any surface-wave pole singularities, and we should take care only of its problematic behavior at the branch point $k_\rho = k$.

First we shall show the strategy for evaluating this integral using DE quadrature formulas. Introducing the transformation

$$x = \frac{k_\rho}{k} \quad (2.38)$$

the above integral can be written in the following form:

$$\int_0^1 \frac{1}{k\sqrt{(1-x)(1+x)}} J_0(k\rho x) k^2 x dx. \quad (2.39)$$

Now, in order to map the integration interval from $(0, 1)$ into $(-1, 1)$ we introduce another change of variables:

$$x = \frac{y+1}{2} \quad \Rightarrow \quad 1-x = \frac{1-y}{2} \quad (2.40)$$

$$1+x = \frac{3+y}{2} \quad (2.41)$$

that leads us to the final form of the integral:

$$\int_{-1}^1 \frac{1}{\underbrace{\sqrt{(3+y)(1-y)}}_H} \cdot J_0\left(\frac{k}{2} \underbrace{\rho(y+1)}_\Xi\right) \cdot \frac{k^2}{4} \underbrace{(y+1)}_\Xi dy \quad (2.42)$$

which is very convenient for application of the DE quadrature. Furthermore, since the binomials H and Ξ are easily identified in the integrand, and our target is to compute the

integral (2.42) with the highest possible accuracy, the second implementation strategy for the DE quadrature is selected.

The integral (2.37) is also evaluated with the help of the variable transformation (2.18), which transforms it into the following finite integral with a smooth integrand:

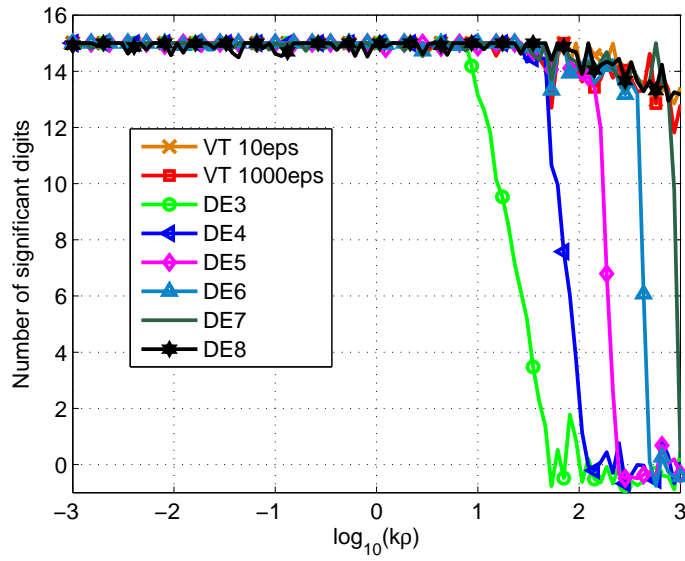
$$\int_0^{\frac{\pi}{2}} J_0(k\rho \cos t) k \cos t dt \quad (2.43)$$

that can be efficiently evaluated using the adaptive quadrature based on Patterson's formulas. As stopping criteria for the adaptive quadrature, two levels of error have been tested: 10eps and 1000eps. The first level of error is selected to test the performance of this approach when we want to obtain results with the highest possible precision. However, in many practical situation we can relax this condition, and we want to test its effect on the computational time.

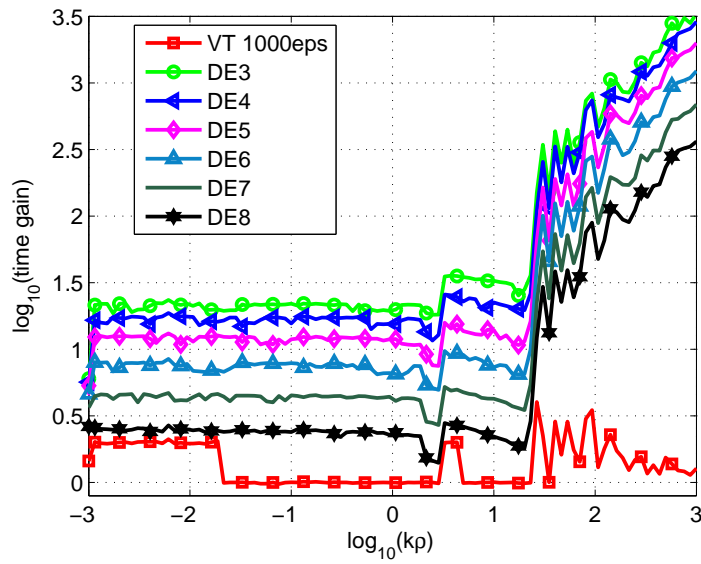
The number of significant digits of the obtained results, when the integral (2.37) is evaluated with the help of the above described approaches, versus the normalized horizontal distance between the source and observation points, $k\rho$, is shown in Fig. 2.6(a). One can see that the change of variable (2.18) together with the adaptive Patterson quadrature leads to very accurate results for all values of ρ considered. In the case that the DE quadrature is used to compute the integral (2.37), the required level M of quadrature depends directly on the horizontal distance between the source and observation points, ρ . For small values of ρ , already level $M = 3$ gives a result with 15 digits precision, which is considered to be the exact result in double arithmetics. For higher values of ρ , to reach this precision, higher quadrature levels must be used.

Now we want to compare the above described different approaches in terms of computational times. Time needed for the evaluation of the integral (2.37) employing change of variables (2.18) and setting the error of 10eps as the stopping criterion for the adaptive Patterson quadrature is used as a reference computational time, T_R . The time T needed to evaluate the integral using other discussed approaches is compared with the reference time, and the time gain, computed as $\log_{10}(T_R/T)$, is depicted in Fig. 2.6(b). One can see that for all the distances studied, the DE quadrature formulas significantly reduce the computational time, when compared with the time needed using the traditional change of variable (2.18) together with the adaptive Patterson quadrature. More precisely, for small values of ρ the computational time is reduced approximately 15 times, while for larger values of ρ , the time reduction is even more impressive. For example, for $k\rho = 10^3$ the computational time is reduced more than 300 times.

Indeed, the number of the integration points of the DE quadrature (for the second implementation approach that we use) is directly determined by its level M , and is given as $N = 2n + 1 = 2 \cdot (6 \cdot 2^M) + 1$. Moreover, as can be seen from Fig. 2.6(a), the larger the



(a) Number of significant digits.



(b) Time gain.

Figure 2.6: Performance of the real-axis integration combined with the variable transformation (VT) (2.18) and the DE quadrature for different levels of quadrature M when evaluating the integral (2.37).

distance between the source and observation points ρ , the higher level of quadrature is needed in order to obtain numerically accurate results. This calls for higher number of integration points, and consequently for higher computational time. Note that if the level of the DE quadrature is increased by 1, the number of integration points N increases approximately 2 times. However, since the associated weights and abscissas can be precomputed, the increment in computational time is lower than 2. In the case of adaptive quadrature based on Patterson's formulas, the computational time growth is significant as ρ increases, especially in the case of $\log_{10}(k\rho) > 1$, due to the highly oscillating behavior of the Bessel function. Therefore, for the large values of ρ , method based on the DE quadrature results in the tremendous reduction of computational time, as one can observe in Fig. 2.6(b).

2.4.3.2 Examples without analytical solution

Now, in order to further demonstrate the superior performance of our DE quadrature based approach for the real-axis integration of (2.7) over the two commonly used methods, namely the half-sine contour integration method and the real-axis integration method combined with the change of variables (2.18)-(2.19), we proceed with several representative numerical experiments. In all the examples we focus on the case when the source and the observation planes coincide, i.e., $z = 0$. The upper limit of the integration interval in (2.7) is $\xi_0 = a + \frac{\pi}{\rho}$, where a is given in (2.12).

For the half-sine contour integration approach, the integral is decomposed into two sub-intervals, $(0, a)$ and (a, ξ_0) . In the region $(0, a)$ the integration path is deformed into the first quadrant of the k_ρ -plane to circle around the pole and branch-point singularities, while the integration over (a, ξ_0) is performed along the real axis. Both integrals are evaluated using the adaptive quadrature based on Patterson's formulas [56]. Details related to this approach have been already discussed in Section 2.4.1.

For the real-axis integration of (2.7), the singular behavior of the integrand in the proximity of surface-wave poles (if they exist) is first extracted. The integral is then split into two parts, $(0, k)$ and (k, ξ_0) . The integrals are evaluated using two methods. For canceling the infinite derivative of the integrand at the branch point, the first method uses the traditional change of variable (2.18) and (2.19) over $(0, k)$ and (k, ξ_0) , respectively. The transformed integrals are then evaluated with the help of the adaptive quadrature based on Patterson's formulas. The second method uses the new DE quadrature for evaluating integrals over $(0, k)$ and (k, ξ_0) . Moreover, as our target is to evaluate integrals with the highest possible precision we select the second implementation strategy.

All obtained results are compared in terms of accuracy and computational cost.

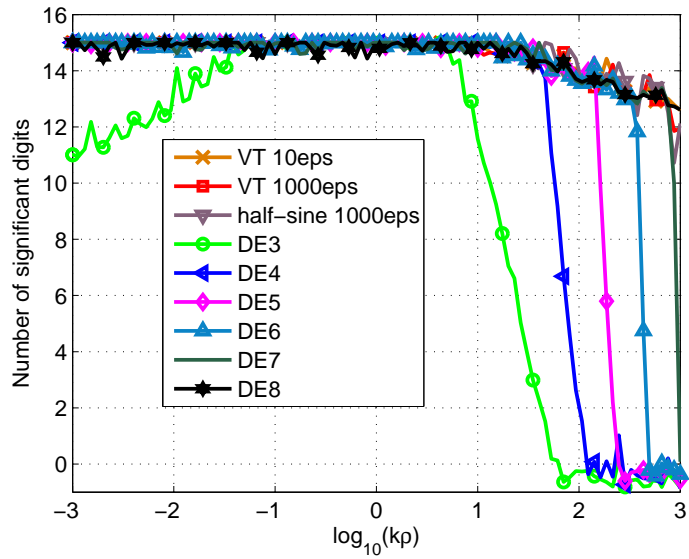
The first example: Sommerfeld identity

As the first example we consider the following integral:

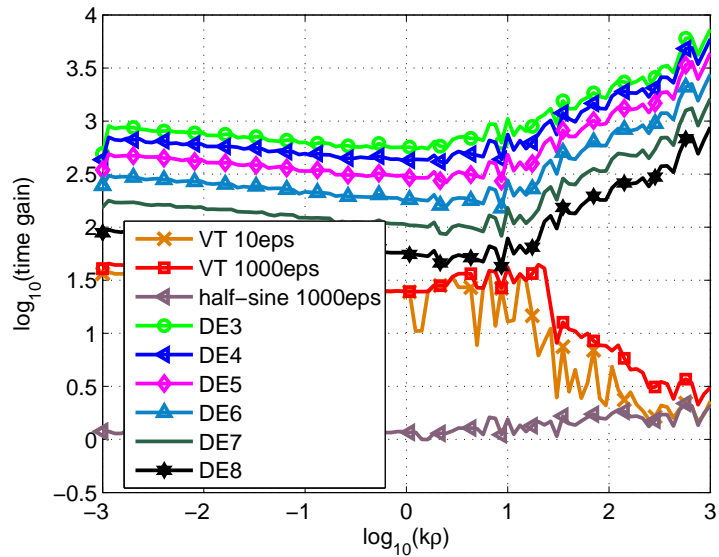
$$\int_0^{\xi_0} \frac{e^{-jk_z|z|}}{jk_z} J_0(k_\rho \rho) k_\rho dk_\rho, \quad (2.44)$$

based on the Sommerfeld identity (2.36). Analytical solution for this integral does not exist. Therefore, we compute it following the half-sine contour approach using the adaptive quadrature based on Patterson's formulas [56] and setting as stopping criterion the accuracy of 10eps in order to obtain a result with the highest possible accuracy. This result, I_R , is used as a reference. The time needed to evaluate the integral in this way is used as a reference time, T_R . Since in many practical applications it is possible to evaluate this integral with relaxed error constrains, we have performed a numerical experiment setting the accuracy of 1000eps as the termination criterion for the adaptive Patterson quadrature, in order to examine its influence on the accuracy and computational cost of the final result. The integral is also evaluated along the real axis employing the change of variable (2.18)-(2.19) (again with two levels of tolerances tested: 10eps and 1000eps), as well as with the help of the DE quadrature formulas. For each of the described approaches, the obtained value of the integral I and the computational time T are compared with the reference results. The number of significant digits, evaluated as $-\log_{10} |(I - I_R)/I_R|$, is represented in Fig. 2.7(a). To account for possible uncertainties in the reference solution and for the incidental presence of error propagation effects, we cautiously assume a result to be numerically exact if its relative error is lower than 10^{-15} with respect to the reference results. The time gain, evaluated as $\log_{10}(T_R/T)$, is plotted in Fig. 2.7(b).

It can be seen that in the case of evaluating the integral using the half-sine contour approach, as well as using the real-axis integration combined with the change of variables (2.18)-(2.19), highly accurate results are obtained for all considered values of ρ . For the DE quadrature formulas, highly accurate results are obtained as well, but the required level of quadrature directly depends on the source-observer distance ρ : the larger the distance, the higher the level of the quadrature is needed, which consequently leads to higher computational time. Although the DE formulas significantly reduce the computational time for all the values of ρ , the highest reduction is obtained for large values of ρ , when compared to the other two approaches. For example, for $\log_{10}(k\rho) = 3$, a DE quadrature of order 8 is needed to obtain numerically accurate result, and the time reduction, compared to the half-sine approach integration, is about 1000 times. The real-axis integration combined with a change of variables also leads to the time reduction when compared with the half-sine contour approach, especially for small values of ρ . Nevertheless, the DE quadrature is computationally the most efficient method for all the considered values of the source-observer distances ρ , as can be seen in Fig. 2.7(b).



(a) Number of significant digits .



(b) Time ratio.

Figure 2.7: Performance of half-sine contour approach combined with the adaptive quadrature based on Patterson's formulas and the real-axis approach combined with the variable transformation (VT) (2.18)-(2.19) and with the DE quadrature formulas, for evaluation of the first part of the Sommerfeld identity (2.44), when $z = 0$.

The second example: ρ -derivative of the Sommerfeld identity

As the second example that we study:

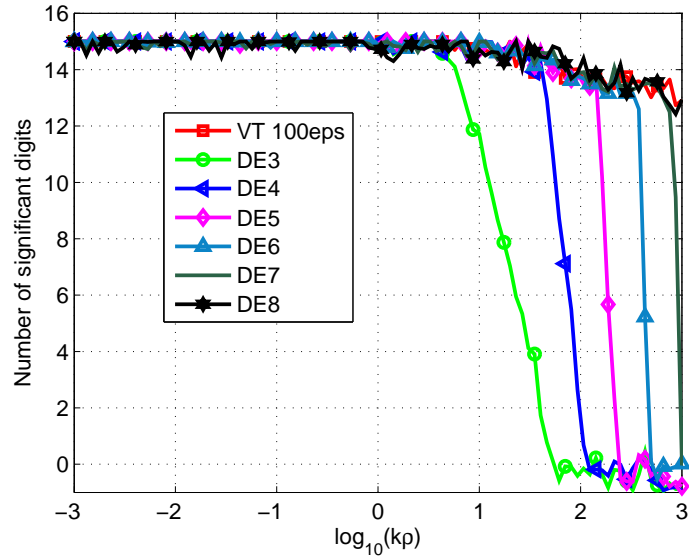
$$\int_0^{\xi_0} \frac{e^{-jk_z|z|}}{jk_z} J_1(k_\rho \rho) k_\rho^2 dk_\rho \quad (2.45)$$

that is based on the ρ derivative of the Sommerfeld identity:

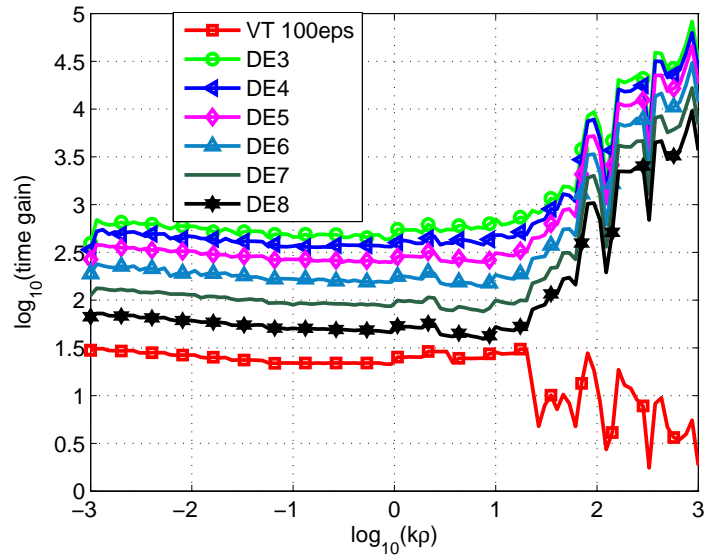
$$\int_0^\infty \frac{e^{-jk_z|z|}}{jk_z} J_1(k_\rho \rho) k_\rho^2 dk_\rho = (1 + jkr) \frac{\rho e^{-jkr}}{r^3} \quad (2.46)$$

Again, the value of the integral obtained following the half-sine contour path integration approach is used as the reference, I_R . As the terminating criterion for the adaptive quadrature based on Patterson's formulas, the tolerance of 100eps is set, because the lower tolerance (10 eps) required more than 10^{25} intervals to converge, which is unacceptable in terms of the computational cost. The integral is also evaluated along the real axis, using two other approaches. For each of them, the obtained value of the integral I and computational time T are compared with the reference results. The number of significant digits of the relative error and the relative computational time are shown in Fig. 2.8. By using the real-axis integration combined with the change of variables (2.18)-(2.19), the computational time is reduced when compared with the half-sine contour integration. The reduction is higher (up to 30 times) for lower values of ρ , while for the higher values of ρ the time is reduced only 2-3 times. In the case of evaluating the integrals using the DE quadrature approach one can see that, again, the level of quadrature that must be used depends on the value of ρ : the larger the distance ρ the higher the value of the quadrature level is needed.

Once the appropriate level is chosen, highly accurate results are obtained. The time gain is significant for all the values of ρ considered. As in all previous examples, the larger the ρ , the higher is the computational time gain. For the largest value of ρ considered ($\rho = 10^3/k$) the computational time is reduced more than 300 times.



(a) Number of significant digits .



(b) Time ratio.

Figure 2.8: Performance of the half-sine contour approach combined with the adaptive quadrature based on Patterson's formulas and the real-axis approach combined with the variable transformation (VT) (2.18)-(2.19) and with the DE quadrature formulas, for evaluation of the first part of the Sommerfeld identity (2.44), when $z = 0$.

The third example: three-layers geometry

After the examples developed from the Sommerfeld identity, which possess only the branch-point singularity, it is time to demonstrate the efficiency of the proposed technique when applied to an integral with surface-wave pole singularities.

For that purpose, we study the geometry consisting of a single-layer substrate of relative permittivity $\varepsilon_r = 4$ and thickness $d = \lambda$, backed by a perfect electric conductor (PEC). A horizontal electric dipole (HED) is at the interface and the frequency is 8 GHz. We focus on the integral arising in the evaluation of the component G_{xx}^A of the vector potential dyadic Green's function. The spectral-domain Green's function has three poles:

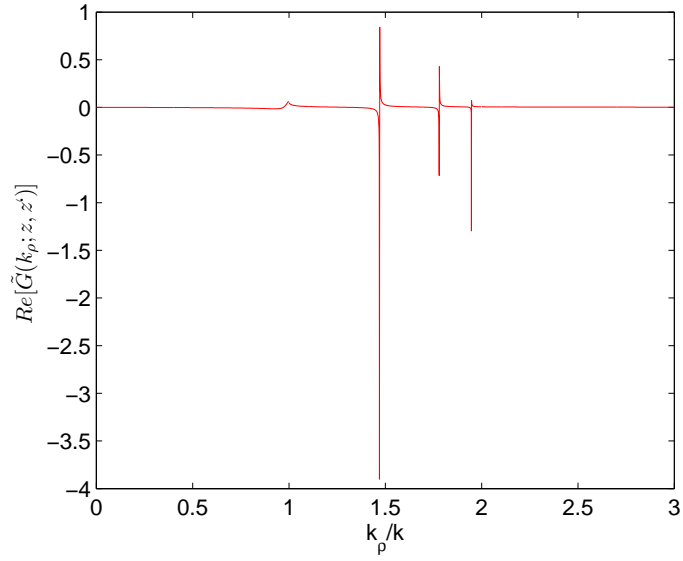
$$P_1 = 1.47017648882187 \cdot k, \quad R_1 = 0.11554707906619 \quad (2.47)$$

$$P_2 = 1.78036944337168 \cdot k, \quad R_2 = 0.04462885274180 \quad (2.48)$$

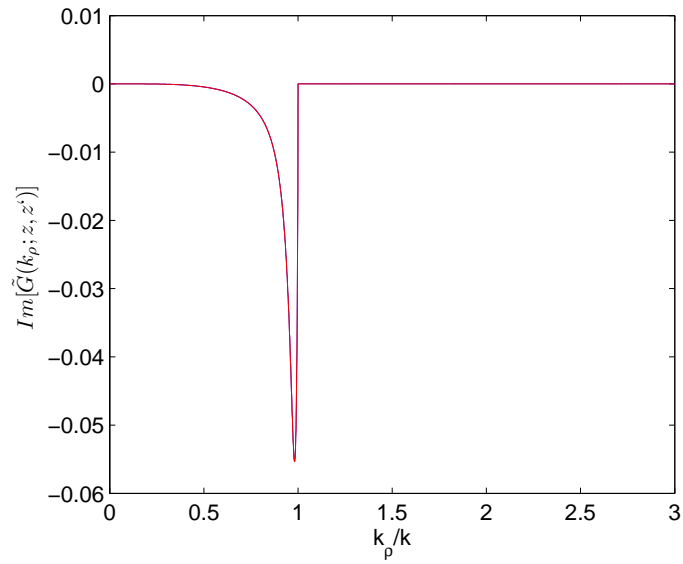
$$P_3 = 1.94704764513553 \cdot k, \quad R_3 = 0.01039239585919 \quad (2.49)$$

which are detected using the pole extractor from [54]. Here P_i and R_i , $i = 1, 2, 3$, are positions and residues of the poles.

Fig. 2.9 shows the original spectral-domain GF, $\tilde{G}(k_\rho; z|z')$. The modified spectral-domain GF, $\tilde{G}(k_\rho; z|z') - f_{\text{sing}}$, after subtracting the poles is depicted in Fig. 2.10. There we can see that the poles are completely removed and the remaining function is smooth everywhere, except at the branch point $k_\rho = k$ where it possesses an infinite derivative. We evaluate the spatial domain counterpart of the original spectral-domain GF in the following way. The Sommerfeld integral of the modified GF is evaluated along the real axis, by splitting the integral into three parts: $(0, k)$, (k, ξ_0) and (ξ_0, ∞) . In the first two regions, the DE quadrature is used, because of the infinite derivative of the integrand at the endpoints of the integration interval. The remaining integral over the region (ξ_0, ∞) is evaluated to the machine precision accuracy, using the integration-then-summation technique combined with the weighted averages extrapolation method, which will be discussed in detail later in this chapter. The spatial domain GF is also evaluated by integrating the original spectral-domain GF along the real-axis path partially deformed into the first quadrant of k_ρ -plane and the so obtained value is used as a reference value. The integral is split into three parts: $(0, a)$, (a, ξ_0) and (ξ_0, ∞) . The integral over the first interval is performed along the half-sine contour path, while the second part is integrated along the real axis. The remaining third part is evaluated in the same way as in the case of the real-axis integration. The results obtained using the two approaches are compared. The number of significant digits of the relative error and the time gain are depicted in Fig. 2.11. One can see that an excellent agreement between the results obtained following both approaches is acquired, while the real-axis approach combined with the pole extractor and the DE quadrature results in significant reduction of the computational time. Note that for large values of ρ , the surface-wave poles have the dominant contribution (Fig. 2.12). However, this is only the case for strictly lossless structures. For a nonzero loss tangent, the poles are

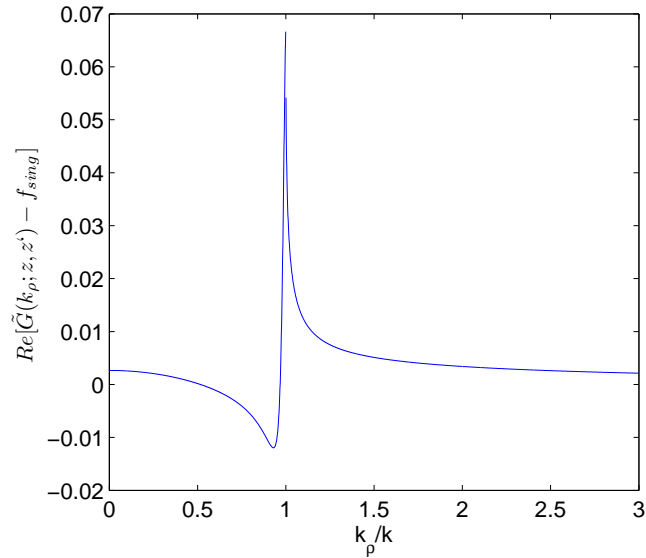


(a) Real part.

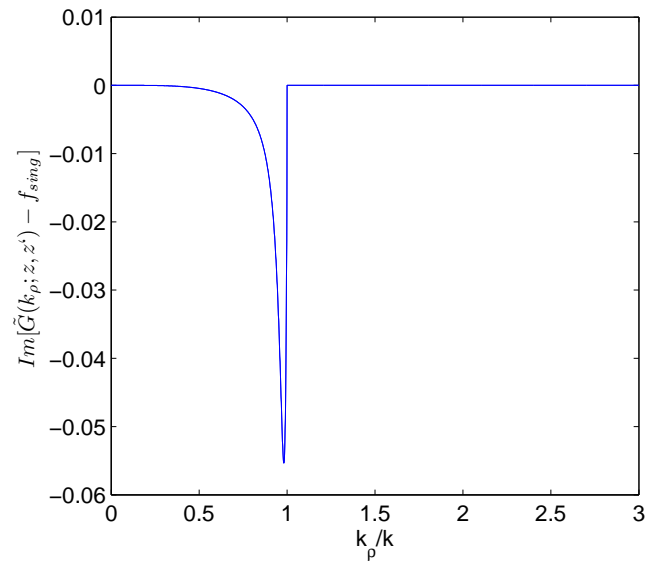


(b) Imaginary part.

Figure 2.9: The original spectral-domain component G_A^{xx} of the vector potential dyadic Green's function for the single-layer substrate of permittivity $\varepsilon_r = 4$ and thickness $d = \lambda$ at 8 GHz.

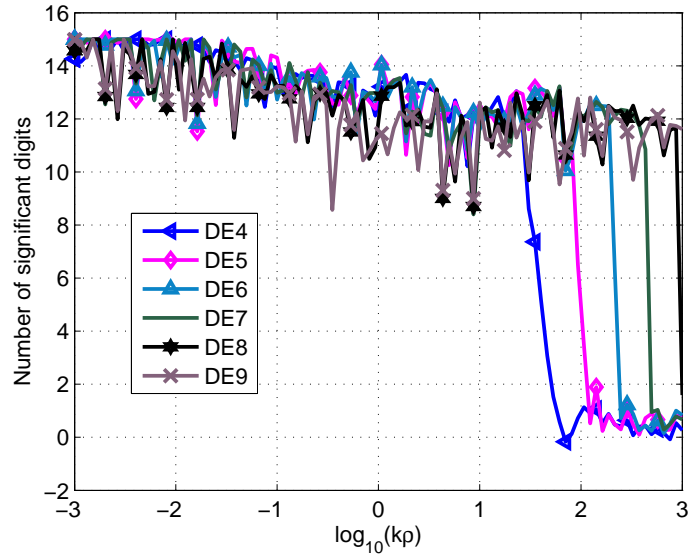


(a) Real part.

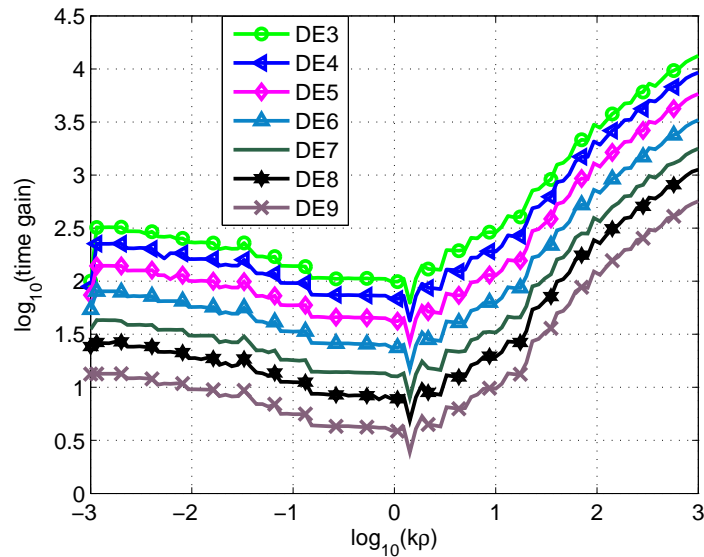


(b) Imaginary part.

Figure 2.10: The modified spectral-domain component G_A^{xx} of the vector potential dyadic Green's function for the single-layer substrate of permittivity $\varepsilon_r = 4$ and thickness $d = \lambda$ at 8 GHz, obtained by annihilating the singular behavior in the proximity of surface-wave poles.



(a) Number of significant digits.



(b) Time ratio.

Figure 2.11: Performance of the real-axis and half-sine contour integration for component G_{xx}^A of the vector potential dyadic Green's function for a single-layer substrate: $\epsilon_r = 4$, $d = \lambda$, $f = 8\text{GHz}$, backed by perfect electric conductor (PEC). Horizontal electric dipole (HED) is at the interface.

located in the fourth quadrant of the complex k_ρ -plane, introducing a small exponential decay in the Hankel function, which results in the domination of the surface-wave poles only up to a certain distance, after which the numerically evaluated term takes over [64].

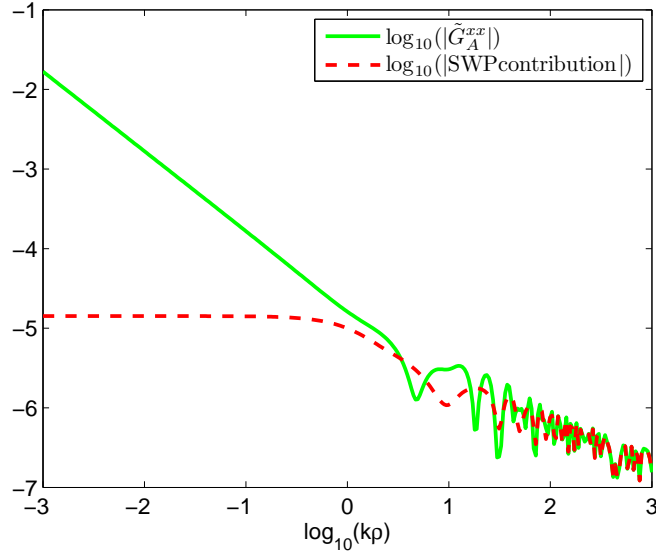


Figure 2.12: Magnitude of the component G_{xx}^A of the vector potential dyadic Green's function and surface-wave pole (SWP) contribution for a single-layer substrate: $\varepsilon_r = 4$, $d = \lambda$, $f = 8\text{GHz}$, backed by perfect electric conductor (PEC). HED is at the interface.

Conclusion on numerical results

To conclude, in all the examples studied, an excellent agreement is observed between the results obtained following the newly proposed method (a real-axis integration, combined with the DE quadrature formulas and the pole extraction technique), and the methods traditionally used for the evaluation of (2.7). Moreover, the new approach significantly reduces the computational time and is valid for both small and large values of the source-observer distances ρ . The level of the quadrature that should be used directly depends on the distance ρ : the larger is ρ , the higher is the required level of the quadrature. Not only is the proposed technique very accurate and efficient, but it is also very easy to implement, since the weights and abscissas of the DE quadrature can be precomputed and the pole extractor can be embedded in a completely automatic way into the routines for the numerical evaluation of the SIs. Finally, the computational time only slightly increases, with the frequency and thickness of the substrate (when the number of poles can be large) and for the large values of the source-observer distances.

2.5 Sommerfeld integral tail

The part of the integral that remains to be solved is the so-called Sommerfeld integral tail:

$$T_n = \int_{\xi_0}^{\infty} \tilde{G}(k_\rho; z|z') J_n(k_\rho \rho) k_\rho dk_\rho. \quad (2.50)$$

Although it is free of singularities, this integral is difficult to evaluate since the integration interval extends to infinity and the integrand is oscillating and slowly converging, or even diverging. More precisely, if the source and observer are at different levels with respect to the stratified medium interface, i.e., $z \neq z'$, the integral (2.50) is defined in the traditional Riemann sense, since due to (2.4) its integrand converges exponentially at infinity. However, for $z = z'$ there is no exponential decrease to guarantee convergence. Indeed, if the asymptotic behavior of the spectral-domain GF (2.4) is given by a power $\mu \leq 0.5$, the integrand in (2.50) does not converge, and the integral is not defined in the Riemann sense. In these cases, a physical meaning can still be assigned to the integral T_n defining it in the Abel sense, i.e., considering the improper Sommerfeld integral as a limiting case when the observer's level tends towards the source's level [65, 66]:

$$T_n|_{z=z'} = \lim_{z \rightarrow z'} T_n|_{z \neq z'}. \quad (2.51)$$

The Abel definition of convergence for improper integrals is a concept derived from the definition of “Abel’s summability” for infinite divergent series and has a fully rigorous mathematical interpretation [67]. However, any electrical engineer can understand “Abel’s summability” in a very intuitive way, relating it to our understanding of electromagnetic phenomena arising in lossless media. A lossless medium is an ideal abstraction, exhibiting a pure imaginary propagation constant. Its direct mathematical treatment involves frequently some difficulties. But the lossless situation can be always viewed as the limiting case of a physical lossy medium, with a complex propagation constant, when the losses vanish. Using the Abel’s definition, it is easy to obtain results for improper integrals that have no meaning in the Riemann sense.

Obviously, it is possible to directly discretize the Abel limiting process of the SI tail (2.50). Within this strategy, a series of values of the integral T_n is numerically computed for some small values of $|z - z'|$ and an extrapolation is made to obtain the value of the integral for $|z - z'| = 0$. However, usually this approach is not very efficient. An extrapolation towards zero is only accurate when made from situations corresponding to very small values of $|z - z'|$. Yet, integrals with very small values of $|z - z'|$ are hard to evaluate numerically. What is needed here is a numerical method that can deal directly with the case $z = z'$ and obtain Abel’s values as the result of a simple arithmetic process. This was the historical goal of specially tailored techniques for the numerical evaluation of SIs.

The proven and most popular approach for numerical evaluation of the SI tails is the integration-then-summation procedure, in which the integral is calculated as an infinite sum of series of partial integrals over finite subintervals, i.e.,

$$T_n = \sum_{i=0}^{\infty} u_{n_i} = \sum_{i=0}^{\infty} \int_{\xi_i}^{\xi_{i+1}} \tilde{G}(k_\rho; z|z') J_n(k_\rho \rho) k_\rho dk_\rho. \quad (2.52)$$

Possible choices of break points ξ_i include asymptotic half-periods, exact zero crossings and extrema of Bessel functions. The conventional approach for evaluating this infinite series consists of finding the limit of the sequence of partial sums:

$$T_n = \lim_{N \rightarrow \infty} T_{n_N} = \lim_{N \rightarrow \infty} \sum_{i=0}^N u_{n_i}. \quad (2.53)$$

Since this sequence converges extremely slowly, i.e., the remainders $r_N = T_{n_N} - T_n$ do not decay rapidly as $N \rightarrow \infty$, in order to achieve high accuracy via direct sum, we need to evaluate an extremely large number of partial integrals, u_{n_i} . One way to tackle the aforementioned deficiency and accelerate the convergence of the sequence $\{T_{n_N}\}$ is by the means of a transformation (linear or nonlinear) from the original sequence $\{T_{n_N}\}$ to a new sequence $\{T'_{n_N}\}$ with rapidly decaying remainders r'_N . These sequence transformations, also referred to as extrapolation methods [26], allow us to infer the limit value in (2.53) by calculating just a few partial integrals u_{n_i} . Among numerous extrapolation techniques, the WA method was shown to be one of the most versatile and efficient ones when dealing with SI tails [26].

2.5.1 Weighted averages method

The weighted averages method is a more sophisticated version of the Euler transformation, which uses the weighted means of consecutive partial sums:

$$T'_{n_N} = \frac{W_N T_{n_N} + W_{N+1} T_{n_{N+1}}}{W_N + W_{N+1}}. \quad (2.54)$$

Since $T'_{n_N} = T_n + r'_N$, the above formula can be written as

$$T'_{n_N} = T_n + \underbrace{\frac{W_N r_N + W_{N+1} r_{N+1}}{W_N + W_{N+1}}}_{r'_N}. \quad (2.55)$$

Obviously, the optimal solution would come from the annihilation of the remainders r'_N of the linearly transformed sequence by imposing an appropriate ratio of the weights,

$$\eta = \frac{W_{N+1}}{W_N} = -\frac{r_N}{r_{N+1}}. \quad (2.56)$$

At this point, the weighted-averages method could be considered complete if the remainders r_N were explicitly known, which is, unfortunately, not the case for the sequences of our interest. Instead, we adopt the following modal sequence

$$T_{n_N} \sim T_n + \underbrace{\omega_N \sum_{i=0}^{\infty} a_i \xi_N^{-i}}_{r_N}, \quad N \rightarrow \infty \quad (2.57)$$

based on the asymptotic expansion of the remainders. Here ω_N are the associated remainder estimates, which can accommodate explicitly the structural information on the N -dependence of r_N , i.e., the behavior of the dominant term of the remainder for large values of N . Now, the ratio of the remainders is

$$\frac{r_N}{r_{N+1}} = \frac{\omega_N}{\omega_{N+1}} [1 + O(\xi_N^{-2})], \quad N \rightarrow \infty \quad (2.58)$$

which suggests that we choose

$$\eta = -\frac{\omega_N}{\omega_{N+1}}. \quad (2.59)$$

Then, if

$$1 + \eta = O(\xi_N^{-\sigma}) \quad (2.60)$$

the ratio of the remainders for the original and transformed sequence becomes

$$\frac{|r'_N|}{|r_N|} \sim O(\xi_N^{-p}) \quad (2.61)$$

where $p = 2 - \sigma$, clearly showing the acceleration property of the aforementioned transformation, when $\sigma < 2$. The remainders of the sequence after the transformation have the same form as the original ones together with a scaling factor ξ_N^{-p} . Finally, the incorporation of the above weights to the weighted-averages transformation (2.54) leads to the following recursive scheme:

$$T_{n_N}^{(l+1)} = \frac{T_{n_N}^{(l)} + \eta_N^{(l)} T_{n_N}^{(l)}}{1 + \eta_N^{(l)}}, \quad N, l \geq 0 \quad (2.62)$$

with

$$\eta_N^{(l)} = -\frac{\omega_N}{\omega_{N+1}} \left(\frac{\xi_{N+1}}{\xi_N} \right)^{pl} \quad (2.63)$$

or the asymptotic form

$$\eta_N^{(l)} \approx -\frac{\omega_N}{\omega_{N+1}} \left(1 + pl \frac{q_N}{\xi_N} \right) \quad (2.64)$$

where $q_N = \xi_{N+1} - \xi_N$.

The recursion (2.62) can be represented by a triangular scheme

$$\begin{array}{ccccccc}
 T_{n_0}^{(0)} & T_{n_0}^{(1)} & \dots\dots\dots & T_{n_0}^{(l)} & & & \\
 T_{n_1}^{(0)} & T_{n_1}^{(1)} & \dots & T_{n_1}^{(l-1)} & & & \\
 T_{n_2}^{(0)} & \dots & T_{n_2}^{(l-2)} & & & & \\
 \vdots & \ddots & & & & & \\
 T_{n_l}^{(0)} & & & & & &
 \end{array} \tag{2.65}$$

where in the first column $T_{n_N}^{(0)} = T_{n_N}$ and $T_{n_0}^{(l)}$ is the best approximation of T_n , given the partial sums T_{n_0}, \dots, T_{n_l} . This recursion, together with the coefficients $\eta_N^{(l)}$, is a linear transformation, known as the weighted averages (WA) method.

The remaining point is to develop explicit analytical expressions for the remainder estimates ω_N , based on the asymptotic form of the spectral-domain Green’s function (2.4). In [26], by taking equidistant break points separated by the asymptotic half-period of the Bessel function, $q = \pi/\rho$, the following remainder estimates are obtained:

$$\omega_N = (-1)^{N+1} e^{-Nq|z-z'|} \cdot \xi_N^\alpha \tag{2.66}$$

for $\rho > 0$, where $\alpha = 0.5 - \mu$ and exponent μ can be easily determined by inspection of the relevant expressions for spectral-domain GFs [8, 22]. The series of thus obtained partial integrals (2.52) is asymptotically alternating. Moreover, the convergence is linear for $|z - z'| > 0$, and logarithmic for $|z - z'| = 0$. In the special case when $\rho = 0$, the interval length of partial integrals must be chosen based on the exponential behavior of $\tilde{G}(k_\rho; z|z')$ (2.4) rather than oscillations of the Bessel function, and the value $q = \pi/|z - z'|$ is suggested [26]. The convergence of the series of partial integrals (2.52) is, in this case, linear monotone and the remained estimates are given by

$$\omega_N = -e^{-Nq|z-z'|} \cdot \xi_N^\alpha. \tag{2.67}$$

Using these analytical remainder estimates in (2.60), we find that $\sigma = 0$, i.e., $p = 2$. Furthermore, replacing ω_N in (2.63) - (2.64) by (2.66) - (2.67) we obtain the following final expressions for the weights:

$$\eta_N^{(l)} = \pm e^{q\zeta} \left(\frac{\xi_{N+1}}{\xi_N} \right)^{-\alpha+pl} \tag{2.68}$$

$$\approx \pm e^{q\zeta} \left(1 + \frac{-\alpha + p \cdot l}{\beta + N} \right). \tag{2.69}$$

Here, the plus and minus sign apply to the alternating ($\rho > 0$) and linear monotone cases ($\rho = 0$), respectively, and $\beta = \xi_0/q$.

The original formulation of the WA algorithm, proposed by Mosig in the early eighties [6, 23], was essentially heuristic and based on intuitive considerations. No attempt was made to connect it to the existing mathematical knowledge and its use was solely justified a posteriori by the excellent results it usually yielded. Moreover, the attention was limited only to the alternating case ($\rho > 0$). The asymptotic expansion of the remainders was developed by applying the integration by parts, and slightly diverges from the one in (2.57). The obtained coefficients η_N^k are consequently different, but they are equivalent to those in (2.68) - (2.69) for $N \gg 1$.

In 1998, a seminal paper by Michalski [26] provided a rigorous mathematical frame for the WA, which we have recalled in this section. Since then, the WA methods have been extensively used in our community, either *per se* or as a benchmark to check the validity and accuracy of other approximated strategies for stratified media Green's functions (for instance complex images, [68]). WA is also referred to as the Mosig-Michalski transformation in the specialized literature [52].

2.5.2 New weighted averages method

As previously stated, the currently used WA algorithms are essentially more powerful versions of the Euler transformation [26], in which simple arithmetic means are replaced by weighted means. However, it is well known that the Euler transformation can be easily generalized as the Hölder means [67], acting simultaneously on N members of a given sequence, rather than on two consecutive elements each time.

The same strategy could be applied to the WA. Hence, the generalized New WA procedure will also start with a sequence of N partial integrals. But now, the best possible evaluation of the infinite integral will be obtained by performing a unique weighted average applied simultaneously to all the partial integrals.

For the sake of simplicity, let us start with the following complex integral:

$$I = \int_a^\infty f(x)e^{-\gamma x} dx \quad (2.70)$$

where

- $[a, \infty]$ is a semiinfinite interval on the real axis x ,
- γ is a complex parameter $\gamma = \alpha + j\beta$ [†] satisfying the conditions: $\alpha \geq 0$ and $|\gamma| \neq 0$,
- the function f will be considered, for the sake of simplicity, as being real-valued and behaving asymptotically as a power function $O(x^q)$; complex functions can be dealt with by considering successively their real and imaginary parts.

[†]Here, α and β must not be confused with the same symbols used in Section 2.5.1

At the end, the obtained results will be discussed in the context of Sommerfeld integral tails of our interest.

To provide a way of numerically evaluating the basic integral (2.70), we introduce partial integrals

$$I_i = \int_a^{x_i} f(x)e^{-\gamma x} dx \quad (2.71)$$

and remainders

$$I - I_i = \int_{x_i}^{\infty} f(x)e^{-\gamma x} dx \quad (2.72)$$

where the abscissas x_i are, at this level of the development, completely arbitrary.

Assume now that we have a set of N partial integrals I_i , $i = 1, 2, \dots, N$, which have been carefully evaluated by any numerical quadrature rule. The question that immediately arises is how to extrapolate, from these partial integrals I_i and by simple means, a better estimation I^* of the true value I . Similarly to the approach already employed in the original WA formulation [23], the remainders (2.72) can be approximated integrating by parts the integral (2.72). This yields an infinite-series expansion for the remainder:

$$I - I_i = e^{-\gamma x_i} \sum_{k=1}^{\infty} {}^{(k-1)}f_i \cdot \gamma^{-k} \quad (2.73)$$

where the coefficients ${}^{(k-1)}f_i$ stand for the $(k-1)$ th order derivatives: $\frac{\partial^{k-1}f}{\partial x^{k-1}}|_{x=x_i}$. Of course, for numerical purpose, this infinite series has to be truncated.

Assuming that a good estimate of the true value of the integral I can be obtained by truncating the infinite series after the first N terms:

$$I_N^* - I_i = e^{-\gamma x_i} \sum_{k=1}^{N-1} {}^{(k-1)}f_i \cdot \gamma^{-k} \quad (2.74)$$

and considering N different partial integrals I_i obtained for N different abscissas x_i , the following linear system of equations is obtained:

$$-I_i \cdot e^{\gamma x_i} = -I_N^* e^{\gamma x_i} + \sum_{k=1}^{N-1} {}^{(k-1)}f_i \cdot \gamma^{-k} \quad (2.75)$$

the N unknowns being I_N^* and $\gamma^{-1}, \gamma^{-2}, \dots, \gamma^{-N+1}$.

The determinant of the system is

$$D_N = \begin{vmatrix} -e^{\gamma x_1} & {}^{(0)}f_1 & {}^{(1)}f_1 & \dots & {}^{(N-2)}f_1 \\ -e^{\gamma x_2} & {}^{(0)}f_2 & {}^{(1)}f_2 & \dots & {}^{(N-2)}f_2 \\ \vdots & \vdots & \vdots & \ddots & \vdots \\ -e^{\gamma x_N} & {}^{(0)}f_N & {}^{(1)}f_N & \dots & {}^{(N-2)}f_N \end{vmatrix} \quad (2.76)$$

and therefore, by using Cramer's rule, we can obtain the unknown I_N^* as a quotient, the denominator being the determinant (2.76) and the numerator a related determinant obtained by replacing in (2.76) the first column's elements by $-I_i e^{\gamma x_i}$. Both determinants can be expanded by the first column and the final expression is

$$I_N^* = \frac{\sum_{i=1}^N (-1)^{i+1} M_i \cdot e^{\gamma x_i} \cdot I_i}{\sum_{i=1}^N (-1)^{i+1} M_i \cdot e^{\gamma x_i}}, \quad (2.77)$$

where M_i are the minors of the determinants obtained by deleting the first column and the i -th row. The final expression clearly shows that a good estimate of the integral can be obtained as a linear combination of weighted linear averages of the partial integrals I_i :

$$I_N^* = \frac{\sum_{i=1}^N w_i I_i}{\sum_{i=1}^N w_i}, \quad (2.78)$$

where the generalized weights w_i are given as:

$$w_i = (-1)^{i+1} M_i \cdot e^{\gamma x_i}. \quad (2.79)$$

The generalized weights

However, the expression (2.79) for the generalized weights is of little practical interest, as it involves the computation of determinants whose elements are the values of the function f and its derivatives at N points x_i . As an illustration, for the trivial case $N = 2$, the following expression is obtained from (2.77):

$$I_N^* = \frac{\frac{\exp(\gamma x_1)}{f(x_1)} I_1 - \frac{\exp(\gamma x_2)}{f(x_2)} I_2}{\frac{\exp(\gamma x_1)}{f(x_1)} - \frac{\exp(\gamma x_2)}{f(x_2)}}, \quad (2.80)$$

but for $N > 2$, it is necessary to know the law of formation of the derivatives. Moreover, computing determinants is usually a cumbersome and time-consuming task. Fortunately enough, an interesting analytical treatment is possible in some cases of interest.

It has been stated at the beginning of the development that the function $f(x)$ asymptotically behaves as a power, i.e.,:

$$\lim_{x \rightarrow \infty} [f(x) - Cx^q] = 0 \quad (2.81)$$

with C and q being some real constants, since this is true for wide class of functions $f(x)$ appearing in practical problems.

If we replace $f(x)$ by its asymptotical approximation, the minor M_i in (2.77) can be calculated as:

$$M_i = V_i \cdot C^{N-1} \left[\prod_{j=1}^{N-2} \frac{q!}{(q-j)!} \right] \cdot \left[\frac{1}{x_i} \prod_{j=1}^N x_j \right]^{q-N+2} \quad (2.82)$$

where V_i is the Vandermonde's determinant:

$$V_i = \begin{vmatrix} 1 & x_1 & x_1^2 & \dots & x_1^{N-2} \\ 1 & x_2 & x_2^2 & \dots & x_2^{N-2} \\ \vdots & \vdots & \vdots & \ddots & \vdots \\ 1 & x_{i-1} & x_{i-1}^2 & \dots & x_{i-1}^{N-2} \\ 1 & x_{i+1} & x_{i+1}^2 & \dots & x_{i+1}^{N-2} \\ \vdots & \vdots & \vdots & \ddots & \vdots \\ 1 & x_N & x_N^2 & \dots & x_N^{N-2} \end{vmatrix}. \quad (2.83)$$

These Vandermonde's determinants have a well-known analytical expression:

$$V_i = \prod_{\substack{1 \leq k < j \leq N \\ k, j \neq i}} (x_j - x_k) = \frac{\prod_{\substack{j=1 \\ k < j}}^N (x_j - x_k)}{\prod_{\substack{j=1 \\ j \neq i}}^N |x_i - x_j|}. \quad (2.84)$$

When used, the following expression for the weights, devoid of determinants, is obtained:

$$w_i = \frac{(-1)^{i+1} e^{\gamma x_i}}{x_i^{q-N+2} \prod_{\substack{j=1 \\ j \neq i}}^N |x_i - x_j|}. \quad (2.85)$$

The above expression for the weights is perhaps not yet very tractable, but it has the merit to be quite general. In particular, the abscissas x_i can have arbitrary values.

Equidistant abscissas

Much simpler expressions for the weights are obtained if some restrictions are applied to the choice of the abscissas. If their values are not conditioned by external circumstances, the obvious choice is to select equidistant abscissas such as $x_{i+1} - x_i = h$. Then, the solution of the Vandermonde's determinant is even easier:

$$V_i = \frac{(N-1)!(N-2)! \dots 2! h^{\frac{N(N-1)}{2}}}{(N-i)!(i-1)! h^{N-1}} \quad (2.86)$$

and a much more compact expression for the weights is obtained:

$$w_i = (-1)^{i+1} \binom{N-1}{i-1} e^{\gamma x_i} x_i^{N-2-q}. \quad (2.87)$$

Moreover, this form is very convenient for numerical purposes since it includes binomial coefficients which are easily computed by recursion.

In the general case, the weights w_i are complex quantities due to the terms $e^{\gamma x_i}$. However, it is possible to always use real values with the following choices. If $\beta = \text{Im}(\gamma) \neq 0$, we can always select x_i

$$\beta x_i = ik\pi + \varphi \quad (2.88)$$

where k is a fixed integer. If k is even, the difference between two successive partial estimations is an integer number of periods. The sequence I_i will approach the true value I monotonically. Since

$$e^{\gamma x_i} = e^{\alpha x_i} e^{j\varphi} \quad (2.89)$$

we can use in (2.78) the real weights

$$w_i = (-1)^{i+1} \binom{N-1}{i-1} e^{\alpha x_i} x_i^{N-2-q} \quad (2.90)$$

which alternate in sign. If k is odd, then the sequence I_i will oscillate around I . This is a numerically stable algorithm because now the weights

$$w_i = \binom{N-1}{i-1} e^{\alpha x_i} x_i^{N-2-q} \quad (2.91)$$

are always positive and the formula (2.78) is a true weighted average including only additions and multiplications by constant coefficients. In the special case when $\beta = 0$, equidistant

abscissas separated by π/α should be used, yielding the following expression for weights:

$$w_i = (-1)^{i+1} \binom{N-1}{i-1} e^{\alpha x_i} x_i^{N-2-q}. \quad (2.92)$$

Exact solutions

Note that if the function $f(x)$ is a polynomial of degree N , the derivatives of order higher than N vanish. Therefore, the infinite series in (2.73) stops after the term γ^{-N} and an extrapolation based upon $N+1$ partial integrals I_i must provide the exact solution $I^* = I$ regardless of the choice of the abscissas x_i .

Applying the New WA technique to Sommerfeld-type integrals

At the end, taking into account the asymptotic behavior of spectral-domain GFs (2.4) and Bessel function (2.5) and by careful examination of the SI tail (2.50), one can see that by setting

$$\alpha = |z - z'| \quad (2.93)$$

$$\beta = \rho \quad (2.94)$$

$$q = 0.5 - \mu \quad (2.95)$$

the integrand in (2.50) is asymptotically equivalent to the real part of the kernel involved in (2.70). Therefore, the New WA technique can be straightforwardly applied to our Sommerfeld-type integrals.

2.5.3 Double exponential-type quadrature formulas

Despite the promises of the New WA method to evaluate Sommerfeld integral tails, the quest for efficient strategies should not be stopped.

Previously in this chapter, we have discussed the DE transformation, originally introduced by Takahasi and Mori in 1974 [55] and tailored for integrals with integrable singularities at the end of the integration interval. The transformation was named after its key attribute: the double-exponential decay of the integrand after the transformation. Unfortunately, the original formula was not efficient when computing slowly decaying oscillatory functions over $(0, \infty)$. Hence, to overcome this weakness, Ooura and Mori proposed a robust DE formula for Fourier-type integrals [69]. The key idea of the new transformation was slightly different: the nodes of the new quadrature approach rapidly (double-exponentially) to the zeros of sine/cosine function, thus allowing computation of the Fourier-type integrals with a small number of function evaluations. A variant with Bessel function zeros as nodes was proposed in [70–72]. Finally, following the same idea, a very efficient tool for the evaluation

of semi-infinite integrals with Bessel function kernels, i.e., Hankel transform integrals, was suggested in [73].

Here we use the aforementioned original study by Ogata and Sugihara [73] in order to introduce the following transformation [74, 75], specifically tailored for the SI tails of our interest:

$$k_\rho \cdot \rho = \Phi(t) \quad (2.96)$$

with

$$\begin{aligned} \Phi(t) &= \frac{\pi}{h} t \cdot \tanh\left(\frac{\pi}{2} \sinh(t)\right) + b \cdot \operatorname{sech}\left(\frac{\pi}{2} \sinh(t)\right) \\ &= \Phi_1(t) + \Phi_2(t), \end{aligned} \quad (2.97)$$

where $b = \xi_0 \cdot \rho$ and h is the so-called step size that has to be chosen carefully since it directly influences the algorithm performance.

In Fig. 2.13 the behavior of the transformation $\Phi(t)$ is shown for different values of the step size h . As it can be seen, the role of the second part of the transformation (2.97), $\Phi_2(t)$, is actually to map the starting point of the integration interval from $k_\rho = \xi_0$ into $t = 0$, and its influence vanishes quickly as $t \rightarrow \infty$. The first part of the transformation, $\Phi_1(t)$, has the dominant effect for larger values of t , approaching rapidly the transformation's asymptotic behavior:

$$\Phi(t) \sim \frac{\pi}{h} |t| \quad (2.98)$$

that will be shown later to be the key attribute of the method.

Applying the aforementioned transformation to the SI tail (2.50), we obtain

$$T_n = \int_0^\infty \mathcal{F}_n(\Phi(t)) \cdot \left(\frac{d\Phi(t)}{dt}\right) dt \quad (2.99)$$

where

$$\mathcal{F}_n(t) = \frac{1}{\rho^2} t \cdot \tilde{G}\left(\frac{1}{\rho} t; z|z'\right) \cdot J_n(t). \quad (2.100)$$

Since the integrand in (2.99) is an odd function with respect to t , the integral can be written as

$$T_n = \frac{1}{2} \int_{-\infty}^\infty \operatorname{sgn}(t) \cdot \mathcal{F}_n(\Phi(t)) \cdot \left(\frac{d\Phi(t)}{dt}\right) dt \quad (2.101)$$

and approximated with the help of an appropriate quadrature formula based on the zeros of

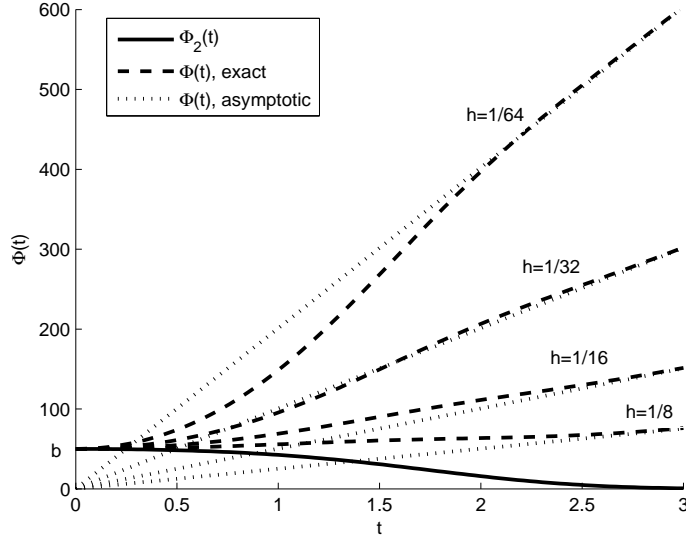


Figure 2.13: Behavior of the DE transformation for different values of step size parameter h .

Bessel functions, according to [73],

$$\begin{aligned}
 T_n \approx & h \sum_{k=1}^{\infty} w_{nk} \mathcal{F}_n\left(\Phi\left(h \frac{\xi_{nk}}{\pi}\right)\right) \Phi'\left(h \frac{\xi_{nk}}{\pi}\right) \\
 & + \frac{h}{\pi} \sum_{\lambda=0}^{n-1} c_{\lambda}^{(n)} h^{2\lambda+1} \frac{\partial^{2\lambda+1} \{\mathcal{F}_n(\Phi(t)) \Phi'(t)\}}{\partial t^{2\lambda+1}} \Big|_{t=0}
 \end{aligned} \tag{2.102}$$

where ξ_{nk} is the k -th zero of the Bessel function J_n . Also,

$$c_{\lambda}^{(n)} = \frac{\pi^{-2\lambda+1}}{(2\lambda+1)!} \sum_{m=0}^{n-\lambda-1} \frac{(n-m-1)!}{m!} 2^{n-2m} b_{n-\lambda-m-1}^{(n)} \tag{2.103}$$

and $b_m^{(n)}$, $m = 0, 1, 2, \dots$, are the coefficients of the Laurent series expansion of $1/J_n$ around the point $x = 0$:

$$\frac{1}{J_n(x)} = \sum_{m=0}^{\infty} b_m^{(n)} x^{2m-n}. \tag{2.104}$$

Moreover, the weights w_{nk} are given as follows:

$$w_{nk} = \frac{Y_n(\xi_{nk})}{J_{n+1}(\xi_{nk})} = \frac{2}{\pi \xi_{nk} J_{n+1}^2(\xi_{nk})}. \tag{2.105}$$

Finally, after some algebraic manipulations, we derive the DE-type quadrature formulas for the SI tails (2.50). In particular, for the two most used indexes $n = 0, 1$ of the Bessel functions, we get

$$T_0 \approx h \sum_{k=1}^N w_{0k} \mathcal{F}_0(\Phi(h \frac{\xi_{0k}}{\pi})) \Phi'(h \frac{\xi_{0k}}{\pi}) \quad (2.106)$$

and

$$T_1 \approx h \sum_{k=1}^N w_{1k} \mathcal{F}_1(\Phi(h \frac{\xi_{1k}}{\pi})) \Phi'(h \frac{\xi_{1k}}{\pi}) + \left(2h - \frac{1}{2}bh^2\right) \mathcal{F}_1(b). \quad (2.107)$$

Actually, the key feature of the aforementioned transformation is that since

$$\Phi(t) \sim \frac{\pi}{h}|t| \quad \text{double exponentially as } t \rightarrow \pm\infty$$

as shown in Fig. 2.13, the quadrature nodes of the final formulas approach double exponentially the zeros of the associated Bessel functions, i.e.,

$$\Phi(h \frac{\xi_{nk}}{\pi}) \sim \xi_{nk} \quad \text{as } k \rightarrow \infty.$$

More specifically, for large values of k we have

$$J_n \left(\Phi \left(h \cdot \frac{\xi_{nk}}{\pi} \right) \right) \simeq J_n \left(\frac{\pi}{h} \cdot h \cdot \frac{\xi_{nk}}{\pi} \right) = 0 \quad (2.108)$$

allowing us to truncate the infinite sum (2.102) at moderate N , as shown in (2.106)-(2.107), without loss of accuracy.

2.5.4 Numerical results

In this section, we perform several numerical experiments in order to demonstrate the accuracy and efficiency of the above described newly developed methods for numerical evaluation of SI tails. For the purpose of comparison, we choose one of the most proven methods for these tails: the integration-then-summation procedure combined with the Mosig-Michalski method and utilizing equidistant break points separated by the asymptotic half-period of the associated Bessel functions [26]. All the calculations are performed in double precision arithmetics (machine precision accuracy is $\text{eps} = 2^{-52}$).

While, thanks to the Sommerfeld identity, analytical solutions exist for a family of Sommerfeld integrals (for instance, the free-space case), nothing comparable can be said for general Sommerfeld tails, especially if their starting point ξ_0 is taken at an arbitrary point of the real axis. This amounts to say that for very simple layered problems we can rearrange formula (2.6) as

$$T_n = S_n - I_n = \text{analytical value} - I_n. \quad (2.109)$$

Therefore, if we try in these cases to assess the absolute error or precision of an algorithm for evaluating the tail T_n , we need to be sure that we are numerically evaluating the finite integral I_n with the best precision, close to machine precision if possible. The basic tail can be obtained by applying the scheme in (2.109) to the Sommerfeld identity (2.36)

$$\int_{\xi_0}^{\infty} \frac{e^{-jk_z|z|}}{jk_z} J_0(k_\rho \rho) k_\rho dk_\rho = \frac{e^{-jkr}}{r} - \int_0^{\xi_0} \frac{e^{-jk_z|z|}}{jk_z} J_0(k_\rho \rho) k_\rho dk_\rho \quad (2.110)$$

where $k_z = \sqrt{k^2 - k_\rho^2}$. Our test cases also include the ρ -derivative of the above:

$$\int_{\xi_0}^{\infty} \frac{e^{-jk_z|z|}}{jk_z} J_1(k_\rho \rho) k_\rho^2 dk_\rho = (1 + jkr) \frac{\rho e^{-jkr}}{r^3} - \int_0^{\xi_0} \frac{e^{-jk_z|z|}}{jk_z} J_1(k_\rho \rho) k_\rho^2 dk_\rho \quad (2.111)$$

its z -derivative:

$$\int_{\xi_0}^{\infty} e^{-jk_z|z|} J_0(k_\rho \rho) k_\rho dk_\rho = ze^{-jkr} \frac{1 + jkr}{r^3} - \int_0^{\xi_0} e^{-jk_z|z|} J_0(k_\rho \rho) k_\rho dk_\rho, \quad (2.112)$$

as well as its second derivative with respect to ρ and z :

$$\begin{aligned} \int_{\xi_0}^{\infty} e^{-jk_z|z|} J_1(k_\rho \rho) k_\rho^2 dk_\rho \\ = z\rho e^{-jkr} \frac{3 + 3jkr - r^2 k^2}{r^5} - \int_0^{\xi_0} e^{-jk_z|z|} J_1(k_\rho \rho) k_\rho^2 dk_\rho. \end{aligned} \quad (2.113)$$

The integrals I_n on the right-hand sides of (2.110) - (2.113) are computed close to machine precision by an adaptive quadrature based on Patterson's formulas [56]. Then the tails T_n (integrals on the left-hand sides of (2.110) - (2.113)) are evaluated with the Mosig-Michalski transformation, the New WA algorithm and the DE technique. In the Mosig-Michalski and New WA algorithms, the partial integrals u_{n_i} in (2.52) must be computed using a Gauss-Legendre quadrature of order 16, as suggested in [22], because in the case of negligibly small integrands, numerical experiments have shown that the adaptive Patterson quadrature rule can fail trying to integrate what is essentially numerical noise.

The key parameter in the DE quadrature is the step size h in (2.106) - (2.107). It directly influences the performance of the formulas and, therefore, it has to be chosen carefully. We

have found experimentally that the value $h = 1/32$ stands as the best trade-off between accuracy and computational cost for the SI tails. We also set, following again the suggestions in [26], a maximum of 160 integration points (ten integration intervals for WA methods) for the three algorithms, if the predefined accuracy (10eps) is not reached.

In Figs. 2.14 - 2.17, the number of significant digits of the relative error in the evaluation of the Sommerfeld identity tail (2.110), its ρ -derivative (2.111), z -derivative (2.112), as well as its second derivative with respect to ρ and z (2.113), versus $k\rho$, for the most challenging case, i.e., $z = 0$, is presented.

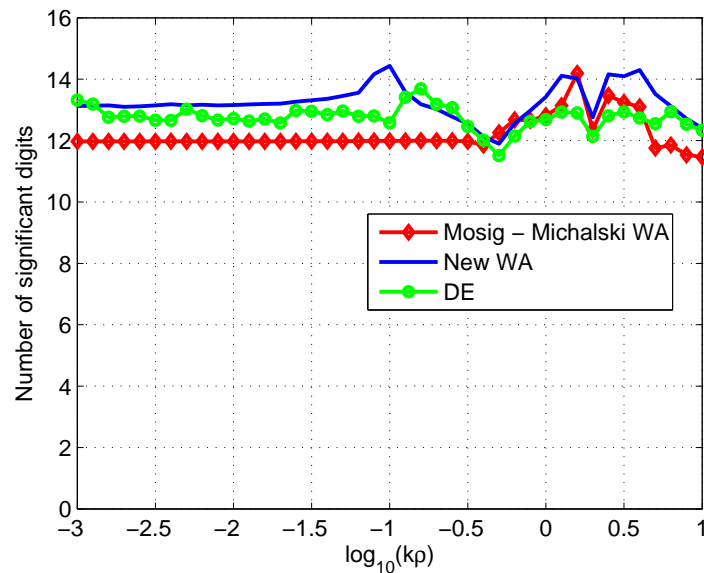


Figure 2.14: Performance of DE formulas, New and Mosig-Michalski WA methods when applied to the Sommerfeld identity tail (2.110) for $z = 0$.

Indeed, when $z = 0$, the exponential function in (2.110)-(2.113) vanishes, and consequently the corresponding integrands have the slowest decay. To account for possible uncertainties in the reference solution and incidental presence of error propagation effects, we cautiously assume a result to be numerically exact if its relative error is lower than 10^{-15} with respect to the reference results. From the results presented, one can see that for the first three examples, all the methods provide very accurate results, with accuracy of more than 10 exact digits for all the values of ρ studied. However, for (2.113), the accuracy of the New WA method is significantly higher than that obtained by using the other two methods. Here, the poorest performance is provided by the DE method, which yields only 7 significant digits of accuracy for some values of ρ . Still, in all the cases studied, the DE-type algorithm needs in average up to 25% fewer integration points than the WA methods.

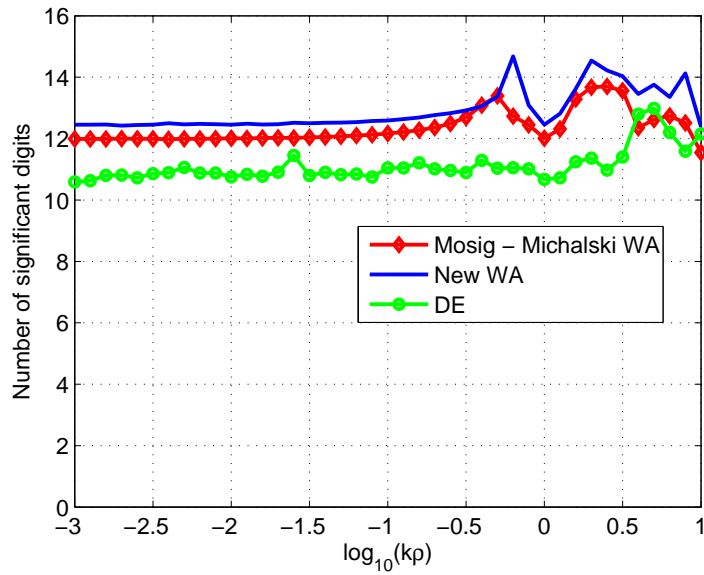


Figure 2.15: Performance of DE formulas, New and Mosig-Michalski WA methods when applied to the ρ -derivative of the Sommerfeld identity tail (2.111) for $z = 0$.

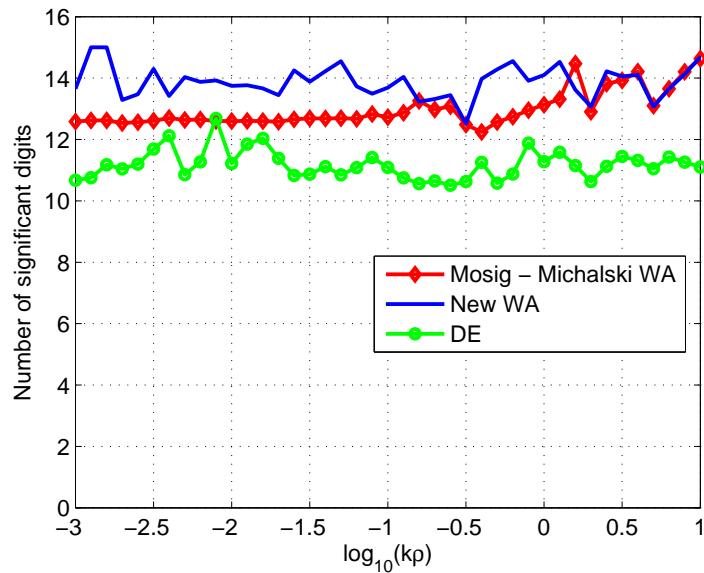


Figure 2.16: Performance of DE formulas, New and Mosig-Michalski WA methods when applied to the z -derivative of the Sommerfeld identity tail (2.112) for $z = 0$.

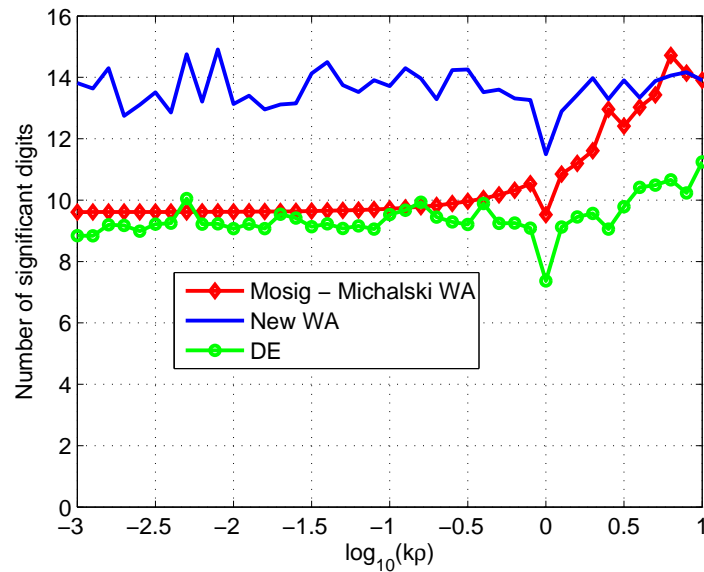
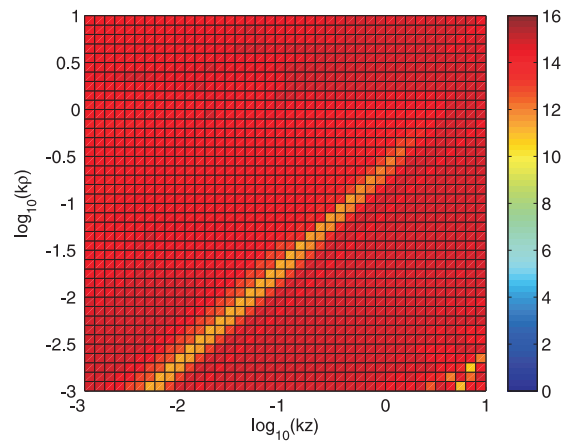
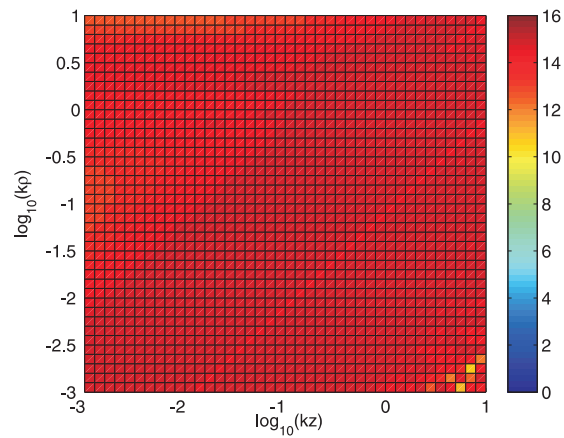


Figure 2.17: Performance of DE formulas, New and Mosig-Michalski WA methods when applied to the second derivative of the Sommerfeld identity tail with respect to ρ and z (2.113) for $z = 0$.

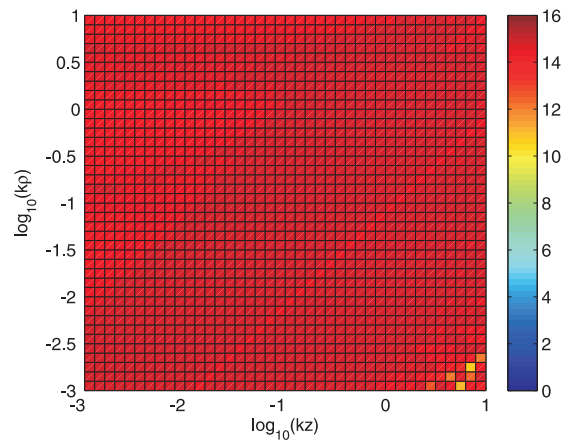
Next, we proceed to a more elaborate numerical experiment including a wide range of distances from the source ($-3 \leq \log_{10}(k\rho), \log_{10}(kz) \leq 1$). To be more specific, the obtained number of significant digits, when the SI tails (2.110)-(2.113) are evaluated with the help of DE, Mosig-Michalski and New WA method are presented in Figs. 2.18 - 2.21. There, one can see that the best results are obtained by using the New WA technique. The other two methods give very good results as well, leading to the accuracy of more than 8 significant digits for all the distances considered.



(a) DE algorithm.

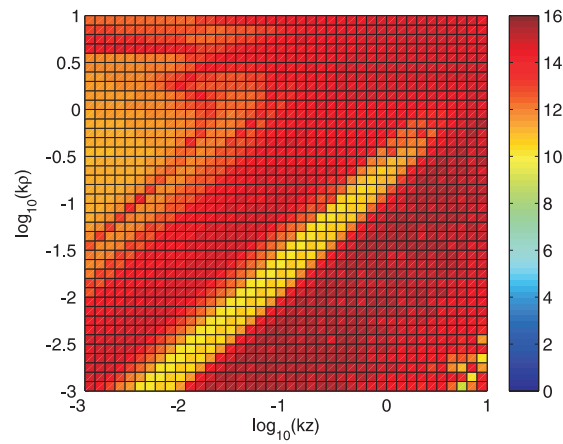


(b) Mosig-Michalski WA transformation.

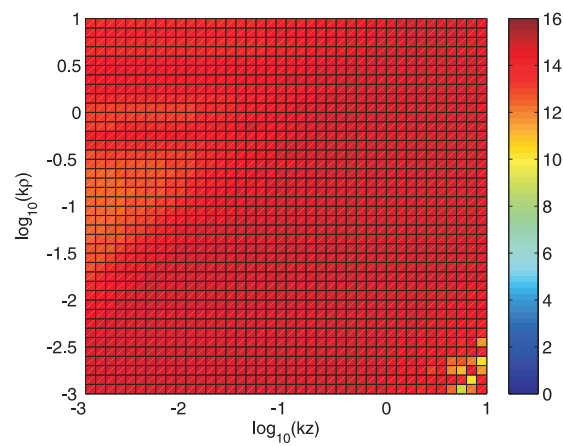


(c) New WA algorithm.

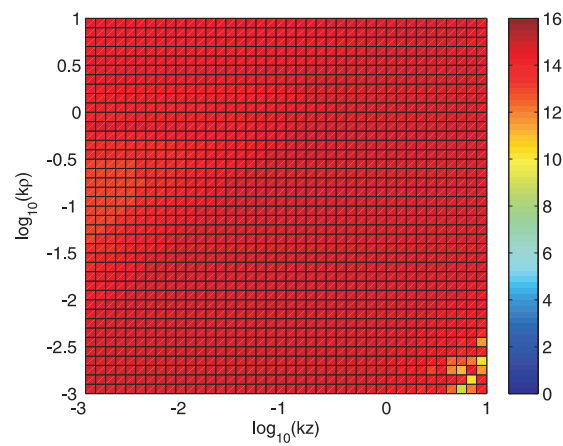
Figure 2.18: Number of significant digits for the SI tail (2.110) for a wide range of distances from the source.



(a) DE algorithm.

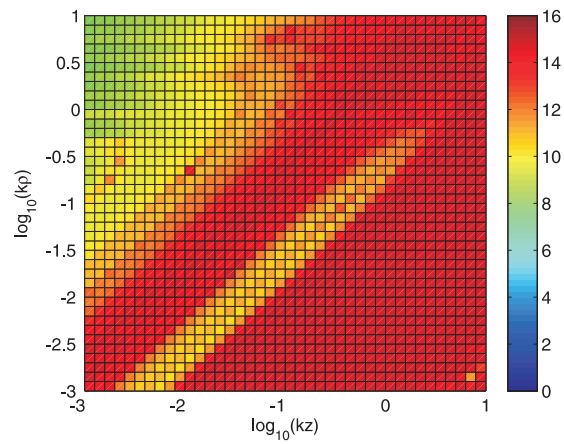


(b) Mosig-Michalski WA transformation.

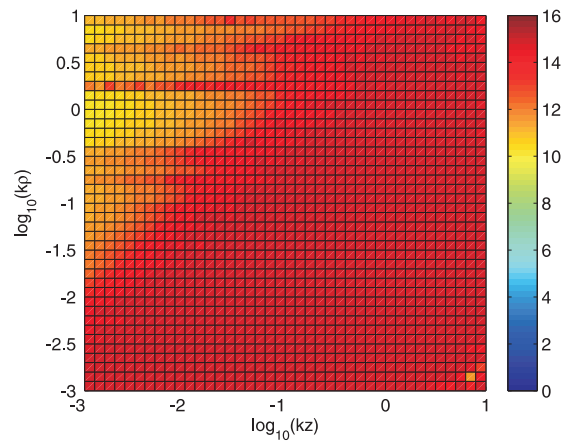


(c) New WA algorithm.

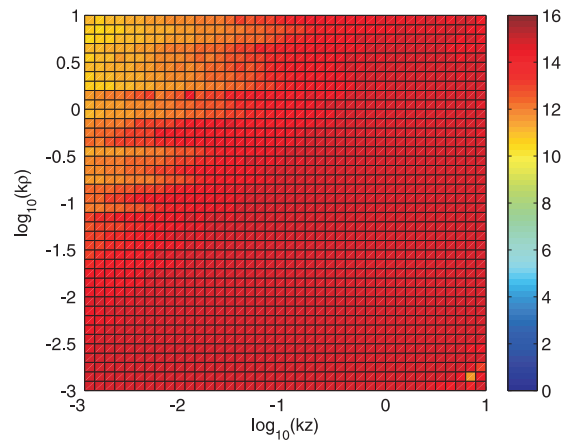
Figure 2.19: Number of significant digits for the SI tail (2.111) for a wide range of distances from the source.



(a) DE algorithm.

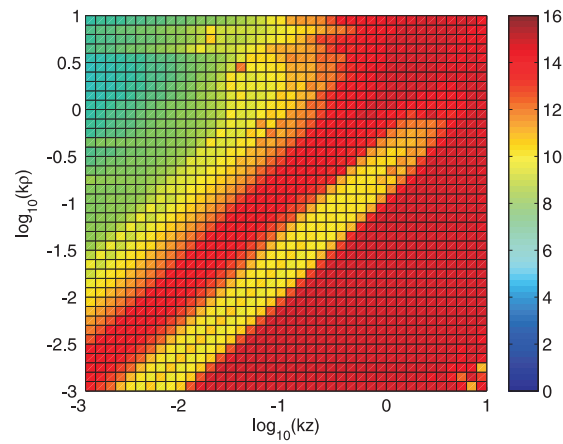


(b) Mosig-Michalski WA transformation.

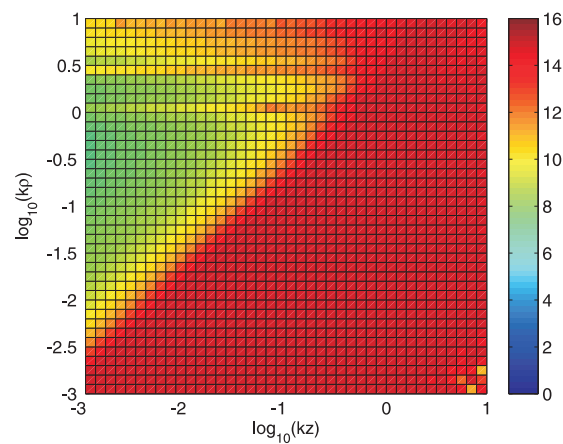


(c) New WA algorithm.

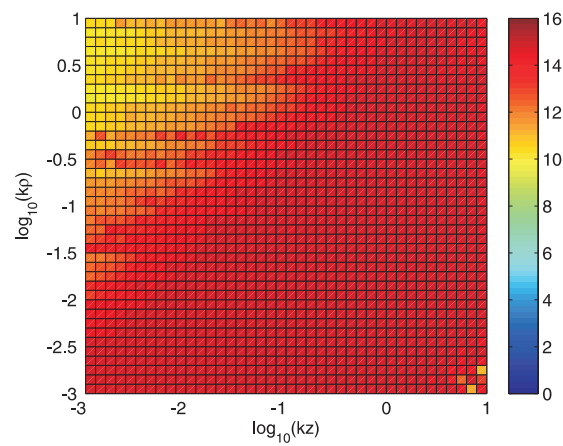
Figure 2.20: Number of significant digits for the SI tail (2.112) for a wide range of distances from the source.



(a) DE algorithm.



(b) Mosig-Michalski WA transformation.



(c) New WA algorithm.

Figure 2.21: Number of significant digits for the SI tail (2.113) for a wide range of distances from the source.

The relative number of integration points $N_{\text{DE}}/N_{\text{WA}}$ (%) is presented in Figs. 2.22 - 2.25 for the tails of (2.110)-(2.113), respectively. Here N_{WA} denotes the number of integration points when the Mosig-Michalski and New WA techniques are used, while N_{DE} is the number of integration points in the case of the DE quadrature. In the lower right part of each of these figures, the contribution of the tail is zero. Neglecting these parts, it is clear that the DE integration scheme is much more efficient than the Mosig-Michalski and New WA techniques in a plethora of observation points.

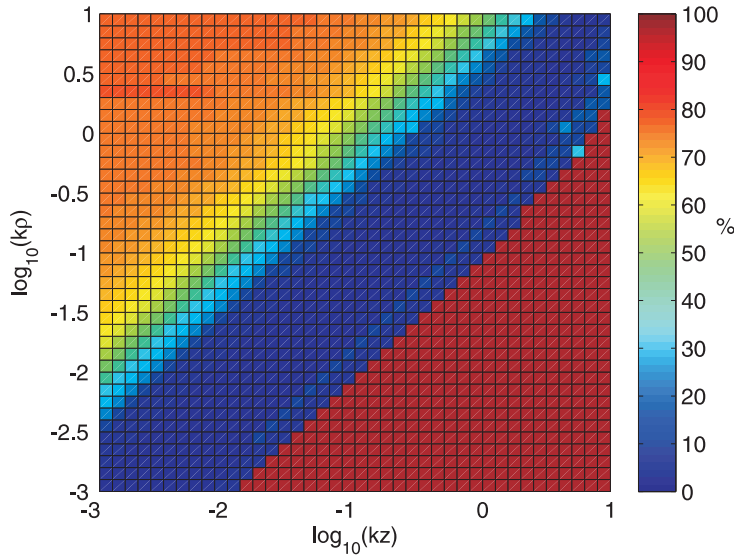


Figure 2.22: Relative number of integration points $N_{\text{DE}}/N_{\text{WA}}$ for the SI tail (2.110) for a wide range of distances from the source.

In the end, we will demonstrate the worthiness of the proposed schemes in two *real life* applications, i.e., a two-layer microstrip antenna geometry (at $f = 8$ GHz):

- layer-1: $\varepsilon_{r1} = 4$, $d_1 = 1\lambda$,
- layer-2: free-space,

and a three-layer antenna geometry (at $f = 1, 30$ GHz):

- layer-1: $\varepsilon_{r1} = 4$, $d_1 = 0.1$ cm,
- layer-2: $\varepsilon_{r2} = 12.6$, $d_2 = 0.1$ cm,
- layer-3: free-space,

terminated by PEC. In both cases, the source (HED) is placed at the interface between the dielectric stack and the free space. Also, we consider only the most challenging case when the

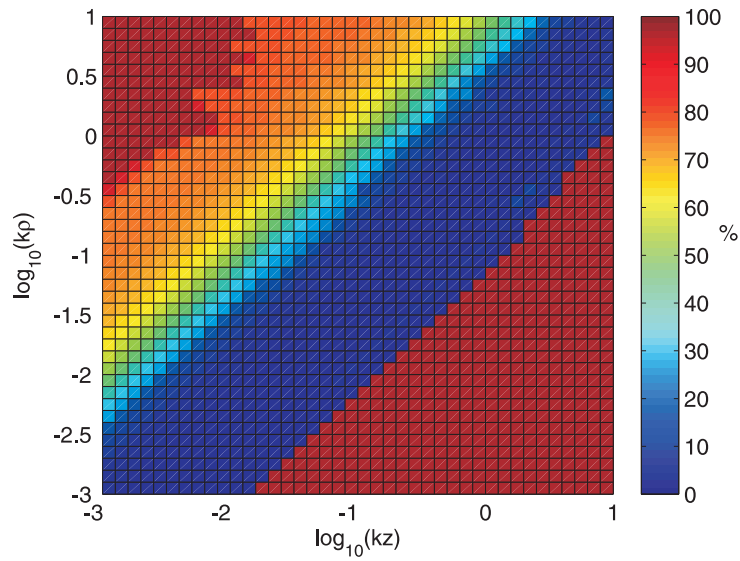


Figure 2.23: Relative number of integration points N_{DE}/N_{WA} for the SI tail (2.111) for a wide range of distances from the source.

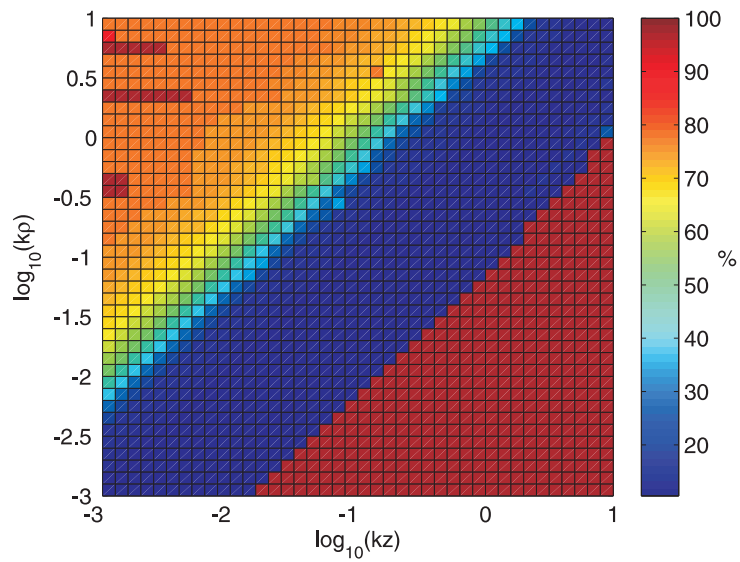


Figure 2.24: Relative number of integration points N_{DE}/N_{WA} for the SI tail (2.112) for a wide range of distances from the source.

observation plane coincides with the source plane, $z = z' = 0$. The average relative numbers of the associated integration points for the evaluation of the tails of the Green's functions

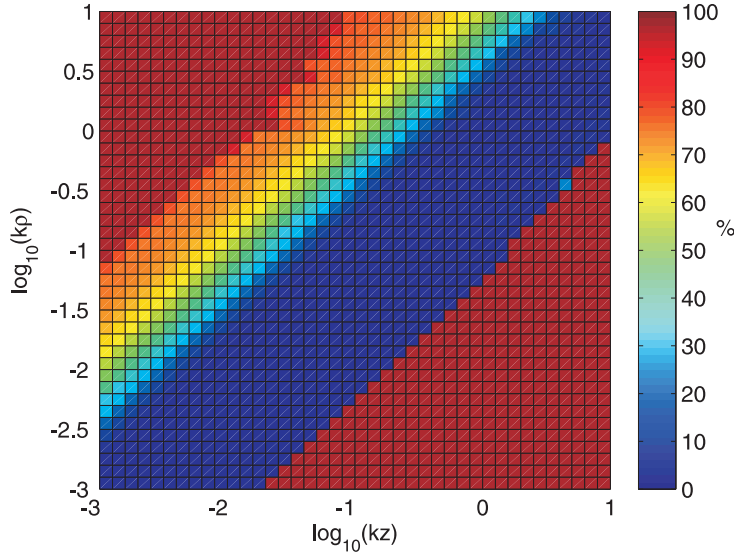


Figure 2.25: Relative number of integration points N_{DE}/N_{WA} for the SI tail (2.113) for a wide range of distances from the source.

$G_{xx}^A(\rho; z, z')$ and $G_x^q(\rho; z, z')$ are shown in Table 2.2.

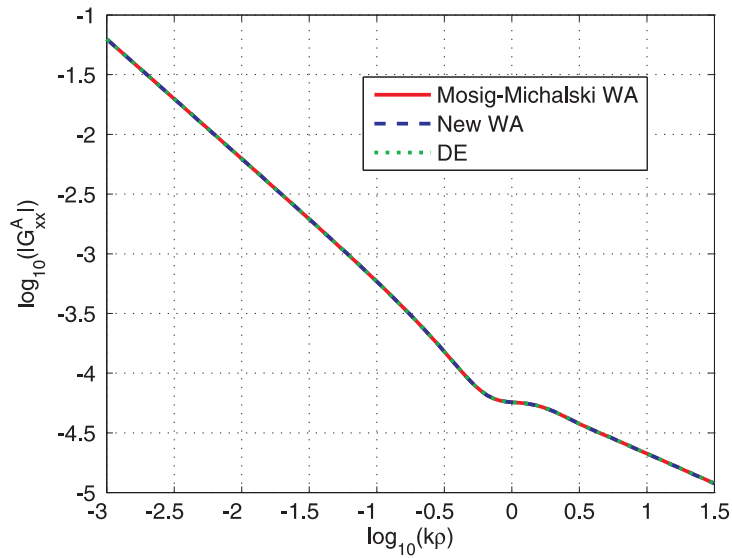
Based on the presented results, we can conclude that the DE formulas require less integration points to achieve the predefined accuracy. Furthermore, very good agreement between the results obtained using the DE, Mosig-Michalski and New WA methods is acquired. For the sake of illustration, in Fig. 2.26 we present the obtained scalar potential GF G_x^q and the component G_{xx}^A of the vector potential dyadic GF, for the three-layer geometry at 30 GHz. There is a perfect agreement between the three techniques with the curves on top of each other for the full range of distances. Furthermore, since the analytical solution does not exist in this case, in order to assess the accuracy of the obtained results, we took as reference the results obtained applying the Mosig-Michalski algorithm until machine precision was reached. The results obtained using the other two methods were then compared with the reference result. Fig. 2.27 gives the number of significant digits. One can see that the three methods agree in more than 11 decimal digits, though the DE method needs approximately 25% fewer integration points.

A final word must be said on the computational time and on the efficient implementation of the above described methods for numerical evaluation of SI tails. Since the value of the step-size parameter h of the DE quadrature is chosen a priori, the associated weights and abscissas can be precomputed. Therefore, the direct application of the formulas (2.106)-(2.107) using as default the maximal number of points (160) can be implemented in MATLAB as a simple

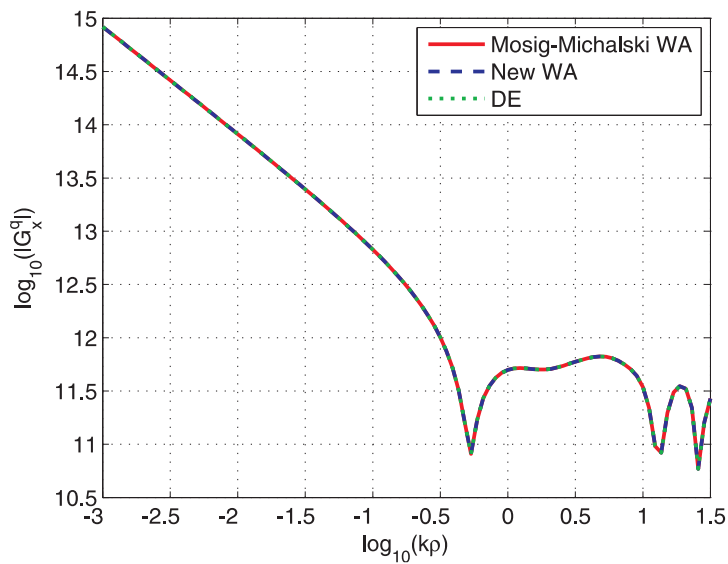
Table 2.2: Average relative number of integration points needed for the evaluation of SI tails

	$N_{\text{DE}}/N_{\text{WA}}$ (%)
two-layer geometry	
$G_x^q _{f=8 \text{ GHz}}$	77.25
$G_{xx}^A _{f=8 \text{ GHz}}$	77.19
three-layer geometry	
$G_x^q _{f=1 \text{ GHz}}$	77.37
$G_{xx}^A _{f=1 \text{ GHz}}$	77.31
$G_x^q _{f=30 \text{ GHz}}$	78.13
$G_{xx}^A _{f=30 \text{ GHz}}$	78.38

matrix multiplication, which is very convenient and indeed leads to lower computational time than the iterative procedure described above, while resulting in same accuracy of the final results. Under these assumptions, the DE transformation takes, approximately 5 times less computational time than the two other methods. The weights (2.68)-(2.69) involved in the Mosig-Michalski WA technique are very easy to evaluate, but the method calls for the recursion (2.62)-(2.65). On the other hand, the evaluation of the weights (2.91)-(2.92) involved in the New WA algorithm is more complex, since it calls for the computation of binomial coefficients. However, this is not a problem since many programming languages have built-in functions for evaluation of binomial coefficients. Alternatively, an iterative procedure might be used. Roughly, it amounts to say that the overhead of the Mosig-Michalski WA transformation is time-wise equivalent to the evaluation of more complicated weights in the New WA method. However the dominant part of the computational time goes to accurate evaluation of the sequence of partial sums, T_{n_i} .



(a) $G_{xx}^A(\rho; z, z')$.



(b) $G_x^q(\rho; z, z')$.

Figure 2.26: Spatial domain Green's function of three-layer geometry problem at 30 GHz.

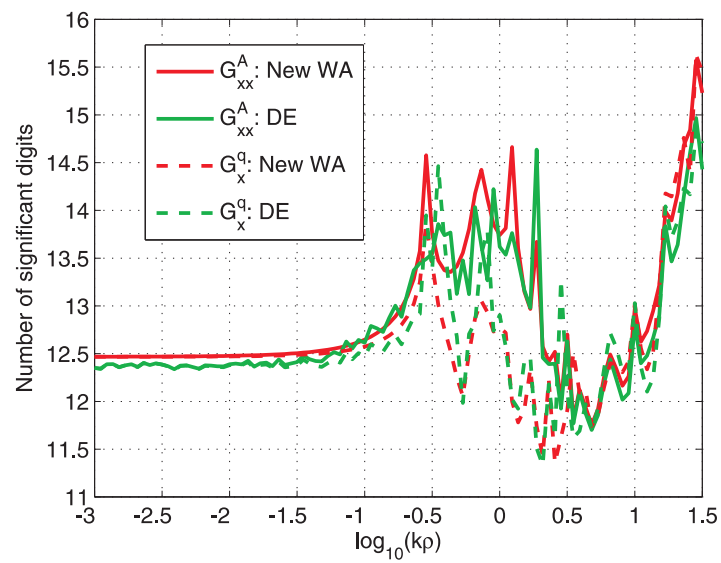


Figure 2.27: Number of significant digits for three-layer geometry at 30 GHz.

2.6 Conclusion

In this chapter we have proposed several schemes for efficient numerical evaluation of Sommerfeld integrals, arising in the formulation of Green's functions for planar multilayered media. These integrals are known to be very difficult to evaluate, because of two complications:

- i) the presence of surface-wave poles and branch-point singularities on and/or near the integration path;
- ii) oscillating and slowly converging integrands over semi-infinite intervals.

Luckily enough, by adequately dividing the integration interval, these two problems can be always separately treated.

First SI part: Finite singular integrals

The difficulty in evaluating the first part of the SI is due to the possible presence of the singularities in the integrand. In order to tackle this problem, we propose a new method based on the double exponential transformation. The integration of the SI is performed along the real axis. The first step is extraction of the pole singularities, and for that purpose we use a very efficient and robust pole extractor from [54], which can be embedded in the routines for numerical evaluation of the SIs in a fully automatic way. The remaining problem, namely the removable singularity of the integrand at the branch point, is taken care of by using a DE quadrature. The accuracy and efficiency of this approach have been verified by investigating several representative examples. In every case, the DE technique is compared with the two most popular techniques for evaluating the first part of the SI: the half-sine contour path integration, and the real-axis integration combined with the pole extraction and variable transformation for treating branch-point singularities. From the presented results, one can see that the new technique yields highly accurate results, while the computational time is dramatically reduced, especially in the case of large source-observer distances.

Second SI part: Infinite interval integrals (tails)

In the second part of this chapter, we have developed two techniques for efficient numerical evaluation of SI tails. These two techniques are a new version of the Weighted Averages (New WA) algorithm and a specially tailored Double Exponential (DE) quadrature formula. The performances of the methods are compared throughout a series of representative numerical examples, with the target of assessing the advantages and disadvantages of their application. As a reference, the Mosig-Michalski WA transformation, which has been traditionally employed for evaluation of the SI tails, is selected. In general, the New WA algorithm is shown to be the winner in terms of accuracy. It converges faster towards the final values, when compared to the Mosig-Michalski WA technique. This may be an important asset, as the computational time is usually dominated by the evaluation of the partial integrals in the sequence. Hence,

the New WA can be used advantageously as an alternative to the classic WA algorithm, that is the most currently used extrapolation method for integration-then-summation techniques. The second strategy, the DE quadrature formula, although on average gives lower accuracy when compared with the WA methods, still yields very good results. More precisely, it always yields more than 9 significant digits of accuracy, except in the case of (2.113), when it leads to only 7 digits accuracy for some combinations of ρ and z values. Fortunately, in the MPIE formulation, this type of integrals only arises in the postprocessing related to the fields evaluations. On the other hand, the lack of accuracy of DE technique is somewhat compensated by an important increase in speed. When properly implemented, the DE always performed significantly faster than both versions of the WA (up to 5 times). This is to be considered in applications where speed is the primordial parameter. Moreover, the convergence of the DE quadrature formulas could be even further improved by changing the value of the coefficient $\pi/2$ in (2.97), as suggested in [76]. This should be a subject of further investigation.

Bibliography

- [1] A. Carlström, M. Viberg, P. Tatalias, J. R. Mosig, E. Suter, and M. Bandinelli, “Antenna CAD and Technology for Future SARs,” Summary Report, Jul. 2001, ESTEC No. 11279/94/NL/PB.
- [2] E. Suter, “Efficient numerical modelling of large scale planar antennas using a subdomain multilevel approach,” Ph.D. dissertation, Ecole Polytechnique Fédérale de Lausanne, Switzerland, 2000, Thèse No. 2286.
- [3] J. R. Mosig, “Arbitrary shaped microstrip structures and their analysis with a mixed potential integral equation,” *IEEE Trans. Microw. Theory Tech.*, vol. 36, no. 2, pp. 314–323, Feb. 1988.
- [4] K. A. Michalski, “The mixed-potential electric field integral equation for objects in layered media,” *Arch. Elek. Ubertragung.*, vol. 39, no. 5, pp. 317–322, Sept. 1985.
- [5] K. A. Michalski and D. Zheng, “Electromagnetic scattering and radiation by surfaces of arbitrary shape in layered media, Part 1: Theory,” *IEEE Trans. Antennas Propag.*, vol. 38, no. 3, pp. 335–344, Mar. 1990.
- [6] J. R. Mosig and F. E. Gardiol, “Dynamical radiation model for microstrip structures,” in *Advances in Electronics and Electron Physics*. New York: Academic Press, 1982, pp. 139–237.
- [7] L. Felsen and N. Marcuvitz, *Radiation and scattering of waves*. New Jersey: Prentice-Hall.
- [8] K. A. Michalski and J. R. Mosig, “Multilayered media Green’s functions in integral equation formulations,” *IEEE Trans. Antennas Propag.*, vol. 45, no. 3, pp. 508–519, Mar. 1997.
- [9] A. A. Melcón, “Application of the integral equation technique to the analysis and synthesis of multilayered printed shielded microwave circuits and cavity backed antennas,” Ph.D. dissertation, Ecole Polytechnique Fédérale de Lausanne, Switzerland, 1998, Thèse No. 1901.
- [10] T. M. Grzegorzcyk, “Integrated 3d antennas for millimeter-wave applications: theoretical study and technological realization,” Ph.D. dissertation, Ecole Polytechnique Fédérale de Lausanne, Switzerland, 2000, Thèse No. 2299.

-
- [11] A. Sommerfeld, *Partial Differential Equations in Physics*. New York: Academic, 1949.
- [12] M. I. Aksun and G. Dural, "Clarification of issues on the closed-form Green's functions in stratified media," *IEEE Trans. Antennas Propag.*, vol. 53, no. 11, pp. 3644–3653, Nov. 2005.
- [13] M. Yuan, T. K. Sarkar, and M. Salazar-Palma, "A direct discrete complex image method from the closed-form Green's functions in multilayered media," *IEEE Trans. Microw. Theory Tech.*, vol. 54, no. 3, pp. 1025–1032, Mar. 2006.
- [14] V. N. Kourkoulos and A. C. Cangellaris, "Accurate approximation of Green's functions in planar stratified media in terms of a finite sum of spherical and cylindrical waves," *IEEE Trans. Antennas Propag.*, vol. 54, no. 5, pp. 1568–1576, May 2006.
- [15] R. R. Boix, F. Mesa, and F. Medina, "Application of total least squares to the derivation of closed-form Green's functions for planar layered media," *IEEE Trans. Microw. Theory Tech.*, vol. 55, no. 2, pp. 268–280, Feb. 2007.
- [16] A. G. Polimeridis, T. V. Yioultsis, and T. D. Tsiboukis, "A robust method for the computation of Green's functions in stratified media," *IEEE Trans. Antennas Propag.*, vol. 55, no. 7, pp. 1963–1969, July 2007.
- [17] —, "Fast numerical computation of Green's functions for unbounded planar stratified media with a finite-difference technique and Gaussian spectral rules," *IEEE Trans. Microw. Theory Tech.*, vol. 55, no. 1, pp. 100–107, Jan. 2007.
- [18] A. G. Polimeridis and T. V. Yioultsis, "On the efficient computation of closed-form Green's functions in planar stratified media," *Int. J. RF Microw. Computer Aided Eng.*, vol. 18, no. 2, pp. 118–126, Mar. 2008.
- [19] T. J. Cui and W. C. Chew, "Fast evaluation of Sommerfeld integrals for EM scattering and radiation by three-dimensional buried objects," *IEEE Trans. Geosci. Remote Sensing*, vol. 37, no. 2, pp. 887–900, Mar. 1999.
- [20] A. Hoorfar, J. X. Zheng, and D. C. Chang, "Numerical modeling of crossover and other junction discontinuities in two-layer microstrip circuits," *Int. J. Microw. Millim. Wave Computer Aided Eng.*, vol. 2, no. 4, pp. 261–272, Mar. 1992.
- [21] P. Gay-Balmaz and J. R. Mosig, "Three-dimensional planar radiating structures in stratified media," *Int. J. Microw. Millim. Wave Computer Aided Eng.*, vol. 7, no. 5, pp. 330–343, Sept. 1997.
- [22] K. A. Michalski, "Application of the complex image method to electromagnetic field computation in planar uniaxial multilayers," in *I Workshop on Integral Techniques for Electromagnetics (INTELECT)*, Lausanne, Switzerland, July 2007.

-
- [23] J. R. Mosig, "Integral equation techniques," in *Numerical Techniques for Microwave and Millimeter-Wave Passive Structures*, T. Itoh, Ed. New York: Wiley, 1989, ch. 3, pp. 133–213.
- [24] F. J. Demuyne and G. A. E. Vandebosch, "The expansion wave concept - part I: efficient calculation of spatial Green's functions in a stratified dielectric medium," *IEEE Trans. Antennas Propag.*, vol. 46, no. 3, pp. 397–406, Mar. 1998.
- [25] N. Kinayman and M. I. Aksun, "Comparative study of acceleration techniques for integrals and series in electromagnetic problems," *Radio Science*, vol. 30, no. 6, pp. 1713–1722, Nov.–Dec. 1995.
- [26] K. A. Michalski, "Extrapolation methods for Sommerfeld integral tails," *IEEE Trans. Antennas Propag.*, vol. 46, no. 10, pp. 1405–1418, Oct. 1998.
- [27] T. Hasegawa and A. Sidi, "An automatic integration procedure for infinite range integrals involving oscillatory kernels," *Numerical Algorithms*, vol. 13, no. 1, pp. 1–19, Mar. 1996.
- [28] T. Ooura, "A continuous Euler transformation and its application to the Fourier transforms of a slowly decaying functions," *J. Comput. Appl. Math.*, vol. 130, no. 1–2, pp. 259–270, May 2001.
- [29] S. Singh and R. Singh, "Computation of Sommerfeld integrals using tanh transformation," *MOTL*, vol. 37, no. 3, pp. 177–180, Mar. 2003.
- [30] T. Ooura, "A generalization of the continuous Euler transformation and its application to numerical quadrature," *J. Comput. Appl. Math.*, vol. 157, no. 2, pp. 251–259, 2003.
- [31] M. Yuan and T. K. Sarkar, "Computation of the Sommerfeld integral tails using the matrix pencil method," *IEEE Trans. Antennas Propag.*, vol. 54, no. 4, pp. 1358–1362, Apr. 2006.
- [32] M. Abramowitz and I. Stegun, *Handbook of mathematical functions*. New York: Dover publications, Inc., 1965.
- [33] R. F. Harrington, *Field computation by moment method*. New York: IEEE Press, 1993.
- [34] J. R. Mosig and T. K. Sarkar, "Comparison of quasi-static and exact electromagnetic fields from a horizontal electric dipole above a lossy dielectric backed by an imperfect ground plane," *IEEE Trans. Microw. Theory Tech.*, vol. 34, no. 4, pp. 379–387, Apr. 1986.
- [35] T. Tamir and A. A. Oliner, "Guided complex waves, part I: fields at an interface," *Proc. IEE*, vol. 110, no. 2, pp. 310–324, Feb. 1963.
- [36] —, "Guided complex waves, part II: relation to radiation patterns," *Proc. IEE*, vol. 110, no. 2, pp. 325–334, Feb. 1963.

-
- [37] W. Shu and J. M. Song, "Complete mode spectrum of a grounded dielectric slab with double negative metamaterials," *Progress in Electromagnetic research, PIER*, vol. 65, pp. 103–123, 2006.
- [38] C. Li, Q. Sui, and F. Li, "Complex guided wave solutions of grounded dielectric slab made of metamaterials," *Progress in Electromagnetic research, PIER*, vol. 51, pp. 187–195, 2005.
- [39] W. C. Chew, *Waves and fields in inhomogeneous media*. New York: Van Nostrand Reinhold, 1990.
- [40] I. M. Longman, "Note on a method for computing infinite integrals of oscillatory functions," *Proc. Cambridge Phil. Soc.*, vol. 52, pp. 764–768, 1956.
- [41] I. A. and T. J., *An introduction to the theory of infinite series*. New York: Macmillan, 1965.
- [42] R. E. Scraton, "A note on the summation of divergent power series," *Proc. Camb. Philos. Soc.*, vol. 66, pp. 109–114, 1969.
- [43] P. Wynn, "A note on the generalized Euler transformation," *Computer J.*, vol. 14, no. 4, pp. 437–441, 1971.
- [44] D. A. Smith and W. F. Ford, "Acceleration of linear and logarithmic convergence," *SIAM J. Num. Anal.*, vol. 16, no. 2, pp. 223–240, Apr. 1979.
- [45] J. E. Drummond, "Convergence speeding, convergence and summability," *J. Comput. Appl. Math.*, vol. 11, no. 2, pp. 145–159, Oct. 1984.
- [46] D. Shanks, "Nonlinear transformation of divergent and slowly convergent sequences," *J. Math. Phys.*, vol. 34, pp. 1–42, 1955.
- [47] D. Levin, "Development of nonlinear transformations for improving convergence of sequences," *Int. J. Comput. Math.*, vol. 3, no. 1–4, pp. 371–388, 1973.
- [48] P. Wynn, "On a device for computing the $e_m(S_n)$ transformation," *Math. tables Aids Comput.*, vol. 10, no. 54, pp. 91–96, Apr. 1956.
- [49] D. A. Smith and W. F. Ford, "Numerical comparisons of nonlinear convergence accelerators," *Math. Comput.*, vol. 38, no. 158, pp. 481–499, Apr. 1982.
- [50] C. Brezinski and M. R. Zaglia, *Extrapolation methods*. Amsterdam: North-Holland, 1991.
- [51] J. R. Mosig and F. E. Gardiol, "Analytical and numerical techniques in the Green's function treatment of microstrip antennas and scatterers," *IEE Proceedings, Part H - Microwaves, Optics and Antennas*, vol. 130, no. 2, pp. 175–182, Mar. 1983.

-
- [52] H. H. H. Homeier, “Scalar Levin-type sequence transformations,” *J. Comput. Appl. Math.*, vol. 122, no. 1–2, pp. 81–147, Oct. 2000.
- [53] J. R. Mosig and A. A. Melcon, “Green’s functions in lossy layered media: integration along the imaginary axis and asymptotic behavior,” *IEEE Trans. Antennas Propag.*, vol. 51, no. 12, pp. 3200–3208, Dec. 2003.
- [54] A. G. Polimeridis, T. V. Yioultis, and T. D. Tsiboukis, “An efficient pole extraction technique for the calculation of Green’s functions in stratified media using a sine transformation,” *IEEE Trans. Antennas Propag.*, vol. 55, no. 1, pp. 227–229, Jan. 2007.
- [55] H. Takahasi and M. Mori, “Double exponential formulas for numerical integration,” *Publ. RIMS, Kyoto Univ.*, vol. 9, no. 3, pp. 721–741, 1974.
- [56] T. N. L. Patterson, “Algorithm 468: algorithm for automatic numerical integration over a finite interval,” *Commun. ACM*, vol. 16, no. 11, pp. 694–699, Nov. 1973.
- [57] S. A. Teo, S. T. Chew, and M. S. Leong, “Error analysis of the discrete complex image method and pole extraction,” *IEEE Trans. Microw. Theory Tech.*, vol. 51, no. 2, pp. 406–413, Feb. 2003.
- [58] H. Takahasi and M. Mori, “Error estimation in the numerical integration of analytic functions,” *Rep. Comput. Centre Univ. Tokyo*, no. 3, pp. 41–108, 1970.
- [59] A. R. Krommer and C. W. Ueberhuber, *Computational integration*. PA: SIAM, 1998.
- [60] M. Sugihara, “Optimality of the double exponential formula - functional analysis approach,” *Numer. Math.*, vol. 75, no. 3, pp. 379–395, 1997.
- [61] M. Mori, “Quadrature formulas obtained by variable transformation and the DE-rule,” *J. Comput. Appl. Math.*, vol. 12-13, pp. 119–130, May 1985.
- [62] —, “Discovery of the double-exponential transformation and its developments,” *Publ. RIMS, Kyoto Univ.*, no. 41, pp. 897–935, 2005.
- [63] A. G. Polimeridis and J. R. Mosig, “Evaluation of weakly singular integrals via generalized Cartesian product rules based on the double exponential formula,” *IEEE Trans. Antennas Propag.*, vol. 58, no. 6, pp. 1980–1988, June 2010.
- [64] J. R. Mosig and A. Alvarez-Melcon, “Green’s functions in lossy layered media: integration along the imaginary axis and asymptotic behavior,” *IEEE Trans. Antennas Propag.*, vol. 51, no. 12, pp. 3200–3208, Dec. 2003.
- [65] J. R. Mosig and R. Golubovic-Niciforovic, “Some new developments of the weighted averages algorithm,” in *5th European Conference on Antennas and Propagation, EuCap 2011*, Rome, Italy, Apr. 11–15, 2011.

-
- [66] J. R. Mosig, “The weighted averages algorithm revisited,” *IEEE Trans. Antennas Propag.*, submitted.
- [67] G. H. Hardy, *Divergent Series*. New York: Oxford University Press, 1949.
- [68] A. Alparslan, M. I. Aksun, and K. A. Michalski, “Closed-form Green’s functions in planar layered media for all ranges and materials,” *IEEE Trans. Microw. Theory Tech.*, vol. 58, no. 3, pp. 602–613, Mar. 2010.
- [69] T. Ooura and M. Mori, “A robust double exponential formula for Fourier-type integrals,” *J. Comput. Appl. Math.*, vol. 112, no. 1–2, pp. 229–241, Nov. 1999.
- [70] C. Frappier and P. Olivier, “A quadrature formula involving zeros of Bessel functions,” *Math. Comp.*, vol. 60, no. 201, pp. 303–316, Jan. 1993.
- [71] G. R. Grozev and Q. I. Rahman, “A quadrature formula with zeros of Bessel functions as nodes,” *Math. Comp.*, vol. 64, no. 210, pp. 715–725, Apr. 1995.
- [72] R. B. Ghanem, “Quadrature formulae using zeros of Bessel function as nodes,” *Math. Comp.*, vol. 67, no. 221, pp. 323–336, Jan. 1998.
- [73] H. Ogata and M. Sugihara, “Quadrature formulae for oscillatory infinite integrals involving the Bessel functions (in Japanese),” *Trans. Japan Soc. Industr. Appl. Math.*, vol. 8, no. 2, pp. 223–256, June 1998.
- [74] R. Golubovic-Niciforovic, A. Polimeridis, and J. R. Mosig, “Fast computation of Sommerfeld integral tails via direct integration based on double exponential-type quadrature formulas,” *IEEE Trans. Antennas Propag.*, vol. 59, no. 2, pp. 694–698, Feb. 2011.
- [75] —, “Double exponential quadrature formulas for the direct calculation of Sommerfeld integral tails,” in *5th European Conference on Antennas and Propagation, EuCap 2011*, Rome, Italy, Apr. 11–15, 2011.
- [76] I. D. Koufogiannis, A. G. Polimeridis, M. Mattes, and J. R. Mosig, “A parametric study of the double exponential algorithm utilized in weakly singular integrals,” in *5th European Conference on Antennas and Propagation, EuCap 2011*, Rome, Italy, Apr. 11–15, 2011.

3 Numerical evaluation of the integrals involving products of Bessel functions of arbitrary order

3.1 Introduction

The previous chapter has extensively dealt with the methods for efficient numerical evaluation of Sommerfeld integrals, i.e., semi-infinite range integrals with Bessel function kernels. It was shown that their numerical evaluation is a cumbersome task because of the oscillatory and slowly converging, or even diverging integrands. In the case that the integrands contain products of two or more Bessel functions, the problem becomes even more difficult, since the integrand now exhibits an irregular oscillatory behavior. Many practical problems in electromagnetics give rise to this type of integrals, for which no analytical solution is known. Therefore, their efficient numerical evaluation is of uppermost relevance and is addressed in this chapter.

Integrals involving product of Bessel functions occur in many different fields. For example, in electromagnetics this type of integrals arises in problems like the analysis of planar transmission lines in microwave applications using the spectral domain Galerkin method [1], or the evaluation of the electromagnetic response of a large circular loop source on a layered earth models (in both quasi-static and non-quasi-static regions) [2], or still in the problem of finding the distribution of the current in the earth, when a DC current enters the ground through a disk electrode [3]. They are also encountered in the hydrodynamics, when dealing with problems involving particle motion in unbounded rotating fluids [4], [5], in elasticity theory when studying the crack problems [6], in acoustics when analyzing the problem of the projection of a wave out of the end of a circular tube [7] and, finally, in biology, associated to problems of distortions of nearly circular lipid domains [8].

Several methods have been proposed in the literature to treat this problem. Inspired by Trefethen's famous 100-Digits challenge, Van Deun and Coolis [9] developed an algorithm for evaluating the infinite integrals containing products of an arbitrary number of Bessel functions of the first kind and the ancillary polynomial function of power n . The oscillating asymptotes are first extracted and evaluated analytically using the incomplete Gamma function with complex argument, while the remaining part is integrated numerically using conventional quadrature methods. Further elaboration of this method is presented in [10], extending it to the integration of the arbitrary product of Bessel functions with an additional exponential or rational factor over a semi-infinite interval. In [1], integrals containing products of two

Bessel functions are represented as a sum of one definite integral that can be calculated with the help of conventional quadrature formulas, and four semi-infinite integrals, such that after deforming the integration path into the complex plane, they are no longer oscillating, and therefore can be evaluated using standard Gauss-Legendre quadratures. The solution for this problem is also offered in [2], for products of only two Bessel functions of the first kind of order 0 and 1. Finally, in [11] a method is presented that requires transformation of the product of two Bessel functions into the sum of two regularly oscillating functions. The method uses the ϵ algorithm and mW transformation of Sidi [12] for accelerating the sequence of partial sums obtained after applying the integration-then-summation procedure to the transformed integral.

Here, we adapt to our needs the original study of [11] and we represent the irregular oscillatory behavior of the product of Bessel functions in a more suitable way, as a sum of asymptotically regularly oscillating functions. Their numerical evaluation is then performed with the help of the robust and efficient New Weighted Averages extrapolation method [13], which has been described in detail in the previous chapter.

3.2 Integrals with products of Bessel functions

Our goal is to accurately and efficiently evaluate the integrals involving products of the Bessel functions of the first kind and an arbitrary order:

$$I_B = \int_0^\infty f_b(x) J_a(px) J_b(qx) dx. \quad (3.1)$$

Having in mind the asymptotic behavior of the Bessel function of the first kind $J_a(x)$,

$$J_a(px) \sim \sqrt{\frac{2}{\pi px}} \cos\left(px - \frac{a\pi}{2} - \frac{\pi}{4}\right) \quad (3.2)$$

the first, simple idea is to start the development considering the related integral whose kernel is the product of two cosine functions:

$$I_C = \int_0^\infty f_c(x) \cos(px) \cos(qx) dx \quad (3.3)$$

and neglecting, for the moment, the additional complexity introduced by the Bessel functions. Replacing the product of the cosine functions by sums, we obtain the following expression:

$$I_C = \frac{1}{2} \int_0^\infty f_c(x) [\cos(\sigma x) + \cos(\delta x)] dx \quad (3.4)$$

where $\sigma = p+q$ and $\delta = |p-q|$. Since $\sigma > \delta$, the oscillatory behavior is mainly due to $\cos(\sigma x)$. The integrand in (3.4) is a typical representation of the amplitude modulation (AM) process, and for an electrical engineer it is natural to consider $\cos(\sigma x)$ as a carrier, and $\cos(\delta x)$ as a

modulator. If σ and δ are rational numbers, i.e. $\sigma = \frac{\sigma_1}{\sigma_2}$ and $\delta = \delta_1/\delta_2$ ($\sigma_1, \sigma_2, \delta_1$ and δ_2 are integers) the sum of two cosine functions in (3.4) is a periodic function, with the period:

$$T = \frac{2\pi}{\tau} = 2\pi \cdot \frac{\text{LCM}(\sigma_2, \delta_2)}{\text{GCD}(\sigma_1, \delta_1)} \quad (3.5)$$

where GCD stands for greatest common divisor and LCD stands for least common multiplier. After simple mathematical manipulations, the above integral can be represented as

$$I_C = \frac{1}{2} \int_0^\infty \left[\frac{\tau}{\sigma} f_c \left(\frac{\tau x}{\sigma} \right) + \frac{\tau}{\delta} f_c \left(\frac{\tau x}{\delta} \right) \right] \cos(\tau x) dx. \quad (3.6)$$

By careful examination, it can be seen that the above integrand is asymptotically equivalent to the real part of the kernel involved in the integral used as a starting point for the development of the New WA method [13, 14]:

$$I = \int_0^\infty f(x) e^{-\alpha x} e^{j\beta x} dx, \quad (3.7)$$

when $\alpha = 0$, $\beta = \tau$ and $f(x) = \frac{\tau}{\sigma} f_c \left(\frac{\tau x}{\sigma} \right) + \frac{\tau}{\delta} f_c \left(\frac{\tau x}{\delta} \right)$. Now, the bold assumption is that we can use the WA algorithm for the numerical evaluation of (3.3) as a classical oscillating integral (involving only a single cosine). In a similar way, the integral (3.1) could be treated, by setting $\alpha = 0$, $\beta = \tau$ and $f(x) = \frac{1}{\pi x \sqrt{pq}} \left[\frac{\tau}{\sigma} f_c \left(\frac{\tau x}{\sigma} \right) + \frac{\tau}{\delta} f_c \left(\frac{\tau x}{\delta} \right) \right]$.

For the sake of validation of the above described reasoning, we have applied it to the following two test integrals:

$$\text{Ex. 1 : } \int_0^\infty J_2(3x) J_1(x) dx = \frac{1}{9} \quad (3.8)$$

and

$$\text{Ex. 2 : } \int_0^\infty J_0(x) J_1(2x) dx = \frac{1}{2}. \quad (3.9)$$

These two test integrals look similar, but the obtained results are quite different. While for the first example (3.8) we have obtained less than 3 significant digits, no matter how many partial integrals we use, the second integral (3.9) is evaluated with 15 digits precision (see dashed curves in Fig. 3.1). In order to have a better insight and understand the reason behind the excellent performance of the method in some cases, and rather poor performance in others, the integrands of (3.8)-(3.9) and the abscissas x_i used as the upper limits of partial integrals have been plotted in Fig. 3.2. There, it can be seen that the answer lies in the irregular oscillatory behavior of the integrands.

As discussed in the previous chapter, a numerically stable algorithm is obtained if equidistant abscissas separated by function's half-period $\frac{\pi}{\beta}$ are used as the upper limits of the partial integrals I_i . Therefore, in the case of simply oscillating integrands, the values of the integrand

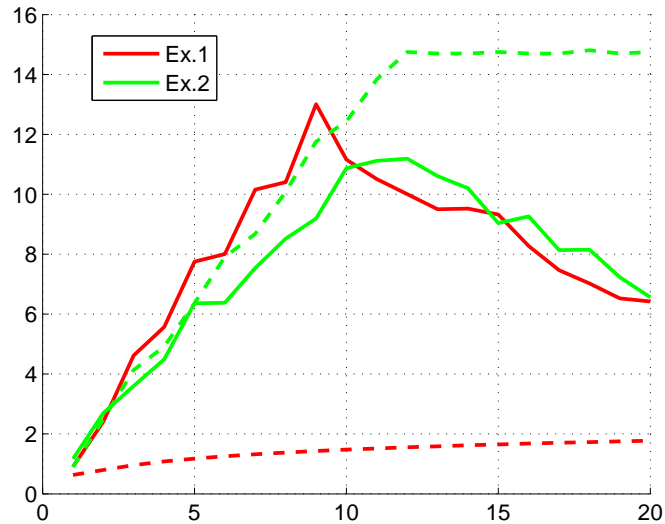
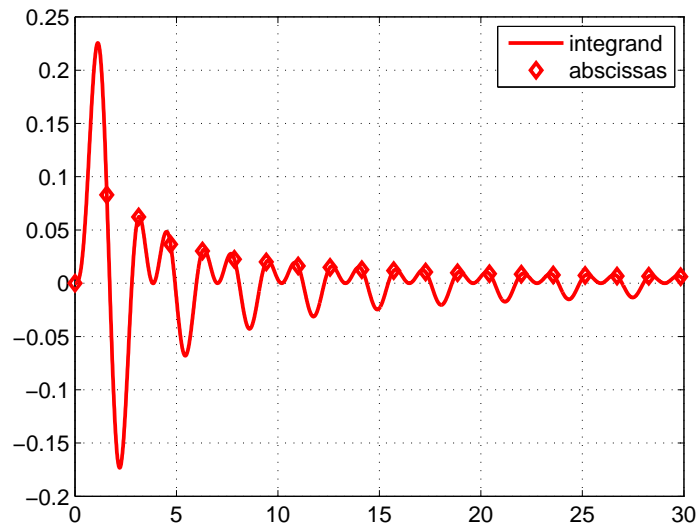


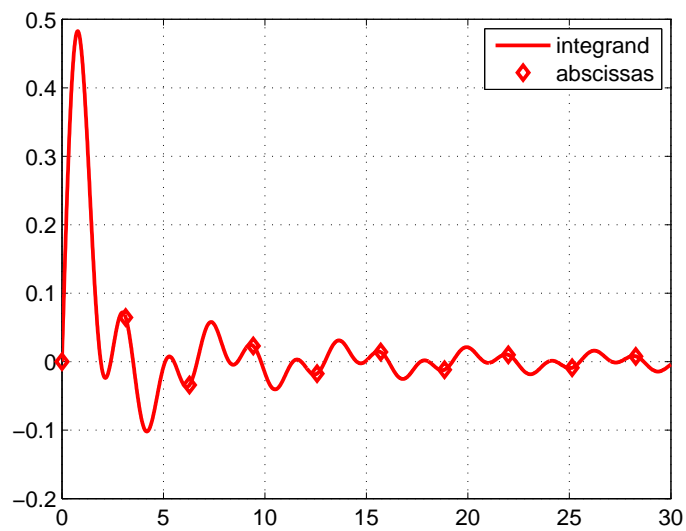
Figure 3.1: Test functions Ex.1 (3.8) and Ex.2 (3.9): Behavior of the algorithm when equidistant break points separated by function's half-period (dashed lines) and by function's period (solid lines) are used as the upper limits of partial integrals.

at the endpoints of two successive partial integrals are of opposite signs.

However, when the integrand involves product of two Bessel functions, its oscillating behavior is more complex, and the above condition could be satisfied depending on the combination of a, b, p and q . In the case that the combination of a, b, p and q is such that the values of the integrands at the endpoints of the successive partial integrals are not always of opposite sign, such as in (3.8), instead of obtaining machine precision accuracy, the final result is not better than the one obtained by simple truncation of the integral at a finite value, assuming that the remaining contribution is negligible. A possible remedy for this problem is to use equidistant abscissas separated by the function's period $\frac{2\pi}{\beta}$ as the upper limits of the partial integrals I_i . However, this choice leads to a numerically unstable algorithm (see solid curves in Fig. 3.1), since the sequence of partial integrals is monotonically approaching the true value of the integral, while the corresponding weights alternate in sign [13, 14]. Therefore, the New WA method, which is very efficient and robust for integrals with simply oscillating integrands, cannot be straightforwardly applied to the functions with irregular oscillatory behavior, like the product of two Bessel functions.



(a) Test function (3.8).



(b) Test function (3.9).

Figure 3.2: Behavior of the integrand (—) and actual positions of the abscissas (◊).

The question that now naturally arises is the possibility of representing the irregular oscillatory behavior of the product of Bessel functions as a linear combination of simply oscillating functions. In [11], Lucas observed that the product of two Bessel function can be written in the following way:

$$J_a(px)J_b(qx) = h_1(x; a, b, p, q) + h_2(x; a, b, p, q) \quad (3.10)$$

where

$$h_1(x; a, b, p, q) = \frac{1}{2}[J_a(px)J_b(qx) - Y_a(px)Y_b(qx)] \quad (3.11)$$

and

$$h_2(x; a, b, p, q) = \frac{1}{2}[J_a(px)J_b(qx) + Y_a(px)Y_b(qx)]. \quad (3.12)$$

This can be considered as the mathematical generalization for the Bessel functions of the classic decomposition of a product of cosine functions into sums. The behavior of the functions h_1 and h_2 is illustrated in Fig. 3.3, for the case of the product of the Bessel functions $J_2(3x)J_1(x)$ from the example (3.8).

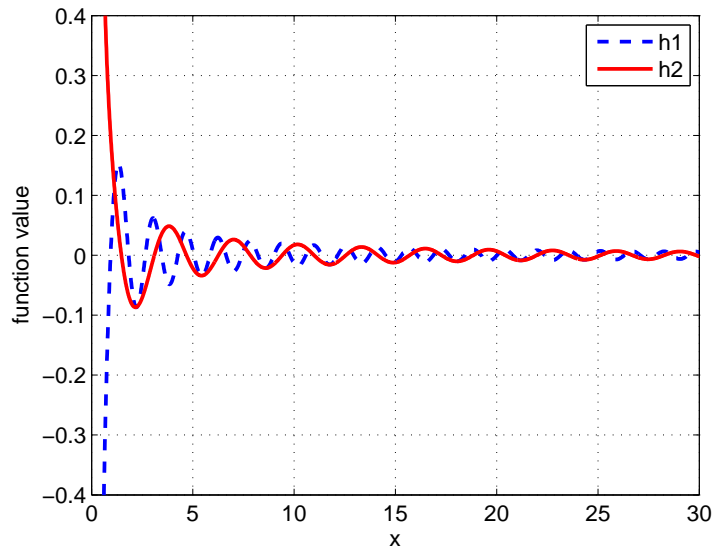


Figure 3.3: Test function (3.8): behavior of h_1 and h_2 .

Taking into account the asymptotic behavior of the Bessel functions of the first kind (3.2) and the second kind:

$$Y_a(px) \sim \sqrt{\frac{2}{\pi px}} \sin\left(px - \frac{a\pi}{2} - \frac{\pi}{4}\right) \quad (3.13)$$

it can be shown that the functions h_1 and h_2 for $p \neq q$ are asymptotically approaching cosine

functions in a similar manner to the Bessel function:

$$h_1(x; a, b, p, q) \sim \frac{1}{\pi\sqrt{pq}x} \cos \left\{ (p+q)x - \frac{(a+b+1)\pi}{2} \right\} \quad (3.14)$$

and

$$h_2(x; a, b, p, q) \sim \frac{1}{\pi\sqrt{pq}x} \cos \left\{ (p-q)x - \frac{(a-b)\pi}{2} \right\}. \quad (3.15)$$

Hence, the WA method should be as efficient for integrating the functions $f_b(x)h_1(x; a, b, p, q)$ and $f_b(x)h_2(x; a, b, p, q)$ over an infinite interval as for integrating $f_b(x)J_a(px)$.

As a conclusion, the New WA method should be able to evaluate the integral I_B in (3.1), including products of Bessel functions, by writing it as:

$$I_B = \int_0^\infty f_b(x)h_1(x; a, b, p, q)dx + \int_0^\infty f_b(x)h_2(x; a, b, p, q)dx \quad (3.16)$$

and evaluating independently each integral.

3.3 Algorithm description

Despite the positive conclusion of the previous paragraph, the direct application of the WA algorithm to the evaluation of the integrals arising in (3.16) is not convenient because of the singular behavior of the Bessel function of the second kind, $Y_a(x)$, at the origin. Depending on the combination of a, b, p and q , it can easily happen that one of the Bessel functions of the second kind has large magnitude, while the other oscillates. Then, the initial oscillations of the product of $Y_a(px)Y_b(qx)$ in equations (3.14)-(3.15) have large magnitudes, and dominate the results of the integrals involving h_1 and h_2 . Moreover, since the contributions of the product of Bessel functions of the second kind to h_1 and h_2 are of opposite sign, loss of accuracy will inevitably occur due to addition of two almost identical large numbers of different signs. To circumvent this drawback, we split the integral (3.1) into three parts, according to [11]:

$$\begin{aligned} I &= I_f + I_{h_1} + I_{h_2} = \\ &= \int_0^{x_{\max}} f_b(x)J_a(px)J_b(qx)dx + \int_{x_{\max}}^\infty f_b(x)h_1(x; a, b, p, q)dx + \int_{x_{\max}}^\infty f_b(x)h_2(x; a, b, p, q)dx \end{aligned} \quad (3.17)$$

thus avoiding the singular behavior of the functions h_1 and h_2 at the origin (see Fig. 3.3). The breakpoint x_{\max} used to split the integral into the finite and infinite parts is chosen to be the largest of the first zeros of $Y_a(px)$ and $Y_b(qx)$. Since the oscillatory behavior of the Bessel function of the second kind begins after its first zero, this choice of x_{\max} guarantees the proper behavior of the functions h_1 and h_2 , for $x > x_{\max}$. The integral I_f is the integral of a smooth and oscillating function on a finite interval. Even if a and b are significantly

different, the product $J_a(px)J_b(qx)$ on $[0, x_{\max}]$ will have only a finite number of oscillations. Therefore, I_f can be accurately calculated using adaptive Patterson quadrature formulas [15].

If $p \neq q$, both h_1 and h_2 are approaching a cosine function and the New WA algorithm can be applied for the evaluation of the semi-infinite integrals I_{h_1} and I_{h_2} . Equidistant break points given by

$$x_{1,i} = x_{\max} + i \frac{\pi}{(p+q)} \quad (3.18)$$

and

$$x_{2,i} = x_{\max} + i \frac{\pi}{|p-q|} \quad (3.19)$$

when $i = 0, 1, \dots$ are employed as upper limits of the partial integrals in the cases of I_{h_1} and I_{h_2} , respectively. The partial integrals are calculated as

$$I_{h_j,i} = \int_{x_{\max}}^{x_{j,i}} f_b(x)h_j(x; a, b, p, q)dx = \sum_{k=0}^i \int_{x_{j,k}}^{x_{j,k+1}} f_b(x)h_j(x; a, b, p, q)dx = \sum_{k=0}^i I_{P_{h_j,k}} \quad (3.20)$$

where $x_{j,0} = x_{\max}$, $j = 1, 2$ and $i = 1, 2, \dots$. Each of the finite integrals in (3.20), $I_{P_{h_j,k}}$, is evaluated using the Gauss-Legendre quadrature of order 16. Now, if we assume that the function f_b behaves asymptotically as

$$f_b(x) \sim C_1 e^{-\alpha_1 x} x^{\mu_1} \quad (3.21)$$

which is true for a wide class of functions appearing in practical problems, then the integrals I_{h_1} and I_{h_2} can be calculated applying WA formulas (2.78):

$$I_{hj} = \frac{\sum_{i=1}^N w_{j,i} I_{h_j,i}}{\sum_{i=1}^N w_{j,i}} \quad (3.22)$$

with

$$w_{j,i} = \binom{N-1}{i-1} e^{\alpha_1 x_{j,i}} x_{j,i}^{N-1-\mu_1}, \quad (3.23)$$

where $j = 1, 2$. The behavior of the transformed integrals I_f , I_{h_1} and I_{h_2} , together with the points $x_{1,i}$ and $x_{2,i}$ used as upper limits of partial integrals in (3.20), is shown in Fig. 3.4.

If $p = q$, the function h_1 still asymptotically approaches the cosine function, and therefore the integral I_{h_1} can be calculated as described above. On the other hand, h_2 now approaches a monotonically decreasing function. Hence, if in (3.21) the coefficient $\alpha_1 \neq 0$, the integral I_{h_2} can be still evaluated using the WA method, but now equidistant abscissas separated by π/α_1 must be used as upper limits of partial integrals in (3.20), and the weights are given

as (2.92):

$$w_{2,i} = (-1)^{i+1} \binom{N-1}{i-1} e^{\alpha_1 x_{2,i}} x_{2,i}^{N-1-\mu_1}, \quad (3.24)$$

Otherwise, for evaluating I_{h_2} one of the routines for adaptive integration over an infinite interval should be applied, as for example dqdagi IMSL routine or quadgk routine of MATLAB. Nevertheless, as soon as p and q are not identical, the function h_2 asymptotically approaches a cosine function, and the integral I_{h_2} can be evaluated using the above described technique.

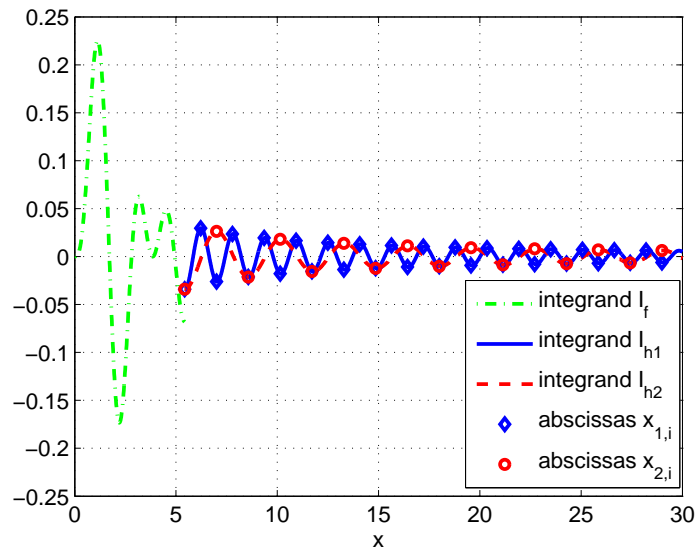


Figure 3.4: Test function (3.8): behavior of the three integrands, I_f , I_{h_1} and I_{h_2} , obtained by applying (3.17) and the abscissas $x_{1,i}$ and $x_{2,i}$ used as upper limits of the partial integrals.

3.4 Numerical results

In this section, we perform several numerical experiments in order to demonstrate the accuracy and efficiency of the proposed method. Besides (3.8) and (3.9), we test 8 more functions:

$$\text{Ex. 3 : } \int_0^{\infty} x^{-4} J_0(x) J_5(2x) dx = \frac{27}{4096} \quad (3.25)$$

$$\text{Ex. 4 : } \int_0^{\infty} x^{-2} J_0(5x) J_3(10x) dx = 0.703125 \quad (3.26)$$

$$\text{Ex. 5 : } \int_0^{\infty} x J_0(2x) J_0(3x) dx = 0 \quad (3.27)$$

$$\text{Ex. 6 : } \int_0^{\infty} J_0(x) J_1(1.5x) dx = \frac{2}{3} \quad (3.28)$$

$$\text{Ex. 7 : } \int_0^{\infty} J_2(4x) J_1(x) dx = \frac{1}{16} \quad (3.29)$$

$$\text{Ex. 8 : } \int_0^{\infty} \frac{x}{1+x^2} J_0(x) J_{20}(1.1x) dx \approx -6.05... \cdot 10^{-3} \quad (3.30)$$

$$\text{Ex. 9 : } \int_0^{\infty} \frac{x}{1+x^2} J_4(x) J_0(1.1x) dx = I_4(1) \cdot K_0(1.1) \quad (3.31)$$

$$\text{Ex. 10 : } \int_0^{\infty} \frac{x}{1+x^2} J_{20}(x) J_0(1.1x) dx = I_{20}(1) \cdot K_0(1.1) \quad (3.32)$$

where I_m is the modified Bessel function of the first kind and order m , and K_0 is the modified Bessel function of the second kind and order 0. Examples (3.25) - (3.27), (3.28) - (3.29) and (3.31)-(3.32) are special cases of the Abramowitz and Stegun [16] equations 11.4.41 and 11.4.42 (Weber-Schafheitlin integral) and Gradshteyn and Ryznik [17] equation 6.577, respectively. Although the integrals in (3.30) and (3.32) look very similar, to the best of author's knowledge, the analytical solution for (3.30) does not exist, and for its result we use the numerical value from [11], which is evaluated with machine precision accuracy. The number of significant digits versus the number of partial integrals is shown in Fig. 3.5, for the ten integrals.

From the presented results, one can easily identify that very high accuracy is obtained in all the cases that are studied. The lowest accuracy, of 11 significant digits, is obtained for the integral Ex. 9 (3.31). The reason is as follows: since p and q are close together, the interval of the finite integrals $I_{P_{h,j,k}}$, which is inversely proportional to $|p - q|$, is clearly becoming quite large. Then, depending on the behavior of the integrand, the order 16 of the Gauss-Legendre quadrature could be insufficient for evaluating the integrals $I_{P_{h,j,k}}$ to machine precision accuracy. The error of evaluating the partial integrals is thus introduced into the WA algorithm. This problem is easily solved by using a higher order of the quadrature rule. As general recommendation, in the cases that p and q are close together, a higher order of

Gauss-Legendre quadrature should be used for evaluating the partial integrals, in order to assure their accurate calculation.

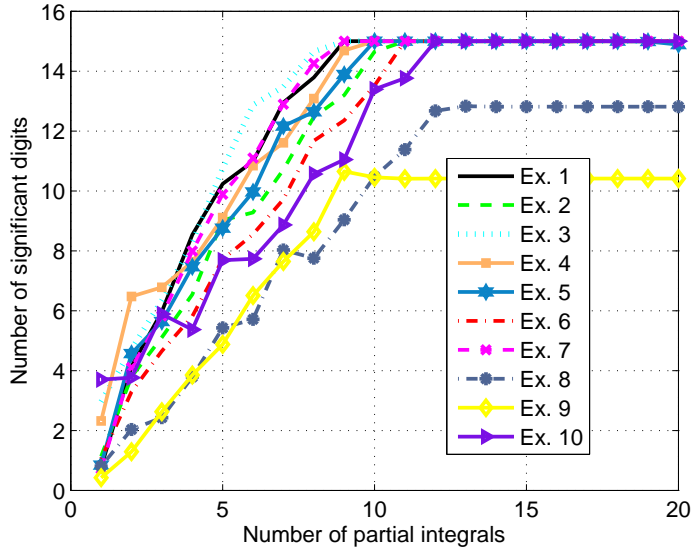
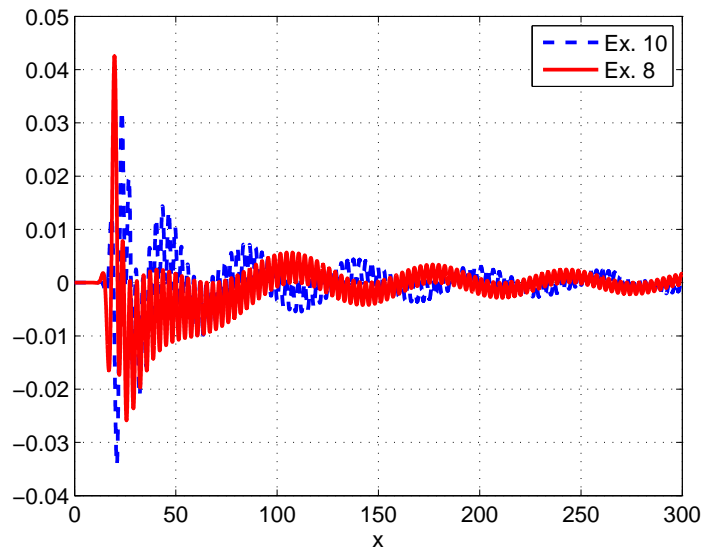


Figure 3.5: Number of significant digits vs. number of partial integrals for Ex. 1 - Ex. 10.

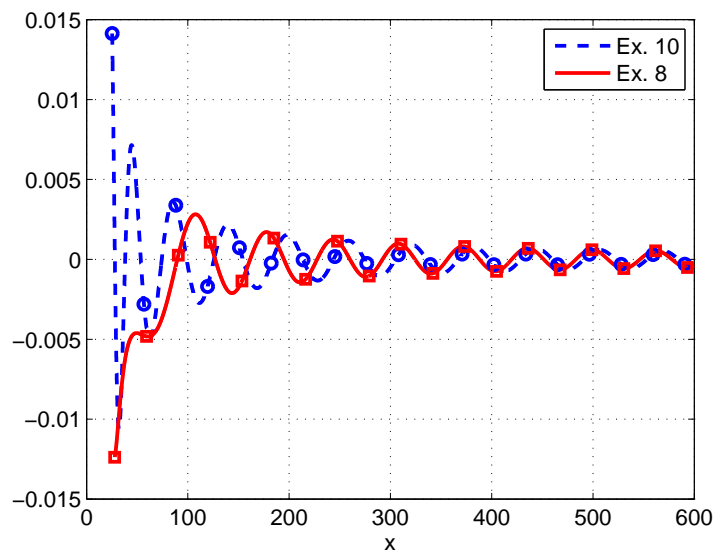
In [11] it was noticed that if a and b are not close together ($|a - b| > 5$), the function h_2 will pass through the transition region before settling into a simple oscillatory behavior of (3.15) for $p \approx q$. The larger the difference between the orders of the Bessel functions, the larger the range of p/q for which the function will exhibit this transition behavior. For p/q sufficiently different from one, the function h_2 does not exhibit this transition behavior and immediately settles into simple oscillations. In the transition region, the function h_2 can behave in two different manners.

The first possibility is that the function will start oscillating immediately, but with a small initial gap between the zeros of the function (see the dashed blue line in Fig. 3.6(b)). This behavior does not affect the performance of the method presented here, since this gap is small and we are not interested in the exact position of the function's zeros.

The second possibility is that the function does not oscillate in the transition region (see the solid red line in Fig. 3.6(b)). The range of this transition behavior depends on the difference between the orders of the Bessel functions. For moderate values of the difference ($|a - b| < 30$), this transition range is small enough so that it does not influence the behavior of the algorithm (see results for Ex. 8 (3.30) in Fig. 3.5), but for large values of the difference between the orders of the Bessel functions, the WA



(a) Behavior of the product of Bessel functions.



(b) Behavior of the function h_2 (—, - - -) and actual positions of the abscissas (\square , \circ).

Figure 3.6: Test functions Ex. 8 (3.30) and Ex. 10 (3.32).

extrapolation method should not be used before the oscillations start. Hence, the simplest approach is to use the higher value of x_{\max} as the lower limit of the integration interval for I_{h2} .

However, since this case was not encountered in any of the practical problems listed at the beginning of this chapter, we have not developed a special strategy for those cases. This should be the subject of further investigation. Finally, as an illustration of the complexity of the integrals we are dealing with, we have depicted in Fig. 3.6(a) the behavior of the products of the Bessel functions appearing in Ex. 8 (3.30) and Ex. 10 (3.32).

3.5 Generalization of the algorithm

The application of the method presented in this chapter is not limited to the integrals involving only the product of two Bessel functions of the first kind, $J_a(px)J_b(qx)$. Following the same philosophy, the method can be easily generalized for a wider class of problems. Indeed, we can use this method to deal with the integration of any irregularly oscillating function, which we are able to express as a linear combination of functions with regular oscillating behavior. Obviously, the method can be applied to products of sine and cosine functions since this was the original case from which the method was developed in Section 3.2. However, since the method is based on the asymptotic behavior of the Bessel functions, it can be generalized to the product of any two Bessel functions of the first and/or second kind, as well as to the product of the sine/cosine and Bessel functions. Here we show the strategy for the integral involving the Bessel function of the second kind, since an additional complication arises in this case. For example, the product of $Y_a(px)J_b(qx)$ can be expressed as

$$Y_a(px)J_b(qx) = h_1(x; a, b, p, q) + h_2(x; a, b, p, q) \quad (3.33)$$

where

$$h_1(x; a, b, p, q) = \frac{1}{2}[Y_a(px)J_b(qx) + J_a(px)Y_b(qx)] \quad (3.34)$$

and

$$h_2(x; a, b, p, q) = \frac{1}{2}[Y_a(px)J_b(qx) - J_a(px)Y_b(qx)]. \quad (3.35)$$

Again, using the asymptotic results for the Bessel functions of the first (3.2) and the second kind (3.13), it can be easily shown that, for $x \gg 1$,

$$h_1(x; a, b, p, q) \sim \frac{1}{\pi\sqrt{pqx}} \sin \left\{ (p+q)x - \frac{(a+b+1)\pi}{2} \right\} \quad (3.36)$$

and

$$h_2(x; a, b, p, q) \sim \frac{1}{\pi\sqrt{pqx}} \sin \left\{ (p-q)x - \frac{(a-b)\pi}{2} \right\}. \quad (3.37)$$

The remaining steps of the method are equivalent to those described within Section 3.3. However, due to the singular behavior of $Y_a(px)$ at $x = 0$, the finite integral I_f has an

endpoint singularity, and instead of the adaptive Patterson quadrature, the double-exponential quadrature [18] should be used, since the latter one has been shown to be very efficient for the integration of functions with singularities at the endpoints of the associated integration interval [19–21].

3.5.1 Products of more than two oscillating functions

This method can be also generalized for integrals involving products of more than two Bessel functions of arbitrary order and/or sine/cosine functions, although the derivation becomes more complicated. The complicated irregular oscillatory behavior of the product of n Bessel functions and/or sine/cosine functions can be rewritten as a sum of 2^{n-1} functions with asymptotically regular oscillatory behavior. As an illustration, we show here the case of the product of three Bessel functions of the first kind. The product of $J_a(px)J_b(qx)J_c(\sigma x)$ can be represented as a sum of four functions:

$$\begin{aligned} J_a(px)J_b(qx)J_c(\sigma x) = & h_1(x; a, b, p, q) + h_2(x; a, b, p, q) \\ & + h_3(x; a, b, p, q) + h_4(x; a, b, p, q) \end{aligned} \quad (3.38)$$

which are given by

$$\begin{aligned} 4h_1(x; a, b, p, q) = & [J_a(px)J_b(qx) - Y_a(px)Y_b(qx)]J_c(\sigma x) \\ & - [Y_a(px)J_b(qx) + J_a(px)Y_b(qx)]Y_c(\sigma x), \end{aligned} \quad (3.39)$$

$$\begin{aligned} 4h_2(x; a, b, p, q) = & [J_a(px)J_b(qx) - Y_a(px)Y_b(qx)]J_c(\sigma x) \\ & + [Y_a(px)J_b(qx) + J_a(px)Y_b(qx)]Y_c(\sigma x), \end{aligned} \quad (3.40)$$

$$\begin{aligned} 4h_3(x; a, b, p, q) = & [J_a(px)J_b(qx) + Y_a(px)Y_b(qx)]J_c(\sigma x) \\ & - [Y_a(px)J_b(qx) - J_a(px)Y_b(qx)]Y_c(\sigma x) \end{aligned} \quad (3.41)$$

$$\begin{aligned} 4h_4(x; a, b, p, q) = & [J_a(px)J_b(qx) + Y_a(px)Y_b(qx)]J_c(\sigma x) \\ & + [Y_a(px)J_b(qx) - J_a(px)Y_b(qx)]Y_c(\sigma x). \end{aligned} \quad (3.42)$$

Considering the asymptotic behavior of the Bessel functions (3.2) and (3.13), it can be straightforwardly shown that each of those four functions is asymptotically approaching cosine functions:

$$h_1(x; a, b, p, q) \sim \frac{\sqrt{2}}{2} \cdot \frac{1}{\sqrt{(px)^3}} \cdot \frac{1}{\sqrt{pq\sigma}} \sin \left\{ (p + q + \sigma)x - \frac{(a + b + c)\pi}{2} - \frac{3\pi}{4} \right\} \quad (3.43)$$

$$h_2(x; a, b, p, q) \sim \frac{\sqrt{2}}{2} \cdot \frac{1}{\sqrt{(px)^3}} \cdot \frac{1}{\sqrt{pq\sigma}} \sin \left\{ (p+q-\sigma)x - \frac{(a+b-c)\pi}{2} - \frac{\pi}{4} \right\} \quad (3.44)$$

$$h_3(x; a, b, p, q) \sim \frac{\sqrt{2}}{2} \cdot \frac{1}{\sqrt{(px)^3}} \cdot \frac{1}{\sqrt{pq\sigma}} \sin \left\{ (p-q+\sigma)x - \frac{(a-b+c)\pi}{2} - \frac{\pi}{4} \right\} \quad (3.45)$$

$$h_4(x; a, b, p, q) \sim \frac{\sqrt{2}}{2} \cdot \frac{1}{\sqrt{(px)^3}} \cdot \frac{1}{\sqrt{pq\sigma}} \sin \left\{ (p-q-\sigma)x - \frac{(a-b-c)\pi}{2} + \frac{\pi}{4} \right\} \quad (3.46)$$

Obviously, the next steps are equivalent to those explained when considering the case of the product of two Bessel functions.

3.5.2 Test cases for the generalized algorithm

To demonstrate the accuracy of this approach, the number of significant digits is shown in Fig. 3.7 for the following test cases:

$$\text{Ex. 11 : } \int_0^{\infty} J_1(x)Y_0(2x)dx = -\frac{1}{\pi} \ln(0.75) \quad (3.47)$$

$$\text{Ex. 12 : } \int_0^{\infty} J_1(3x)Y_0(7x)dx = -\frac{1}{3\pi} \ln\left(\frac{40}{49}\right) \quad (3.48)$$

$$\text{Ex. 13 : } \int_0^{\infty} xJ_3(4x)J_1(2x)J_2(x)dx = 0 \quad (3.49)$$

$$\text{Ex. 14 : } \int_0^{\infty} x^3J_2(x)J_1(2x)J_7(4x)dx = \frac{\Gamma(7)}{2^{10} \cdot \Gamma(2) \cdot \Gamma(3)}. \quad (3.50)$$

Examples (3.47) - (3.48) and (3.49) - (3.50) are special cases of the Gradshteyn and Ryznik [17] equations 6.512.6 and 6.573, respectively. From the presented results, one can see that all the integrals are evaluated with the machine precision accuracy, except the diverging integral Ex. 14 (3.50), which is defined only in the Abel sense. The achieved accuracy is still very high, more than 12 exact digits. In order to illustrate the complexity of the integrals we are coping with, we have depicted in Fig. 3.8 the behavior of the integrands from Ex. 13 (3.49) and Ex. 14 (3.50).

Following the same philosophy, similar formulas can be derived for any combination of the product of the Bessel functions of the first and/or second kind and arbitrary order and/or sine/cosine functions, if the integrals of this type are needed.

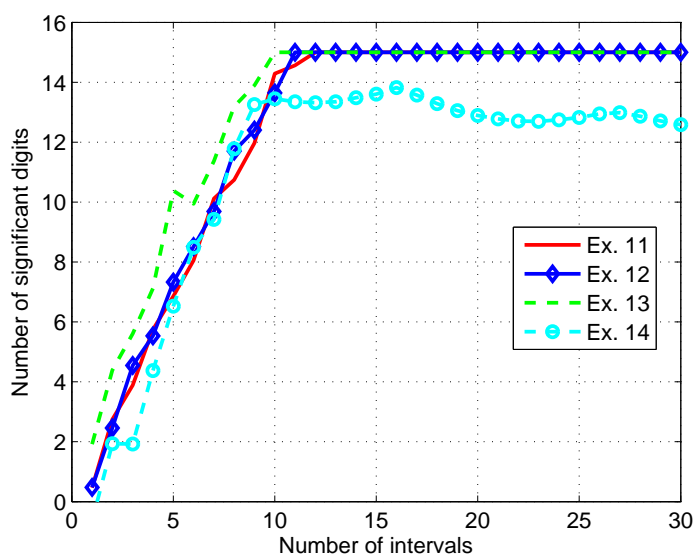
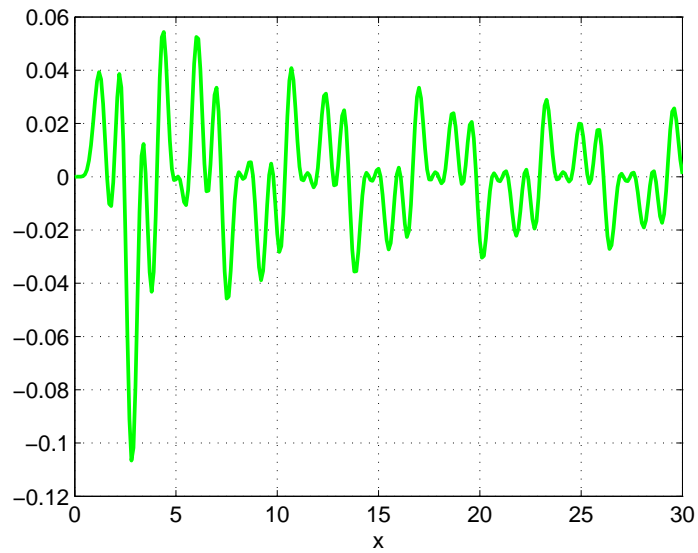
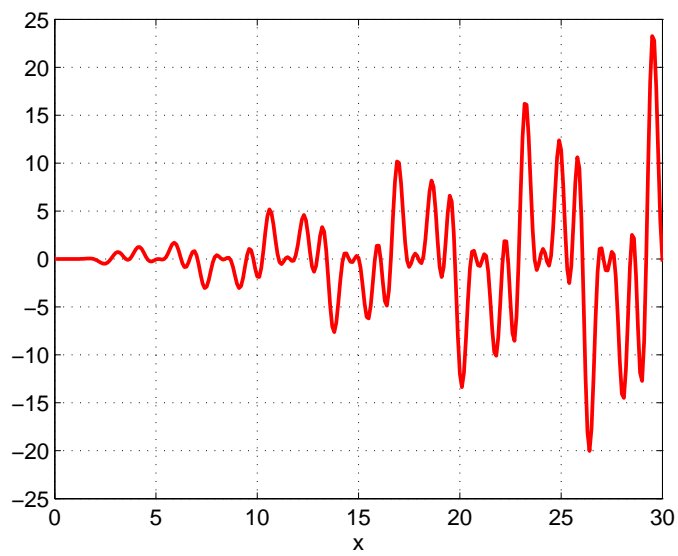


Figure 3.7: Number of significant digits vs. number of partial integrals for Ex. 11 - Ex. 14.



(a) Test function Ex. 13 (3.49).



(b) Test function Ex. 14 (3.50).

Figure 3.8: Behavior of the integrand.

3.6 Conclusion

The integrals involving products of the Bessel functions of the first and/or second kind and/or sine/cosine functions are very demanding to evaluate, due to the irregular oscillatory behavior of their kernels. Direct evaluation of these integrals, by truncating the integral at some finite value and neglecting the contribution of the remaining part (tail or remainder), typically returns at most a few digits of accuracy. The exception are the integrals with quickly converging kernels, for which higher accuracy might be obtained. However, even in these cases, evaluating the integrals with machine precision accuracy is usually computationally unacceptably expensive. On the other hand, for the integrals with diverging kernels, as for example integral Ex. 10 (3.50), which are defined only in the Abel sense, this approach completely fails to evaluate the true value of the integral, regardless of how large value we use for truncating the integral. Therefore, special methods for evaluating this type of integrals are needed.

In this chapter, an algorithm for efficient numerical evaluation of infinite-range integrals involving products of Bessel functions has been presented. The proposed method remains valid even when the integrands are not converging, but are defined only in the sense of Abel's summability. The algorithm requires rewriting the product of Bessel functions as a sum of asymptotically regularly oscillating functions, and makes use of the New WA extrapolation technique for their efficient calculation. First, the case of the product of two Bessel functions of the first kind of an arbitrary order has been described in detail, and possible complications involved in the method have been discussed. The superior performance of the proposed method has been demonstrated throughout numerical experiments.

Also, it has been shown that, by following the same philosophy, the method can be generalized to the product of an arbitrary number of Bessel functions of the first and/or second kind and/or sine/cosine functions, since the irregular oscillatory behavior of the integrand can be represented as a linear combination of functions with asymptotically simple oscillating behavior. The solution to the additional complications arising in the case that the integrand involves the Bessel function of the second kind, caused by its singular behavior at the origin, has been also suggested. Indeed, the method proposed here is the first one dealing with the integrals containing products of Bessel functions of the second kind, although some ideas about extending [9–11] to this type of integrals were suggested therein.

Finally, through the example of the integral containing a product of three Bessel functions of the first kind, the correctness of the approach used to generalize the method to the product of an arbitrary number of sine/cosine and/or Bessel functions has been proven.

A final word must be said on the behavior of the proposed method, when compared with other techniques targeting the same problem. The method presented in [11], which served as inspiration for transforming the product of the Bessel functions into the sum of regularly oscillating functions, uses the ϵ algorithm and the mW transformation of Sidi [12]

for accelerating the sequence of partial sums obtained after applying the integration-then-summation procedure to the transformed integral. The mW algorithm is suggested as the more efficient extrapolation technique for accelerating this sequence, but it calls for accurately locating zeros of h_1 and h_2 , which is not always an easy task. Alternatively, the ϵ extrapolation algorithm, which allows using the zeros of the asymptotic cosine approximation of h_1 and h_2 (3.14)-(3.15) instead of their exact zeros, could be used but this approach leads to less accurate results, because of the poorer convergence properties of the ϵ algorithm. The method that we propose uses the New WA extrapolation technique which has been shown in this thesis to be very robust and efficient for evaluation of semi-infinite range integrals with simply oscillating kernels. This presumption has been confirmed by the author throughout additional and exhaustive numerical experiments which have been submitted for publication [14, 22]. The New WA method uses equidistant break point as endpoints of partial integrals involved in the integration-then-summation technique, and since it obviates the need of locating the zeros of the integrands, it requires less function evaluations when compared with the mW algorithm, while preserving its excellent accuracy. Furthermore, the method from [11] offers solutions for integrals containing product of only two Bessel functions of the first kind.

The method proposed in [9], and further elaborated in [10], deals with integrals of products of an arbitrary number of Bessel functions of only the first kind with additional power, rational or exponential functions. The interval of integration is first split into a finite and an infinite part. The finite part is evaluated using the standard Gauss-Legendre quadrature. The integrand of the infinite path is approximated using asymptotic expansions and this approximation is integrated exactly with the help of the upper incomplete gamma function. Before evaluating these integrals, the breakpoint separating the infinite interval into a finite and a semi-infinite part, as well as the order of an infinite-range approximation, must be automatically determined. These two parameters directly influence the accuracy of the approximation of the infinite integral, and must be therefore carefully selected. There is an infinite number of possible pairs of values of these parameters. An optimization must be performed in order to choose those parameter values that minimize computational effort. Against this complexity, the method proposed here is clearly much easier to implement, since it calls only for the New WA extrapolation method and standard Gauss-Legendre quadrature, while leading to highly accurate results.

Bibliography

- [1] M. Ikonomou, P. Köhler, and A. F. Jacob, “Computation of integrals over the half-line involving products of Bessel functions, with application to microwave transmission lines,” *ZAMM -J. of Appl. Math. and Mech./ Zeitschrift für Angewandte Mathematik und Mechanik*, vol. 75, no. 11, pp. 917–926, Nov. 1995.
- [2] N. P. Singh and T. Mogi, “Electromagnetic response of a large circular loop source on a layered earth: a new computation method,” *Pure App. Geophys.*, vol. 162, no. 1, pp. 181–200, 2005.
- [3] N. N. Lebedev, I. P. Skalskaya, and Y. S. Uflyand, *Worked problems in applied mathematics*. New York: Dover publications, 1965.
- [4] A. M. J. Davis, “Drag modifications for a sphere in a rotational motion at small non-zero Reynolds and Taylor numbers: wake interference and possible Coriolis effects,” *J. Fluid Mech*, vol. 237, pp. 13–22, 1992.
- [5] J. Tanzosh and H. A. Stone, “Motion of rigid particle in a rotating viscous flow: an integral equation approach,” *J. Fluid Mech*, vol. 275, pp. 225–256, 1994.
- [6] M. Tezer, “On the numerical evaluation of an oscillating infinite series,” *J. Comput. Appl. Math.*, vol. 28, pp. 383–390, Dec. 1989.
- [7] P. M. Morse and H. Feshbach, *Methods of theoretical physics: part II*. Minneapolis: Feshbach publishing, LLC, 1981.
- [8] H. A. Stone and H. M. McConnell, “Hydrodynamics of quantized shape transitions of lipid domains,” *Proc. Math. and Phys. Sci.*, vol. 448, no. 1932, pp. 97–111, Jan. 1995.
- [9] J. Van-Deun and R. Coolis, “Algorithm 858: Computing infinite range integrals of an arbitrary product of Bessel functions,” *ACM Trans. Math. Software*, vol. 32, no. 4, pp. 580–596, Dec. 2006.
- [10] —, “Integrating products of Bessel functions with an additional exponential or rational factor,” *Computer Physics Communications*, vol. 178, no. 8, pp. 578–590, Apr. 2008.
- [11] S. K. Lucas, “Evaluating infinite integrals involving products of Bessel functions of arbitrary order,” *J. Comput. Appl. Math.*, vol. 64, no. 3, pp. 269–282, Dec. 1995.
- [12] A. Sidi, “A user-friendly extrapolation method for oscillatory infinite integrals,” *Math. Comp.*, vol. 51, no. 183, pp. 249–266, July 1988.

-
- [13] J. R. Mosig and R. Golubovic-Niciforovic, "Some new developments of the weighted averages algorithm," in *5th European Conference on Antennas and Propagation, EuCap 2011*, Rome, Italy, Apr. 11–15, 2011.
- [14] J. R. Mosig, "The weighted averages algorithm revisited," *IEEE Trans. Antennas Propag.*, submitted.
- [15] T. N. L. Patterson, "Algorithm 468: algorithm for automatic numerical integration over a finite interval," *Commun. ACM*, vol. 16, no. 11, pp. 694–699, Nov. 1973.
- [16] M. Abramowitz and I. Stegun, *Handbook of mathematical functions*. New York: Dover publications, Inc., 1965.
- [17] I. S. Gradshteyn and I. M. Ryzhik, *Table of integrals, series and products*. New York: Academic Press, 1965.
- [18] H. Takahasi and M. Mori, "Double exponential formulas for numerical integration," *Publ. RIMS, Kyoto Univ.*, vol. 9, no. 3, pp. 721–741, 1974.
- [19] M. Mori, "Quadrature formulas obtained by variable transformation and the DE-rule," *J. Comput. Appl. Math.*, vol. 12-13, pp. 119–130, May 1985.
- [20] M. Mori and M. Sugihara, "The double-exponential transformation in numerical analysis," *J. Comput. Appl. Math.*, vol. 127, no. 1–2, pp. 287–296, Jan. 2001.
- [21] M. Mori, "Discovery of the double-exponential transformation and its developments," *Publ. RIMS, Kyoto Univ.*, no. 41, pp. 897–935, 2005.
- [22] R. Golubovic-Niciforovic, A. G. Polimeridis, and J. R. Mosig, "Efficient algorithms for computing Sommerfeld integral tails," *IEEE Trans. Antennas Propag.*, submitted.

4 Particle Swarm Optimization Algorithm

4.1 Introduction

The design of electromagnetic (EM) structures is nowadays almost exclusively performed using one of the numerous electromagnetic simulators available on the market, in conjunction with optimization techniques. An EM structure is described by its physical dimensions and electromagnetic properties of the materials it is made of. These are input parameters to the EM solver, which, with a help of numerical methods, calculates different characteristics of the structure under consideration (for example Z, Y and S parameters, and antenna gain, among others). We can request for each of these characteristics to have the value that is lower, higher or equal to some desired value. These requirements represent the optimization criteria, and their number may vary from one (in the case of the simple optimization problems) to tens or even hundreds (for extremely complex problems). It is clear that in many cases it is enormously difficult to find a desired solution in reasonable time, unless sophisticated optimization methods are used that provide a “faster search” for the best performance of the structure of interest.

Scientists and engineers from all disciplines frequently have to deal with the classical problem of search and optimization. The optimization means an action of finding the best suited solution of some problem within the given constraints and flexibilities [1]. Of course, there might be not only one, but several solutions satisfying the given criteria, in which case we consider all of them to be equally good (according to our requirements). The flowchart describing the typical design procedure of an EM structure is represented in Fig. 4.1. The optimization algorithm is driving the optimization of the structure, while its EM analysis is done using an EM solver, which constitutes the inner step in an optimization loop. To link the optimization algorithm to the physical problem, a function that accurately describes the structure under consideration in terms of its parameters and given optimization criteria has to be defined. This function, which represents in a single number the optimality of the proposed solution, is called the objective, fitness or cost function.

During the last 20 years, the global, derivative-free optimization techniques, and more specifically those called evolutionary algorithms, have evolved as a successful alternatives to the conventional gradient-based local optimization algorithms [2, 3]. The latter ones frequently were not capable of solving real-world problems, for which no *a priori* information about the optimization space is available. In many cases the cost function is noisy and/or non-differentiable, and one cannot trust derivatives or approximate them by finite differences. Moreover, even when it is possible to numerically evaluate function derivatives, in many

practical problems it is very time-consuming. The evolutionary optimization algorithms, on the other hand, do not make any assumption about the optimization problem, and are therefore very well suited for a wide class of practical optimization problems. The well-established global optimization techniques are, among others, the Genetic Algorithm (GA) [4–7], the Simulated Annealing (SA) [8], the Ant Colony Optimization [9], and the more recently developed Particle Swarm Optimization (PSO) algorithm [10–12]. These methods do not rely neither on the derivative information of the cost function nor on its approximation, but use only the information based on the samples of the cost function. They belong to the class of heuristic optimization methods, i.e., there is no strict mathematical proof of their convergence after a finite number of iterations. Also, due to stochastic elements, they do not necessarily produce the same solution each time. Nonetheless, they have been widely used in many different fields, because of the very good results they usually yield. It has now become a well known fact among the researchers that these stochastic search algorithms perform better in complex real life optimization problems when compared to the classical deterministic algorithms.

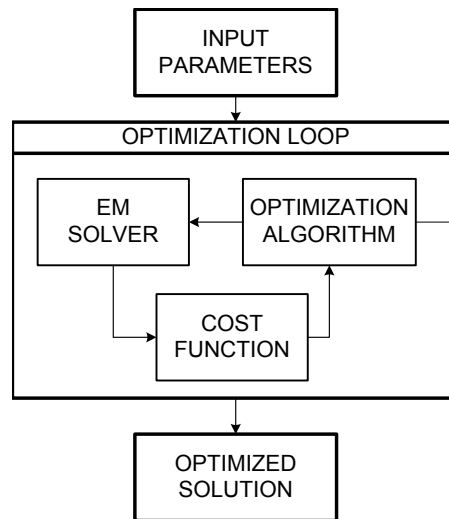


Figure 4.1: Flowchart describing the design procedure of an EM structure.

In this thesis we focus on the Particle Swarm Optimization algorithm, introduced in 1995 by Kennedy (a social psychologist) and Eberhart (an electrical engineer) [10]. By considering the movement of bird flocks or fish schools during the food-searching activities in the nature, they developed the powerful PSO algorithm. The enormous success of the PSO algorithm has been witnessed by more than 1000 papers published since then in different areas, such as antenna design, biological, medical, and pharmaceutical applications, optimization of communication networks, design and restructuring of electricity networks, image and video analysis applications, finance, etc [13]. As researchers have learned about the technique, they have derived new versions, developed new applications, and published theoretical studies of the effects of the various parameters and aspects of the algorithm, which are summarized in [14].

The PSO method was first used by the electromagnetic community in 2004 [11]. Since then, it has been continuously gaining popularity, because of its algorithmic simplicity, robustness and relatively fast convergence. In this chapter, we introduce the basic philosophy of the PSO algorithm in the concept of the optimization of multilayered electromagnetic structures. Moreover, with the aim of even further improvement of the convergence characteristics of the PSO algorithm, we propose a novel Tournament Selection PSO algorithm. This hybrid algorithm introduces the binary tournament selection, typical for the GA, into the classical PSO algorithm. Finally, the performances of both methods are compared through several multilayered EM optimization problems.

A very good performance of the PSO algorithm, when compared to other optimization algorithms, has been demonstrated by many authors [11, 15]. Clearly, the choice of the “best” optimization algorithm is problem dependent. For example, the gradient-based algorithms would be the best choice in case the cost function is differentiable and a good starting point for the algorithm can be easily determined. However, the gradient-based algorithm belong to the class of local optimization methods, since they converge very quickly to the steepest local minimum in the neighborhood of the starting point. Hence, there is a high chance that this algorithm will converge to the local, instead to the global minimum. On the other hand, evolutionary algorithms, being very general and robust, are suitable for a wide class of optimization problems, especially if little or nothing is known about the behavior of the cost function. Among them, we have chosen the PSO algorithm, which, due to its relative simplicity and its suitability for the implementation on the parallel processors, appears to be quite efficient in antenna optimizations. Finally, the purpose of this chapter is not to study which optimization method is the best for EM optimization problems, but rather to improve the performance of the PSO algorithm.

4.2 Classical PSO algorithm

The PSO algorithm is based on the analogy between the movement of bird flocks, fish schools, or bee swarms, on one side, and the optimization, on the other side. It simulates, in a computational way, the social behavior of the bee swarms in the process of food searching.

4.2.1 PSO language

Before describing the concept of the PSO algorithm, we must first introduce its special terminology:

- *Particle* or *agent* denotes each individual (bee).
- All particles searching in the optimization space form a *swarm*.
- *Fitness* or *cost function* links the optimization algorithm to the physical problem. It measures in a single number the optimality of the given solution (represented by the

position vector in the optimization space). Depending on the formulation of the problem, it could be necessary to find the minimum or maximum of this function. As the maximization problems can be straightforwardly reduced to minimization problems (by multiplying the cost function by -1), it is sufficient to observe only one of the formulations. Here we consider only the minimization problems, since they are more often encountered both in the practice and in the literature. Furthermore, when dealing with multiobjective optimizations (for example, in the case of addressing multiple design factors in practical engineering problems), it is possible to formulate a single-objective cost function by using the conventional weighted aggregation (CWA) approach, i.e., by weighting and summing up different factors. However, determining the best trade-off between all factors requires understanding the relative importance of each factor, and typically calls for an extensive tuning of weighting coefficients, especially if the objectives are unrelated. In that case, a more convenient approach is to define separate cost function for each objective, and perform the optimization based on the concept of the Pareto dominance [12, 16].

- \mathbf{p}_{best} is the vector representing the best position that the particle (bee) has found by itself. Each particle has its own \mathbf{p}_{best} , which is determined by the path it has flown. Every time the particle changes its position, it compares the cost function value of its new location to that of \mathbf{p}_{best} . If the new location has a smaller cost function value, \mathbf{p}_{best} is replaced with the new location vector.
- \mathbf{g}_{best} is the vector representing the best position found by the whole swarm together. Therefore, for the whole swarm there is only one \mathbf{g}_{best} . If any particle is at the location of a lower cost function, \mathbf{g}_{best} is replaced by that particle position.

4.2.2 Algorithm description

The PSO algorithm searches for the global minimum of the cost function, i.e., it minimizes the cost function of an EM problem by simulating movement and interaction of particles in a swarm. The position of a particle corresponds to one possible solution of the EM problem, i.e., it represents one point in the optimization space. Therefore, in the N -dimensional optimization space, each particle's position is represented by an N -dimensional vector. Since we assume that there is no *a priori* knowledge of the optimization problem, there is equal possibility of choosing any point in the optimization space at the beginning of the optimization. Hence, PSO starts with randomly chosen positions and velocities of particles. Assume that at a given iteration t a particle is located at \mathbf{x}_t . The particle knows its previous position \mathbf{x}_{t-1} , and the current best positions achieved by itself, \mathbf{p}_{best} and by the swarm, \mathbf{g}_{best} . It has, therefore, three logical directions to progress:

- a) follow its own inertia, defined by the difference $\mathbf{x}_t - \mathbf{x}_{t-1}$,
- b) approach its best result by following the difference $\mathbf{p}_{\text{best}} - \mathbf{x}_t$,

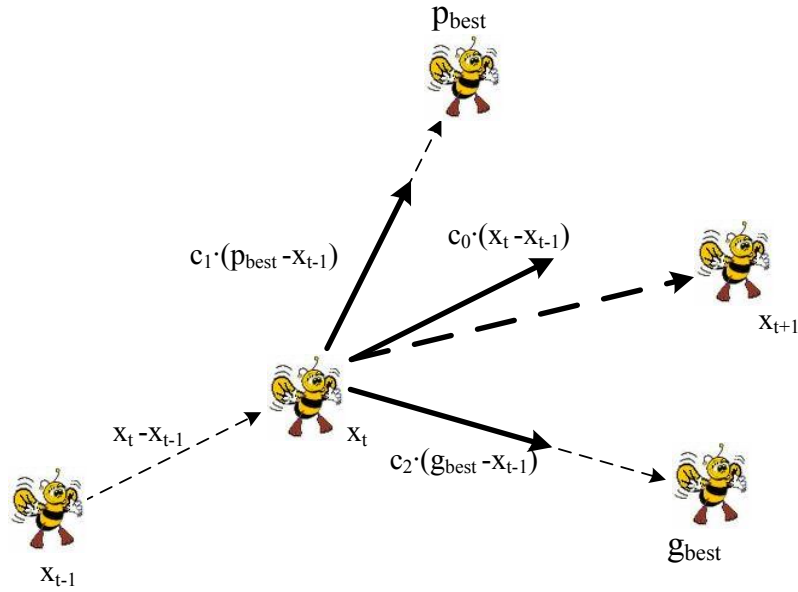


Figure 4.2: Updating the position of the particle.

c) approach the swarm best result by following the difference $\mathbf{g}_{best} - \mathbf{x}_t$.

In practice, a good compromise is to make the particle progress along a linear combination of these three possibilities (Fig. 4.2). Hence, the particle position is updated as:

$$\mathbf{x}_{t+1} = \mathbf{x}_t + \mathbf{v}_{t+1}, \quad (4.1)$$

with

$$\mathbf{v}_{t+1} = c_0 \cdot (\mathbf{x}_t - \mathbf{x}_{t-1}) + c_1 \cdot \text{rand}() \cdot (\mathbf{p}_{best} - \mathbf{x}_t) + c_2 \cdot \text{rand}() \cdot (\mathbf{g}_{best} - \mathbf{x}_t) \quad (4.2)$$

where $\text{rand}()$ is a function that generates uniformly distributed random numbers between 0 and 1. Quite logically the coefficients or weights c_0 , c_1 and c_2 are called, respectively the inertial, cognitive, and social rate coefficients. The absolute values of the coefficients define the acceleration characteristics. For instance, the choice $c_0 = 1$, $c_1 = c_2 = 0$ corresponds to a uniform particle motion, blindly dominated by inertia. A more critical factor is the consideration of the coefficient ratios and of their evolution during the optimization process. Indeed, it has been demonstrated (see [11, 12]) that, commonly, better performances are obtained when the value of the inertial coefficient c_0 (frequently called w in the literature) uniformly decreases during the iterative procedure. Also, as in most societies, a good choice is provided by selecting identical values for c_1 and c_2 . However, a degree of randomness between selfish and social behavior is most welcome (as in many societies) and can be achieved by multiplying c_1 and c_2 by $\text{rand}()$. In that way, some particles will show a somewhat unexpected behavior, deviating from the global trend and exploring

some *a priori* unpromising sections of the optimization space. Our implementation uses two independent random numbers in (4.2) to stochastically vary the relative pull of \mathbf{g}_{best} and \mathbf{p}_{best} .

Finally, the total velocity may undergo a normalization process to fit the optimization space. It has been found that if there are no limits for the velocity of the particles, they might frequently fly out of the meaningful optimization space [10, 11, 17]. Therefore, a maximal velocity V_{max} is introduced as another parameter of the PSO algorithm. V_{max} represents the maximal percentage of the dynamic range of the optimization variable for which the velocity can change in successive movements of the particle. In our implementation of the optimization, all dynamic ranges of the optimization variables are scaled to the interval $[-1.0, 1.0]$, and one unique value for the maximal velocity for all optimization variables is used.

However, experience has shown that this does not always confine the particles within the solution space, i.e., the particles may still occasionally fly to a position beyond the defined search space, and hence produce an invalid solution. To solve this problem, enclosing the search space with boundaries has been suggested in [11]. There are four types of boundary conditions [11, 18]. The characteristics of each boundary condition are depicted in Fig. 4.3, for the example of a two-dimensional optimization space. These boundary conditions are:

- *Absorbing walls.* When a particle hits one of the boundaries of the solution space, its velocity in that dimension is set to zero (see Fig. 4.3(a)).
- *Reflecting walls.* When a particle hits one of the boundaries of the solution space, its velocity in that dimension changes the sign and the particle is reflected back into the optimization space (see Fig. 4.3(b)).
- *Invisible walls.* The particles are allowed to fly out of the optimization space (see Fig. 4.3(c)). The particles that go out of the solution space are “penalized” by being assigned a very high predefined value of the cost function. The motivation for this technique is as follows. Since in many practical applications the most time-consuming part of the optimization process is the evaluation of the cost function, this approach saves computational time by calculating only the cost function for the particles within the allowed optimization space, while not interfering with the natural motion of the swarm.
- *Damping walls* boundary condition combines features of the absorbing and reflecting walls (see Fig. 4.3(d)). When a particle hits one of the boundaries (for example, a boundary of the dimension m), the part of the velocity in that dimension is absorbed by the boundary and the particle is then reflected back to the search space with a damped velocity:

$$v_{t+1,m} = -v_{t+1,m} \cdot \text{rand}(). \quad (4.3)$$

Therefore, the behavior of the proposed damping boundary lies in between the performances of the absorbing (when $\text{rand}() = 0$) and reflecting boundaries (when $\text{rand}() = 1$).

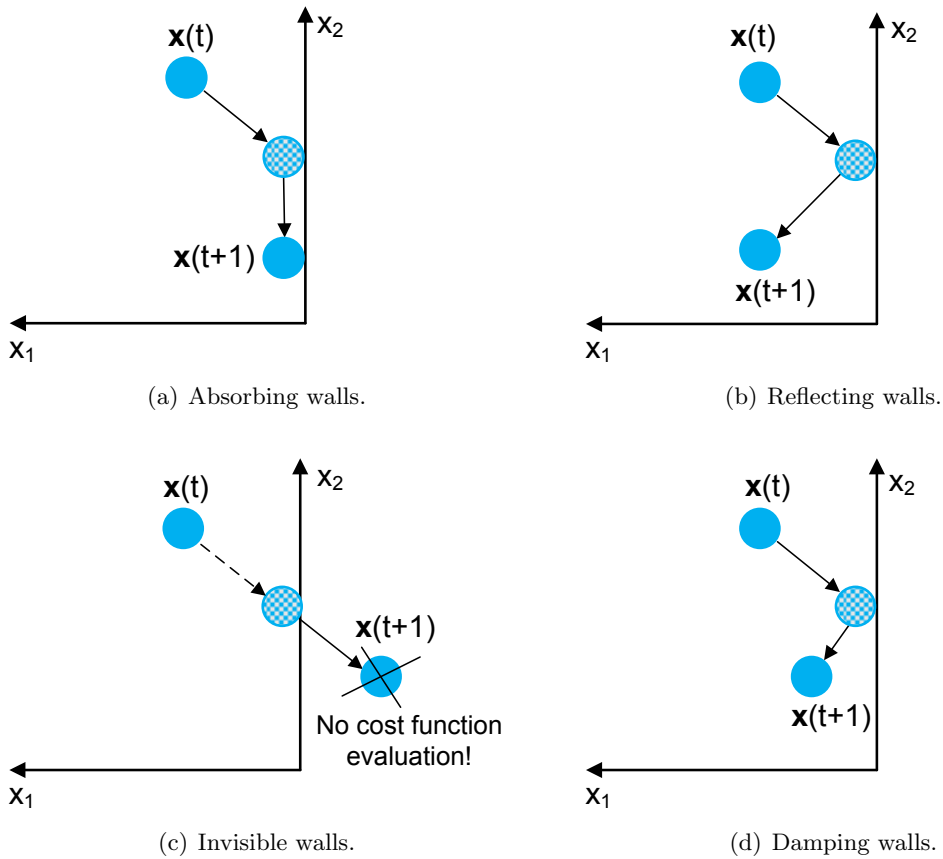


Figure 4.3: Different boundary conditions used for particles trying to escape from the optimization space. (Full circles represent the particle in two consecutive iteration t and $t + 1$. With dotted circle, the intermediate position of the particle, when it hits one of the boundaries, is illustrated).

In our implementation, we use the invisible-walls boundary condition, since it has been shown to outperform the other three conditions in terms of the computational cost [12]. Furthermore, it is easiest to implement, and in the case of well-defined optimization problems, the optimized solution is usually not extremely close to the boundaries of the optimization space.

Finally, trying to find a good trade-off between the global exploration and the local exploitation of the solution space, various values of the coefficients in (4.2) have been tested in the literature. First, for the sake of convergence the following condition must be fulfilled: $c_1 + c_2 < 3$ [17]. Naturally, in order to balance the cognitive part and the social part, most authors suggest $c_1 = c_2 = 1.5$. However, some authors suggest to use $c_1 > c_2$ in order to enforce the global perspective of the PSO. Indeed, increasing c_1 encourages global exploration

of a solution space as the move of each particle is more influenced by its own \mathbf{p}_{best} than by \mathbf{g}_{best} , while increasing c_2 encourages exploitation of the supposed global minima. Therefore, choice the $c_1 > c_2$ according to [19] allows maintaining the population's diversity for a large number of iterations, and consequently, avoids premature convergence to a local minimum, instead of the global minimum. The inertia coefficient c_0 determines the effect of particles previous velocity on the new velocity. The first versions of the PSO algorithm used constant value $c_0 = 0.73$. Note that this value is very close to the mean value of c_1 and c_2 (since in (4.2) they are multiplied by $\text{rand}()$ number). Later, the importance of exploration early in the run (during the first iterations) was observed, along with the increasing importance of exploitation of already found minima as run progresses and a time-varying (linearly decreasing from 0.9 to 0.4 over the course run) coefficient c_0 was suggested in [20]. Actually, it was noticed that larger values of c_0 encourage global exploration of the search space, because then the particle previous velocity has a dominant effect on the new velocity. Similarly, lower values of c_0 promote local exploitation, since the particles are, in that case, rapidly pulled towards \mathbf{p}_{best} and \mathbf{g}_{best} . Note that again, the mean value of c_1 and c_2 roughly corresponds to the value taken by c_0 in the intermediate steps of the optimization run. However, when using a time-varying coefficient c_0 , special care must be taken in choosing the number of iterations: a too large number will cause PSO to stagnate waiting for the decrease of c_0 to begin the exploitation of the minima, while a too low number could result in exploitation of local minima before the swarm had time to adequately explore the optimization space and find the lowest global minimum [11].

4.2.3 Algorithm implementation

This section presents the basic steps in the implementation of the PSO algorithm, which are pictorially shown in Fig. 4.4:

Define the optimization problem. The optimization starts with defining the optimization problem, i.e., describing the configuration of the EM structure (its geometry, material parameters, working frequency) and defining the optimization space (selecting the parameters to be optimized and their respective ranges). In addition, the PSO algorithm needs some internal parameters to be specified: the number of particles p , the coefficients c_0 , c_1 , c_2 and the maximal allowed velocity of the particles, V_{max} . Finally, the cost function f must be carefully defined. The PSO algorithm is “blind”, i.e., to perform an effective search for better and better structures, it only uses samples of the cost functions. Therefore, the cost function is the only connection between the optimization algorithm and the physical problem in hand, and its appropriate choice is a crucial step. All the previous steps must be developed for each optimization, while the following steps are independent of the structure being optimized.

Swarm initialization. To begin searching the solution space, the PSO swarm starts with randomly chosen positions \mathbf{x}_i and velocities \mathbf{v}_i ($i = 1, \dots, p$) of the particles, each of them being an N -dimensional vector, where N is the number of parameters to be optimized (dimension

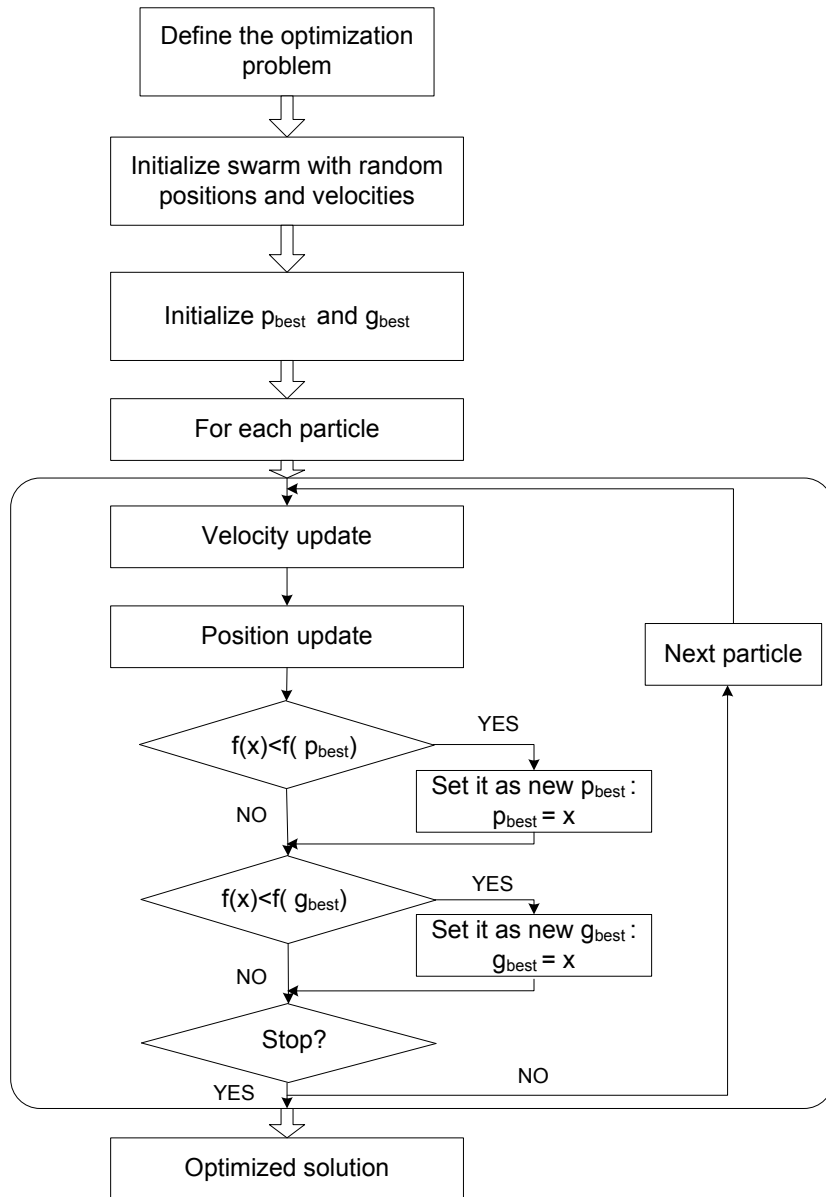


Figure 4.4: Flowchart depicting the PSO algorithm.

of optimization space). Since the initial position of a particle is the only position visited by the particle at the beginning of the optimization, that position becomes particle's \mathbf{p}_{best} . The position of the particle with the lowest cost function becomes \mathbf{g}_{best} .

Search of the optimization space. After the initialization of the algorithm, particles start interacting in the process of searching the optimization space, until the stopping criterion has been reached. As usual, the stopping criterion is either a cost function threshold or the maximum number of iterations. In our implementation, one iteration represents one call of the cost function evaluation, i.e., one call to EM solver. Hence, during one iteration one particle changes its velocity and position according to (4.1) and (4.2). The following steps are performed individually for each particle, cycling throughout the whole swarm:

- Update the particle's velocity according to (4.1)
- Update the particle's position according to (4.2)
- Update the particle's \mathbf{p}_{best} : if $f(\mathbf{x}_i) < f(\mathbf{p}_{\text{best}_i})$ then $\mathbf{p}_{\text{best}_i} = \mathbf{x}_i$
- Update \mathbf{g}_{best} : if $f(\mathbf{x}_i) < f(\mathbf{g}_{\text{best}})$ then $\mathbf{g}_{\text{best}} = \mathbf{x}_i$

Note that interaction of the particles while searching the optimization space is provided only through the information given by the “best” one, i.e., the whole swarm has only the information about the memory of the best member, \mathbf{g}_{best} . This position influences the movement of the whole swarm, while the best positions of the other particles, \mathbf{p}_{best} , influence only their own moves.

4.2.4 Swarm convergence

In order to have a better insight into the behavior of the particles throughout the optimization run, we consider a swarm consisting of 15 particles in the process of searching for a global minimum of the two-dimensional Rastrigin function within the search space $[-5, 5]$. This function is frequently used as a benchmark problem for optimization algorithms. For two independent variables, x_1 and x_2 , the Rastrigin function is defined as:

$$f(x_1, x_2) = 20 + x_1^2 + x_2^2 - 10(\cos(2\pi x_1) + \cos(2\pi x_2)). \quad (4.4)$$

Its behavior is depicted in Figs. 4.5 and 4.6. One can see that this is a fairly difficult optimization problem due to a large number of local minima in the search space. The function has just one global minimum at the point $[0, 0]$ in the x_1x_2 plane, where the value of the function is 0. At any local minimum other than $[0, 0]$, the value of the Rastrigin function is greater than 0. The further is the local minimum from the origin, the larger is the value of the function at that point.

The example of the particles progress throughout the optimization process is shown in Figs. 4.7 and 4.8. The asterisks in the plots represent the positions of the particles, while the

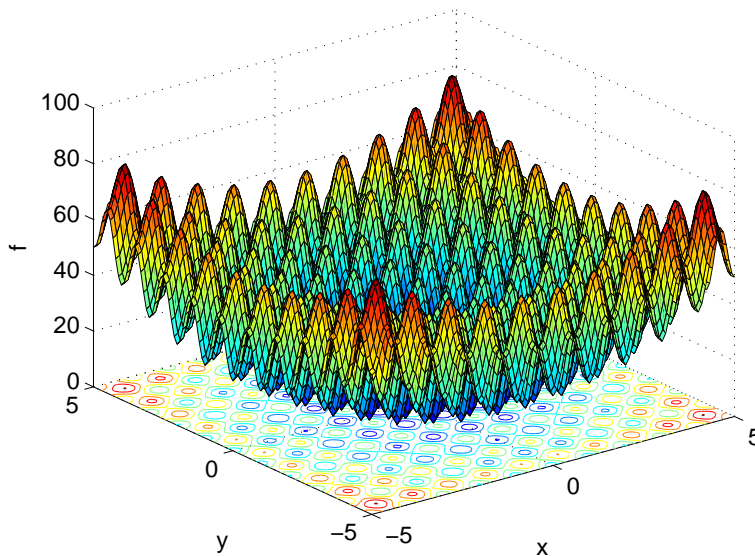


Figure 4.5: Two-dimensional Rastrigin function: 3-D view.

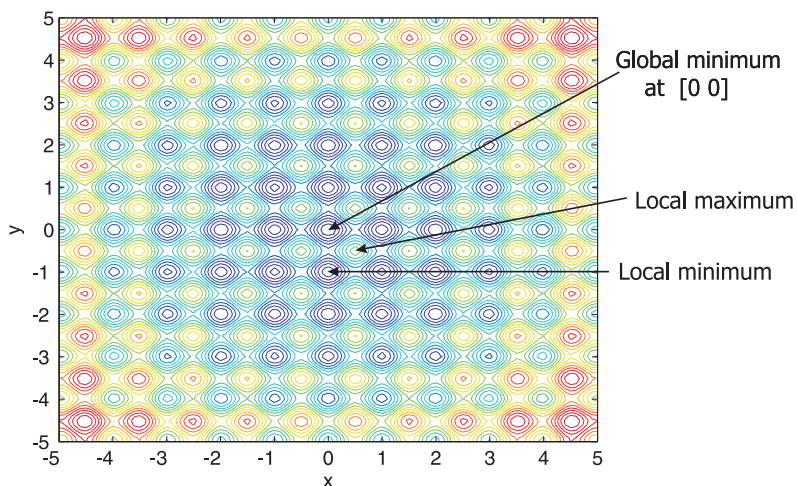


Figure 4.6: Two-dimensional Rastrigin function: alternating maxima and minima.

arrows show their velocity vectors. The particles start searching the optimization space from random positions and with random velocities. In the first few iterations, the swarm is spread within the optimization space. Moreover, the velocities of the particles are fairly large. This is the exploration phase of the optimization process, in which the particles are moving a lot, gathering information about the optimization space. As the optimization advances, and particles have more and more information about the optimization space, the optimization

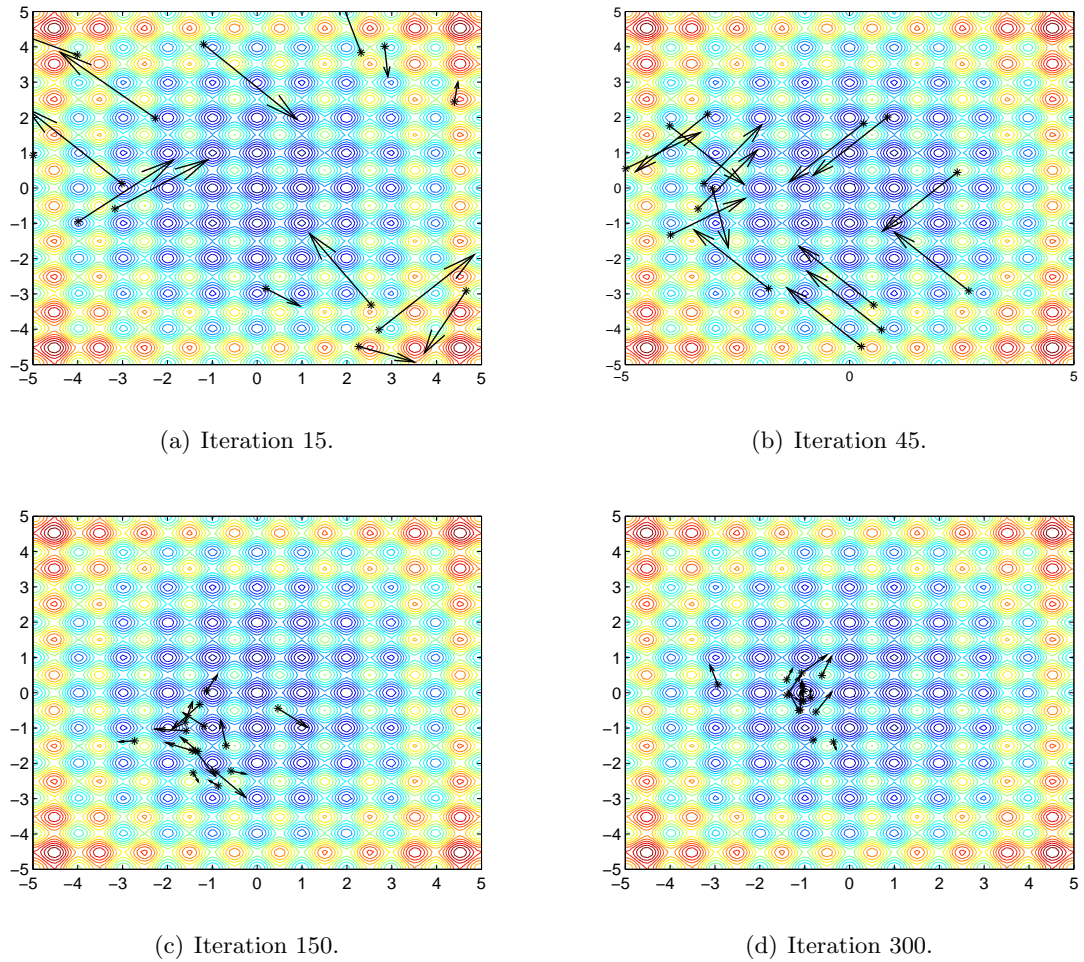


Figure 4.7: Swarm consisting of 15 particles in the process of searching for global minimum of the 2-D Rastrigin function.

slowly progresses towards its exploitation phase. The movement of the particles is less affected by inertia, and the collected information about the optimization space (\mathbf{p}_{best} and \mathbf{g}_{best}) starts having the dominant effect on the next particle positions. However, in our case the swarm starts converging towards the one of the local minima instead towards the global minimum. As can be seen from Figs. 4.8(a) - 4.8(c) at one moment almost all the particles are “trapped” in the local minimum. Their velocities are small, since all the particles have very similar positions and \mathbf{p}_{best} , and the coefficient c_0 has a relatively small value in this stage of the optimization run. Nevertheless, thanks to the `rand()` function in (4.2), some of the particles are still searching the parts of the optimization space that, according to the information the swarm has gathered until that moment (\mathbf{p}_{best} and \mathbf{g}_{best}), are considered

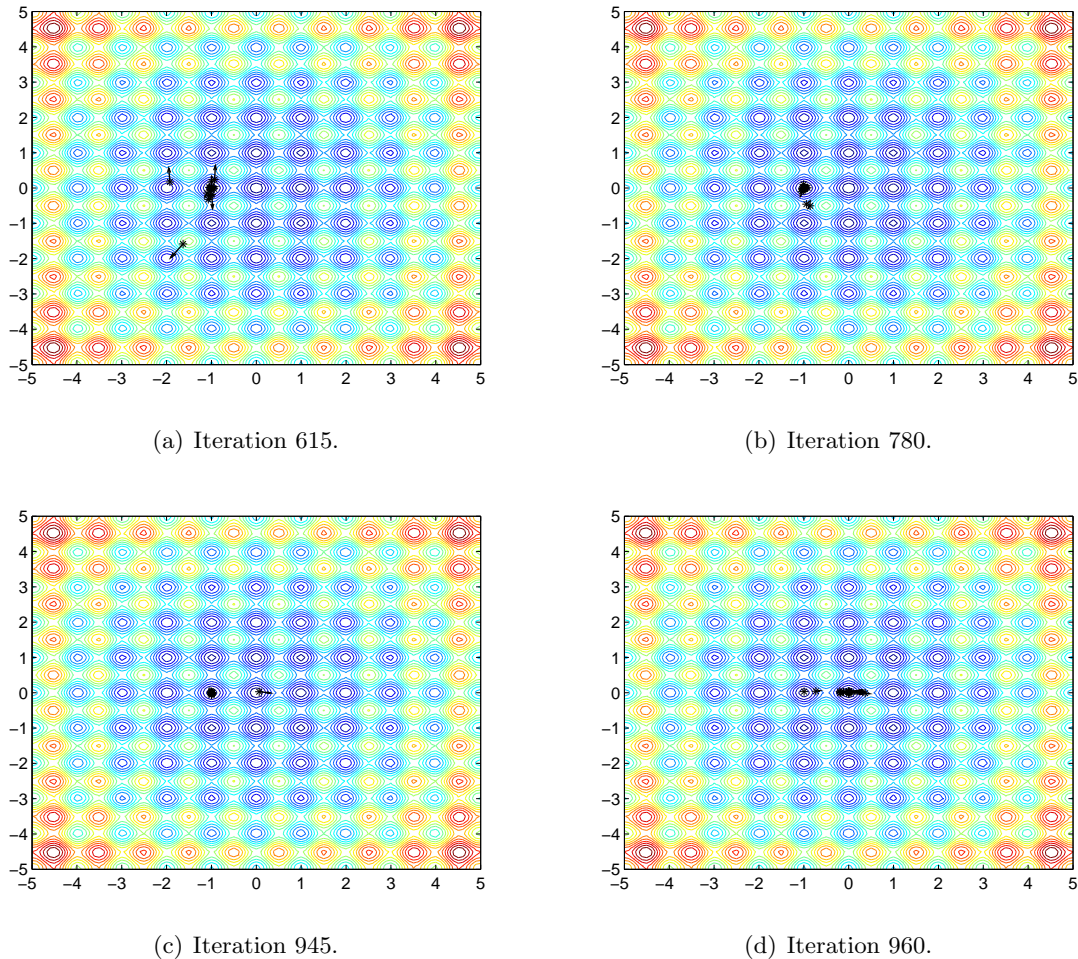


Figure 4.8: Swarm consisting of 15 particles in the process of searching for global minimum of the 2-D Rastrigin function.

unpromising. Thanks to this somewhat unexpected behavior of some particles, which deviate from the global trend, one of the particles “escapes” the local minimum (Fig. 4.8(c)), and finds the lower, global minimum. Already in the next iterations, the whole swarm is pulled towards the newly discovered better position (Fig. 4.8(d)). This move obviously would not be possible without the stochastic terms in (4.2). Therefore, these stochastic terms are one of the secrets of the success of the PSO algorithm in the process of searching the optimization space, and its ability to handle difficult multimodal problems.

Due to the quite large number of local minima in the search space, this optimization problem, although only two-dimensional, is fairly difficult. We have selected a moderate number of particles, which is one of the reasons why the algorithm, at one moment, converged to one of the local minima. This could have been avoided if a larger number of the particles were searching the optimization space. Nevertheless, this example is a very good illustration of the ability of the PSO algorithm to find the global minimum of the optimization problem, even after prematurely converging to one of the local minima.

4.3 Tournament selection PSO

The classical PSO algorithm is known to have very good convergence properties. However, since usually, the EM simulation is the most time-consuming part of the optimization, reducing the overall number of iterations (EM solver calls) is always welcome. Here we introduce the tournament selection strategy, typical for the Genetic Algorithm [7], to see if it can further improve the convergence performances of the classical PSO. This new hybrid algorithm is called the Tournament Selection PSO (TS-PSO) algorithm [21–23].

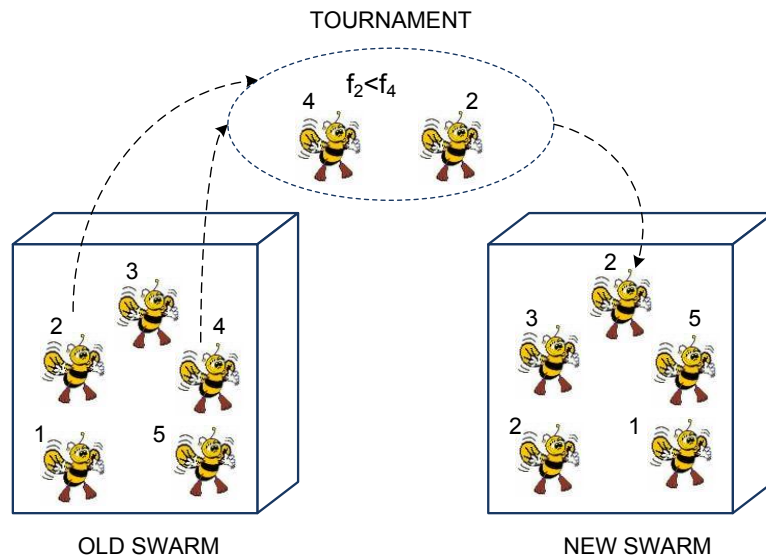


Figure 4.9: Binary tournament selection.

The tournament selection is introduced in the PSO algorithm in the following way. After the whole swarm has moved, the tournament selection is applied to form a new swarm. We randomly choose a subpopulation of M particles. These particles then compete in a tournament, based on the values of their cost functions. The particle with the lowest value of the cost function wins the tournament and becomes the member of a new swarm. All the particles are then placed back to the initial pool of particles, and the process is repeated for p times, where p is the number of particles in the initial swarm. Therefore,

the new swarm, built in this manner, can have several particles with the same starting position.

The implementation of this strategy is fairly straightforward. First, we enumerate all the particles in the swarm. Then, for the tournament played by M particles, we generate M random integers between 1 and the number of the particles in the swarm, p . These numbers indicate the particles participating in the tournament. For the sake of illustration, we consider the case of a binary tournament selection ($M = 2$) and a swarm consisting of $p = 5$ particles (see Fig. 4.9). We generate two random numbers between 1 and 5. If, for example, the numbers 2 and 4 are generated, so that in the tournament selection we should compare the cost functions of the 2nd and 4th particle from the swarm. The one with the smaller cost function is selected for the new swarm. These two particles are then placed back in the pool, and the procedure is repeated 5 times.

The TS - PSO algorithm differs from the classical algorithm only in the tournament selection, i.e., each time the whole swarm has moved, the tournament selection is played in order to build a new swarm. This new swarm continues searching the optimization space (during the next p iterations) in the same manner as the classical PSO algorithm. Note, that in the case of the TS - PSO, the swarm changes after every p iterations.

4.4 Optimization Examples

Both the classical PSO and the new hybrid version of the PSO, called the Tournament Selection PSO algorithm, have been applied to several layered-media problems, in order to compare their convergence performances. Both algorithms are implemented in C/C++ programming language. For the analysis of EM structures, we use an in-house solver (implemented in FORTRAN programming language) based on the mixed-potential integral equations specially tailored to model planar multilayered structures [24, 25]. The interface between the PSO algorithms and the EM simulator is provided by MATLAB, which allows for a proper automation of the exchange and post-processing tasks involved in the computation of the cost function. The implemented PSO parameters are now detailed for each case.

Classical PSO algorithm

For the classical PSO algorithm, the following values of the parameters are used in all the considered optimization examples: time-varying c_0 decreasing from 0.9 to 0.4 over the course run is set, as suggested in [11], and c_1 and c_2 are equal to 1.5. The maximal particle velocity is set to be equal to the dynamic range for each dimension of the optimization space. The invisible-wall boundary condition is applied for particles that go out of the solution space. Note that since c_1 and c_2 are multiplied by a random number $\text{rand}()$, their mean value (0.75) roughly corresponds to the value taken by c_0 in the intermediate steps of the optimization process.

Tournament selection PSO algorithm

For the TS - PSO the binary tournament selection strategy ($M = 2$) is selected because of the following reason. The tournament selection strategy increases the search pressure and speeds up the convergence because several copies of the better individuals can propagate from iteration to iteration, whereas the individuals with larger values of the cost function are more likely to be lost. The search pressure is easily adjusted by changing the tournament size. If the tournament size is larger, weak individuals have smaller chances to propagate. Therefore, the higher is the number of the particles playing the tournament, the faster is the convergence, since the probability of propagating good solutions is increased. However, a too strong pressure often causes the premature convergence of the algorithm into a local minimum, and the swarm diversity is likely to be quickly lost. For that reason, the tournament size $M = 2$ is chosen. Moreover, in order to keep the diversity of the swarm throughout the optimization, the constant value $c_0 = 0.73$ is used.

4.4.1 First optimization problem: microstrip antenna

The first optimization problem is a classical microstrip antenna [26]. It consists of a feeding line, a quarter-wavelength transformer, and a radiating patch, as illustrated in Fig. 4.10. The

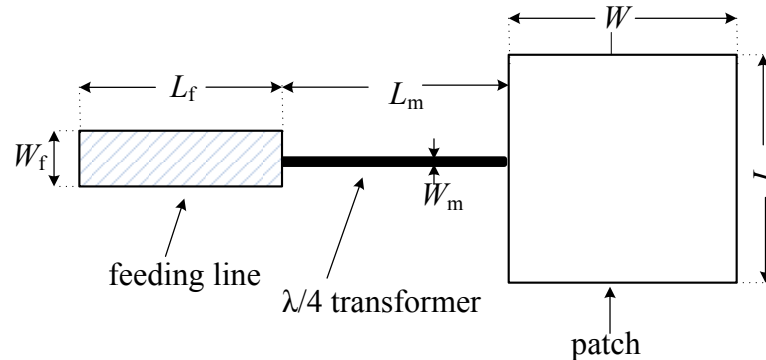


Figure 4.10: Microstrip antenna.

optimization parameters are the length L and the width W of the patch (which determine the operating frequency of the antenna) and the length L_m and the width W_m of the quarter-wavelength transformer (a matching transmission line that ensures the impedance of the patch is matched to the 50Ω feeding line). The length and the width of the 50Ω feeding line are $L_f = 20$ mm, $W_f = 2.403$ mm. The dielectric layer on which the metallization is printed is Duroid with $\epsilon_r = 2.2$ and $\tan \delta = 0.0009$ of thickness $h = 0.7874$ mm and backed by a ground plane.

A microstrip antenna is a narrowband radiator. By optimizing the specified geometry, its bandwidth is not affected, but we will be able to target its operating frequency (in our case set to be $f = 3$ GHz). The optimization goal is to minimize the reflection coefficient of the

structure, s_{11} , at the operation frequency.

The cost-function is defined as:

$$f_{\text{cost}} = s_{11} \text{ [dB]} \quad (4.5)$$

and the boundaries of the optimization space are reported in Table 4.1. By using decibels (dB) the minimum of the cost function is put at $f_{\text{cost}} = -\infty$, instead of the more intuitive $f_{\text{cost}} = 0$, if linear values of the reflection coefficient s_{11} are used. Nevertheless, using dB gives more dynamics to the search. On the other hand, values below -40 dB (10^{-4} in linear scale) are considered negligible in practice.

Both algorithms are run for 10 times to estimate the average outcome of the optimization. The averaged-best found values of s_{11} versus the number of iterations are shown in Fig. 4.11.

Table 4.1: Input and optimized parameters of the microstrip antenna optimization problem.

parameter to optimize	boundaries [mm]	optimized value [mm]
patch length L	$20 \leq L \leq 50$	33.112491
patch width W	$20 \leq W \leq 50$	48.687532
quarter-wavelength transformer length L_m	$10 \leq L_s \leq 30$	20.442849
quarter-wavelength transformer width W_s	$0.1 \leq W_s \leq 10$	0.753805

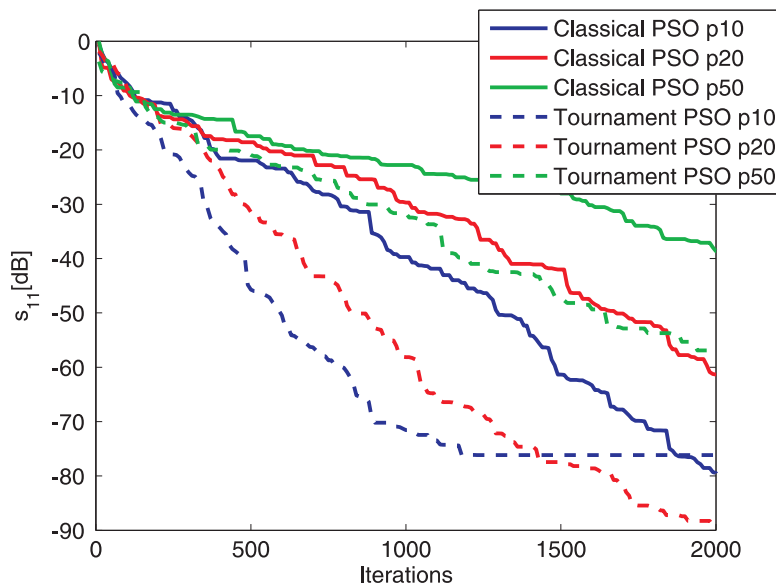


Figure 4.11: Microstrip antenna optimization problem: convergence of the algorithms.

We see that the tournament selection significantly speeds up the convergence of the PSO

algorithm. For example, to find the geometry with $s_{11} = -40$ dB, the TS-PSO needs 500 iterations, whereas the classical PSO requires more than 1000 iterations (cost function evaluations). Therefore, the TS-PSO is twofold more efficient, in terms of computational time, when compared to the classical PSO. Furthermore, the optimum number of particles p is equal to 20 for this 4-dimensional optimization problem. Finally, the parameters of the best among optimized geometries are given in Table 4.1, leading to $s_{11} < -40$ dB.

4.4.2 Second optimization problem: SSFIP antenna

The second optimization problem is an SSFIP (Strip-Slot- Foam-Inverted-Patch) antenna [27], shown in Fig. 4.12. It is well-known that microstrip patch antennas have significant advantages in terms of size, ease of fabrication and compatibility with printed circuits. However, their main drawback is their relative narrow bandwidth. In order to overcome this problem, the SSFIP antenna concept was developed [27]. The coupling from the line to the patch is provided by a slot etched in the ground plane. The slot must not resonate over the operating frequency band of the antenna in order to avoid radiation toward the back of antenna, which would interfere with the radiation from the patch.

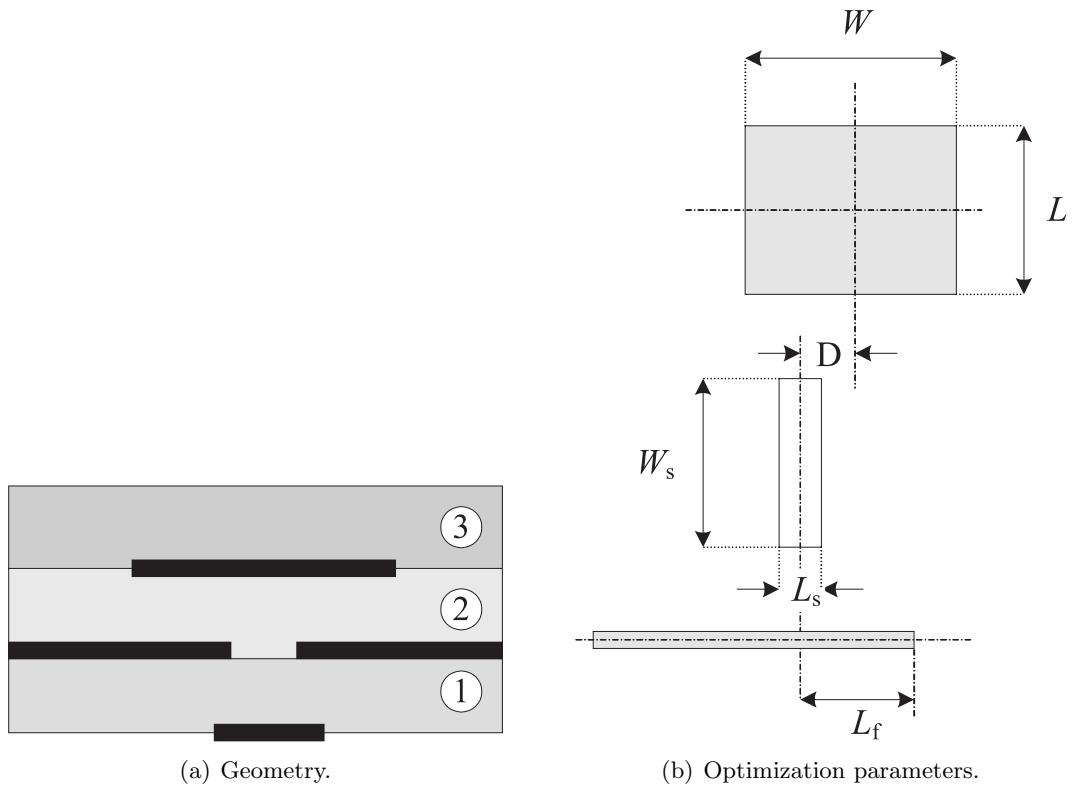


Figure 4.12: SSFIP antenna.

The optimization parameters are: the length L and the width W of the patch antenna, the length L_s and the width W_s of the slot, the offset D between the centers of the patch antenna and the slot, and the length of the feeding line (see Fig. 4.12). The boundaries of the optimization space are reported in Table 4.2.

Table 4.2: Input and optimized parameters of the SSFIP antenna optimization problem.

parameter to optimize	boundaries [mm]	optimized value [mm]
patch length L	$10 \leq L \leq 100$	67.891742
patch width W	$10 \leq W \leq 100$	38.577134
slot length L_s	$0.5 \leq L_s \leq 4$	0.920157
slot width W_s	$10 \leq W_s \leq 90$	64.208835
feeding line length L_f	$0 \leq L_f \leq 50$	44.060315
patch-slot offset D	$-30 \leq D \leq 30$	27.525812

The optimization goal is to minimize s_{11} at the operating frequency (1.75 GHz), while controlling the antenna bandwidth. From our experience, we defined the cost function as follows:

$$f = 1.66 \text{ GHz} \Rightarrow f_{\text{cost1}} = \begin{cases} 0, & \text{if } s_{11}(f) > -5 \text{ dB} \\ |s_{11}(f)| - 5, & \text{if } s_{11}(f) \leq -5 \text{ dB} \end{cases} \quad (4.6)$$

$$f = 1.75 \text{ GHz} \Rightarrow f_{\text{cost2}} = \begin{cases} 0, & \text{if } s_{11}(f) \leq -50 \text{ dB} \\ 50 - |s_{11}(f)|, & \text{if } s_{11}(f) > -50 \text{ dB} \end{cases} \quad (4.7)$$

$$f = 1.84 \text{ GHz} \Rightarrow f_{\text{cost3}} = \begin{cases} 0, & \text{if } s_{11}(f) > -5 \text{ dB} \\ |s_{11}(f)| - 5, & \text{if } s_{11}(f) \leq -5 \text{ dB} \end{cases} \quad (4.8)$$

$$f_{\text{cost}} = f_{\text{cost1}} + f_{\text{cost2}} + f_{\text{cost3}} \quad (4.9)$$

If the optimized structure satisfies our requirements, i.e., if the reflection coefficient of the structure, s_{11} , is greater than -5 dB at the frequencies $f = 1.66$ GHz and $f = 1.84$ GHz, and smaller than -50 dB at $f = 1.75$ GHz, the cost function will have the optimal, minimal value $f_{\text{cost}} = 0$.

Both algorithms are run for 10 times to estimate the average outcome of the optimization. The averaged-best found solutions versus the number of iterations are shown in Fig. 4.13. After 2000 iterations both algorithms converge to practically the same value. Nevertheless, the Tournament Selection PSO algorithm has faster convergence. Within the given optimization space, there are several solutions satisfying our requirements. The geometry of one of those solutions is given in Table 4.2, and the s_{11} parameter corresponding to that solution is depicted in Fig. 4.14. We should point out that both algorithms found solutions satisfying our requirements.

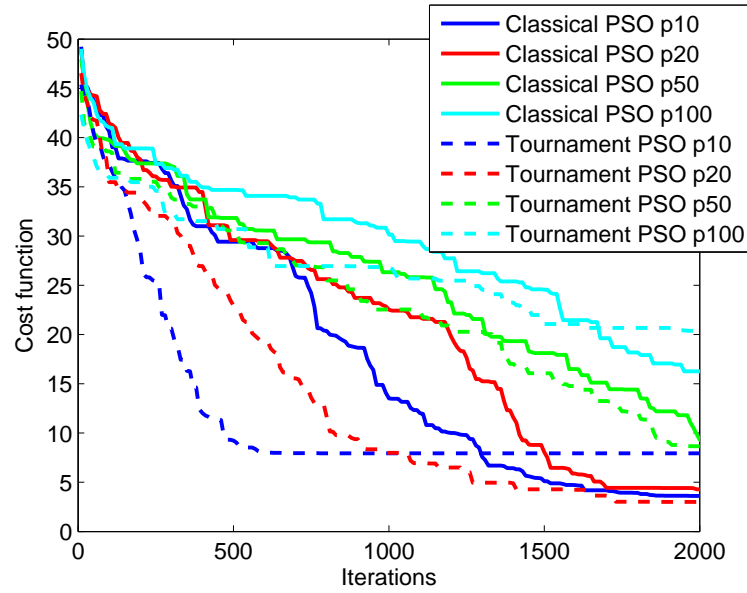


Figure 4.13: SSFIP optimization problem: convergence of the algorithms.

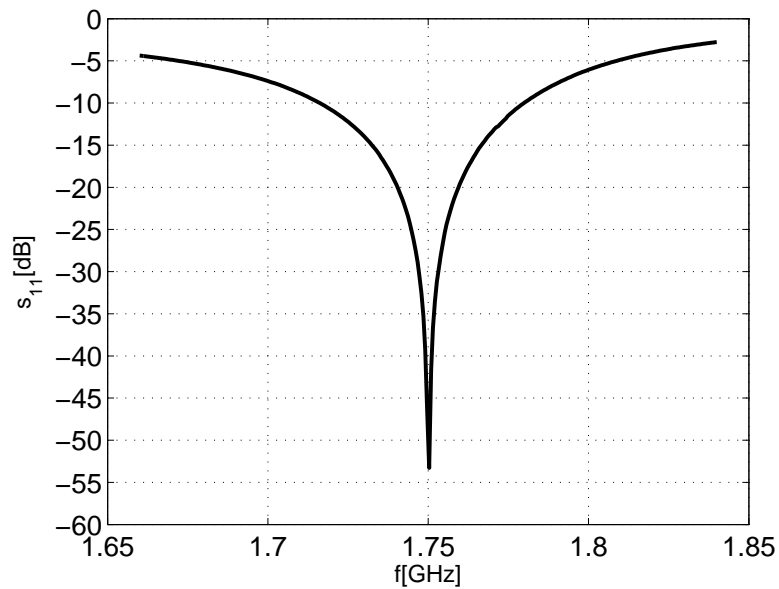


Figure 4.14: The reflection coefficient s_{11} of the SSFIP antenna that satisfies our requirements.

4.4.3 Third optimization problem: Broadside coupled filter

The third optimization problem is a broadside coupled filter, shown in Fig. 4.15. All the resonators are printed on different substrates and placed one above the other. The optimization parameters are the lengths of the resonators, L_1 and L_2 , their width, W and the resonator offsets from the box, dX_2 and dX_3 (see Fig. 4.15). The boundaries of the optimization space are reported in Table 4.3.

We want our filter to have $s_{11} \leq -20$ dB for the band-pass frequencies, and we want to control its bandwidth. For that purpose, the cost-function is defined as:

$$f = 6.835 \text{ GHz} \Rightarrow f_{\text{cost}1} = |s_{11} + 5| \quad (4.10)$$

$$f = 6.840 \text{ GHz} \Rightarrow f_{\text{cost}2} = |s_{11} + 10| \quad (4.11)$$

$$f = 6.865 \text{ GHz} \Rightarrow f_{\text{cost}3} = \begin{cases} 0, & \text{if } s_{11}(f) \leq -20 \text{ dB} \\ 20 - |s_{11}(f)|, & \text{if } s_{11}(f) > -20 \text{ dB} \end{cases} \quad (4.12)$$

$$f = 6.905 \text{ GHz} \Rightarrow f_{\text{cost}4} = \begin{cases} 0, & \text{if } s_{11}(f) \leq -20 \text{ dB} \\ 20 - |s_{11}(f)|, & \text{if } s_{11}(f) > -20 \text{ dB} \end{cases} \quad (4.13)$$

$$f = 6.945 \text{ GHz} \Rightarrow f_{\text{cost}5} = \begin{cases} 0, & \text{if } s_{11}(f) \leq -20 \text{ dB} \\ 20 - |s_{11}(f)|, & \text{if } s_{11}(f) > -20 \text{ dB} \end{cases} \quad (4.14)$$

$$f = 6.965 \text{ GHz} \Rightarrow f_{\text{cost}6} = |s_{11} + 10| \quad (4.15)$$

$$f = 6.875 \text{ GHz} \Rightarrow f_{\text{cost}7} = |s_{11} + 5| \quad (4.16)$$

$$f_{\text{cost}} = \sum_{i=1}^7 f_{\text{cost}i} \quad (4.17)$$

If all our requirements are satisfied, the cost function will have the optimal, minimal value $f_{\text{cost}} = 0$. In the case that any of the requirements is not satisfied, the value of the cost function will be greater than 0.

Both algorithms are run for 10 times. The averaged-best found solutions versus the number of iterations are shown in Fig. 4.16. For a small number of iterations the Tournament Selection PSO algorithm has faster convergence. After 1000 iterations it is slightly outperformed by the classical PSO algorithm. Nevertheless, the Tournament Selection PSO still finds a very good solution. The cost function value of the best of 10 solutions found by the classical PSO is 2.562, while the best solution found by the Tournament Selection PSO gives slightly higher value of the cost function: 2.709. The geometry of the best found solution is reported in Table 4.3, and the s_{11} parameter of the corresponding structure is shown in Fig. 4.17.

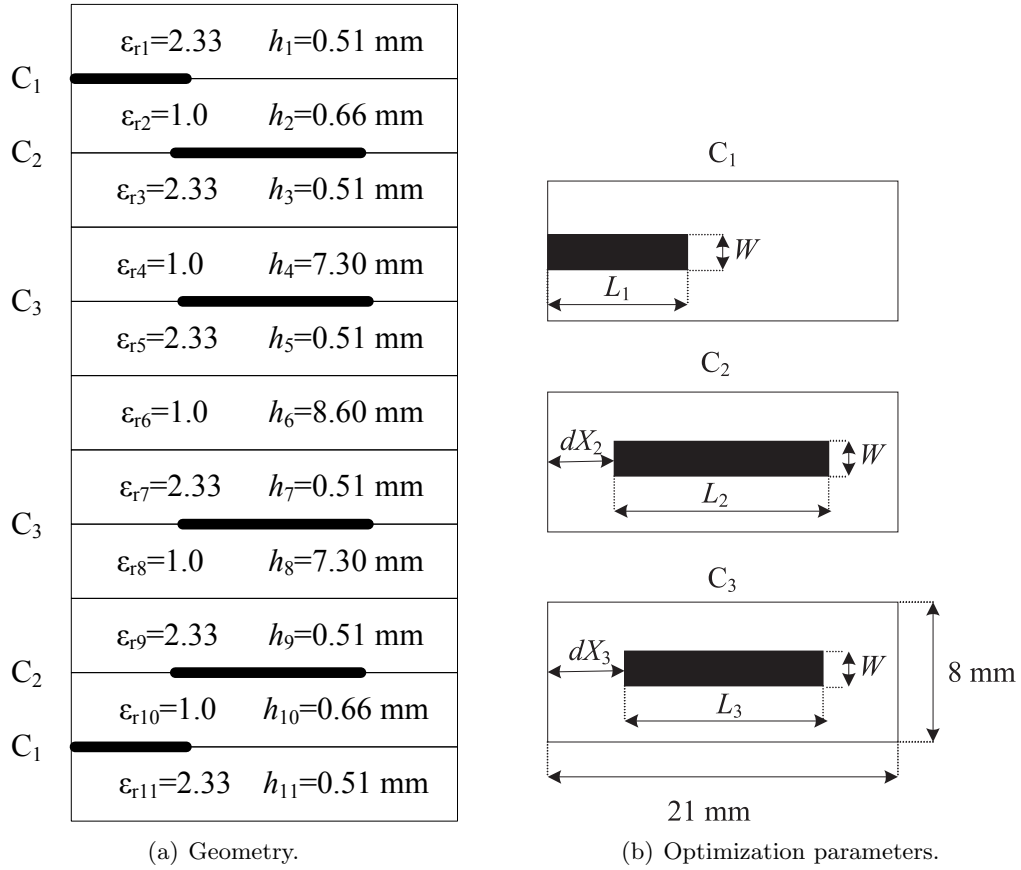


Figure 4.15: Broadside coupled filter.

Table 4.3: Input and optimized parameters of the broadside coupled filter optimization problem.

parameter to optimize	boundaries [mm]	optimized value [mm]
first resonator's length L_1	$3 \leq L_1 \leq 5$	3.673094
second resonator's length L_2	$16 \leq L_2 \leq 18$	16.949250
third resonator's length L_3	$16 \leq L_3 \leq 18$	16.786691
resonator width W	$1 \leq W \leq 2$	1.492699
resonator-box offset dX_2	$1 \leq dX_2 \leq 3$	1.352223
resonator-box offset dX_3	$1 \leq dX_3 \leq 3$	1.084593

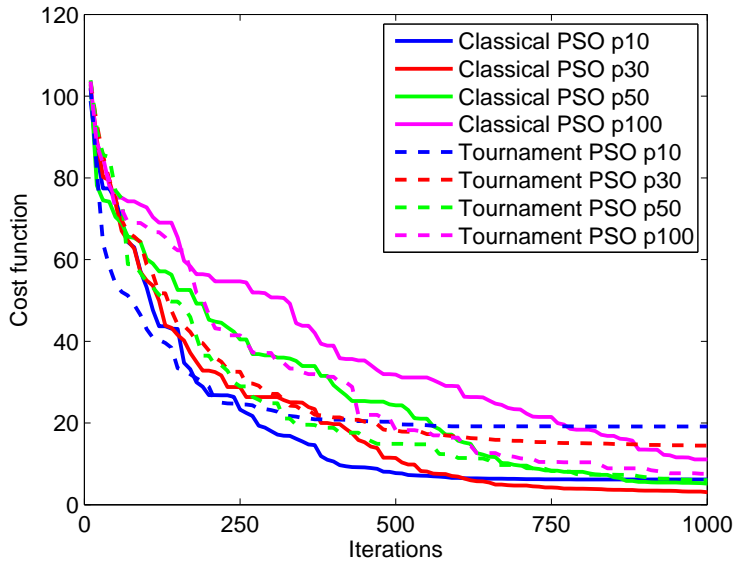


Figure 4.16: Broadside coupled filter optimization problem: convergence of the algorithms.

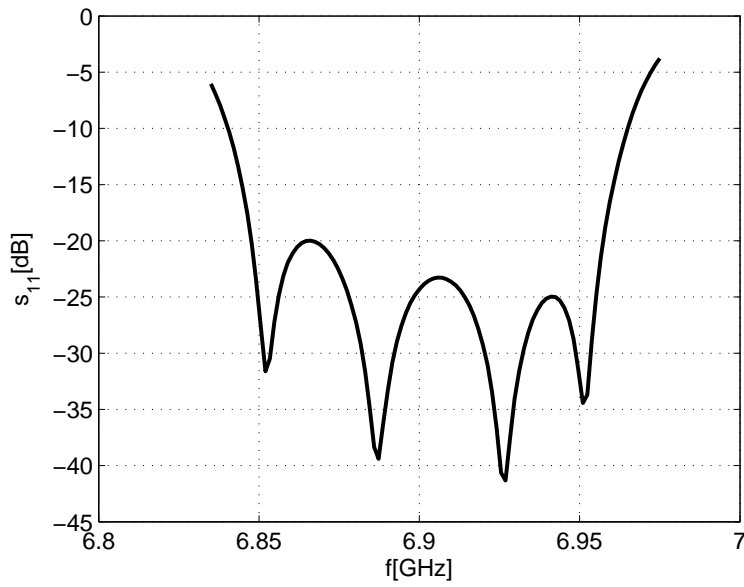


Figure 4.17: The reflection coefficient s_{11} of the optimized broadside coupled filter.

4.5 Conclusion

In this chapter we have introduced the Particle Swarm Optimization algorithm in the context of optimization of multilayered planar structures. The PSO algorithm is known to be very robust (the default values of the PSO parameters suggested in the literature work very well for a wide class of problems), easy to implement and relatively computationally inexpensive (i.e., it has relatively fast convergence). However, when the PSO algorithm is used to perform the optimization of an electromagnetic structure, the cost function is typically based on the results provided by an EM simulator. In each iteration, PSO is suggesting new solution, and the EM analysis for the new geometry must be run. Therefore, as the EM simulation is usually the most time-consuming part of the optimization, reducing the overall number of iterations (EM solver calls) is of uppermost relevance. In that context, we have proposed a new, modified version, the Tournament Selection PSO algorithm. This hybrid algorithm introduces in the classical PSO algorithm the tournament selection, successfully used in genetic algorithm.

To compare the performances of the algorithms, both the classical and the Tournament Selection PSO algorithms have been applied to three multilayered media problems: a microstrip antenna, an SSFIP antenna and a broadside coupled filter. To analyze these structures, the PSO algorithms are coupled to in-house EM solvers based on the mixed-potential integral equations specially tailored to model planar multilayered problems. From the presented results, one can see that the tournament selection always significantly speeds-up the convergence of the PSO algorithm. Although in some cases the Tournament Selection PSO could be slightly outperformed by the classical PSO if given unlimited number of iterations, the Tournament Selection PSO provides a much faster rate of convergence in the first phases of the iterative process. A number of iterations, between 3 and 5 times smaller, is usually needed to reach satisfactory small values of the cost function.

Bibliography

- [1] S. Das and A. Abraham, "Synergy of particle swarm optimization with evolutionary algorithms for intelligent search and optimization," *IEEE International Congress on Evolutionary Computation*, vol. 1, pp. 84–88, 2006.
- [2] B. D. Popovic, M. B. Dragovic, and A. R. Djordjevic, *Analysis and Synthesis of Wire Antennas*. John Wiley & Sons, 1982.
- [3] B. M. Kolundzija and D. I. Olcan, "Multiminima heuristic methods for antenna optimization," *IEEE Trans. Antennas Propag.*, vol. 54, no. 5, pp. 1405–1415, May 2006.
- [4] R. L. Haupt, "An introduction to genetic algorithms for electromagnetics," *IEEE Antennas and Propagation Magazine*, vol. 37, no. 2, pp. 7–15, Apr. 1995.
- [5] D. S. Weile and E. Michielssen, "Genetic algorithm optimization applied to electromagnetics: a review," *IEEE Trans. Antennas Propag.*, vol. 45, no. 3, pp. 343–353, Mar. 1997.
- [6] J. M. Johnson and Y. Rahmat-Samii, "Genetic algorithms in engineering electromagnetics," *IEEE Antennas and Propagation Magazine*, vol. 39, no. 4, pp. 7–21, Aug. 1997.
- [7] Y. Rahmat-Samii and E. Michielssen, *Electromagnetic optimization by genetic algorithm*. New York: John Wiley & Sons, INC, 1999.
- [8] S. Kirkpatrick, C. D. Gelatt, Jr., and M. P. Vecchi, "Optimization by simulated annealing," *Science*, vol. 220, no. 4598, pp. 671–680, May 1983.
- [9] M. Dorigo, M. Birattari, and T. Stutzle, "Ant colony optimization," *IEEE Computational Intelligence Magazine*, vol. 1, no. 4, pp. 28–39, Nov. 2006.
- [10] J. Kennedy and R. Eberhart, "Particle swarm optimization," in *IEEE Int. Conf. Neural Networks*, Perth, WA, Australia, Nov. 17 – Dec. 1, 1995, pp. 1942–1948.
- [11] J. Robinson and Y. Rahmat-Samii, "Particle swarm optimization in electromagnetics," *IEEE Trans. Antennas Propag.*, vol. 52, no. 2, pp. 397–407, Feb. 2004.
- [12] N. Jin and Y. Rahmat-Samii, "Advances in particle swarm optimization for antenna designs: real-number, binary, single-objective and multiobjective implementations," *IEEE Trans. Antennas Propag.*, vol. 55, no. 3, pp. 556–567, Mar. 2007.

-
- [13] R. Poli, "Analysis of the publications on the applications of particle swarm optimisation: review article," *Journal of Artificial Evolution and Applications*, vol. 2008, pp. 4:1–4:10, Jan. 2008.
- [14] R. Poli, J. Kennedy, and T. Blackwell, "Particle swarm optimization: an overview," *Swarm Intelligence*, vol. 1, no. 1, pp. 33–57, Aug. 2007.
- [15] D. Olcan, R. Golubovic, and B. Kolundzija, "On the efficiency of particle swarm optimizer when applied to antenna optimization," in *IEEE-APS Proc.*, Albuquerque, NM, 9–14, 2006, pp. 3297 – 3300.
- [16] D. Velduizen, J. Zydallis, and G. Lamont, "Considerations in engineering parallel multi-objective evolutionary optimizations," *Trans. Evol. Comput.*, vol. 7, no. 2, pp. 144–173, Apr. 2003.
- [17] M. Clerc and J. Kennedy, "The particle swarm explosion, stability, and convergence in the multidimensional complex space," *IEEE Trans. on Evolutionary Computation*, vol. 6, no. 1, pp. 58–73, Feb. 2002.
- [18] T. Huang and A. Mohan, "A hybrid boundary condition for robust particle swarm optimization," *IEEE Antennas Wireless Propag. Lett.*, vol. 4, no. 1, pp. 112–117, 2005.
- [19] K. E. Parsopoulos and M. N. Vrahatis, "Recent approaches to global optimization problems through particle swarm optimization," *Natural Computing*, vol. 1, no. 2–3, pp. 235–306, June 2002.
- [20] R. C. Eberhart and Y. Shi, "Particle swarm optimization: developments, applications and resources," in *Proc. Congr. Evolutionary Computation*, Seoul, South Korea, May 27–30, 2001, pp. 81–86.
- [21] R. Golubovic, D. Olcan, and J. R. Mosig, "Tournament selection particle swarm optimization algorithm applied to em problems," in *IEEE Proc. European Electromagnetics 2008*, Lausanne, Switzerland, July 21–25, 2008.
- [22] J. R. Perez and J. Basterrechea, "Particle swarm optimization with tournament selection for linear array synthesis," *MOTL*, vol. 50, no. 3, pp. 627–632, Mar. 2008.
- [23] R. Golubovic, I. Stevanovic, D. Olcan, and J. R. Mosig, "Can tournament selection improve performances of the classical particle swarm optimization algorithm?" in *3rd European Conference on Antennas and Propagation, EuCap 2009*, Berlin, Germany, Mar. 23–27, 2009, pp. 506 – 509.
- [24] A. A. Melcón, "Application of the integral equation technique to the analysis and synthesis of multilayered printed shielded microwave circuits and cavity backed antennas," Ph.D. dissertation, Ecole Polytechnique Fédérale de Lausanne, Switzerland, 1998, Thèse No. 1901.

-
- [25] J. R. Mosig, "Integral equation techniques," in *Numerical Techniques for Microwave and Millimeter-Wave Passive Structures*, T. Itoh, Ed. New York: Wiley, 1989, ch. 3, pp. 133–213.
- [26] H. Pues and A. V. de Capelle, "Accurate transmission-line model for the rectangular microstrip antenna," *IEE Proceedings Pt. H*, vol. 131, no. 6, pp. 334–340, Dec. 1984.
- [27] F. Gardiol and J.-F. Zürcher, "Broadband patch antennas - a SSFIP update (invited paper)," *Digest of 1996 AP-S International Symposium*, pp. 2–5, 1996.

5 Conclusion

5.1 Thesis assessment

Antennas and electromagnetic sensors are becoming a basic component and a keystone for areas like health care, biology, wireless networks, Earth sciences and even quantum photonics (nanoantennas). All these areas can benefit from a deeper understanding of antenna operation in their specific environment and from the availability of adequate electromagnetic (EM) modeling tools. In that context, we need reappraisal of the existing techniques and the development of the new ones for mathematical modeling and designing innovative antennas and wireless sensors required by future applications. The ultimate goal is the existence of computer models able to efficiently (in terms of accuracy, memory requirement and computational cost) predict and optimize the performance of complex antennas in complex environments. However, in order to be efficient, one must tackle a very reduced part of this large research panorama and do it in a rather deep way. This thesis has addressed some of these specific and very specialized challenges. In doing so, it contributes to the development and improvement of accurate electromagnetic modeling and optimization algorithms for an ubiquitous class of antennas, the planar printed antennas.

Antennas and scatterers embedded in planar stratified media are frequently analyzed by means of integral-equation (IE) formulations combined with a discretization procedure, like the Galerkin Method of Moments (MoM). Among several variants in which the IE model can be cast, the mixed potential integral equation (MPIE) is usually considered to be the most efficient technique because of its weakly singular kernel. In the application of MoM for the solution of MPIE, a key aspect for speed and accuracy is the development of fast and accurate algorithms for the evaluation of Green's functions in spatial domain, which are customarily expressed in terms of the well-known Sommerfeld integrals (SIs). Generally, analytical solution of the SIs is not available, and direct numerical integration is out of question, since the integral kernels may possess singularities on and/or near the integration path, and are, moreover, both highly oscillatory and slowly decaying. Therefore, specially tailored techniques for efficient evaluation of SIs are needed. This problem has been extensively treated for over 30 years and several methods are already available [1–18]. Although it is now a classical one, the problem of efficient evaluation of SIs is still attracting a lot of interest, because of the very important role the SIs play in many EM problems. The recent literature in this area is very extensive, thus witnessing the relevance and the actuality of the topic.

There are mainly two difficulties arising in the evaluation of SIs. The first one is related to the oscillating and slowly converging, or even diverging, kernels of the integrals which are extending over semi-infinite intervals. The second difficulty is due to the possible occurrence of surface-wave poles and branch-point singularities in the integrands. Luckily enough, by decomposing the semi-infinite integration interval into two parts $[0, \infty] = [0, a] \cup [a, \infty]$, the above mentioned difficulties can be separately treated. Here, a is appropriately selected to guarantee that the second interval is free of singularities.

In Chapter 2 of this thesis, both problems have been addressed. First, for the evaluation of the first part of the SI (over $[0, a]$), the real-axis integration path is selected. The pole extraction technique from [19] is used to annihilate the surface-wave pole singularities. For the treatment of the remaining branch-point singularity, the double-exponential (DE) quadrature formulas are utilized. Throughout several representative numerical examples, it was shown that the proposed approach remains valid and computationally inexpensive for both small and large values of the source-observer distances (which acts as a multiplicative parameter in the argument of the Bessel function). More precisely, when compared to the integration along the half-sine path in the complex plane, which has been commonly used, the newly proposed scheme yields the same accuracy of the final results, while substantially reducing the computation time. Not only the proposed technique is very accurate and efficient, but it is also very easy to implement. The pole extractor from [19] can be embedded in routines for numerical evaluation of SIs in an entirely automatic way, while the weights and abscissas of the proposed DE quadrature can be precomputed.

For the evaluation of the remaining semi-infinite SI tail, the classic weighted averages (WA) algorithm was first reviewed. This method is currently recognized as the most competitive algorithm to evaluate Sommerfeld integral tails. In the literature it is also referred to as the Mosig-Michalski transformation. It calls for the transformation of the infinite SI tails into an infinite sequence of partial finite integrals and acts upon this sequence as a convergence accelerator. The reappraisal of the classic WA method led to a new algorithm, called the New WA method, in which iterative and recursive nature of the classic WA is eliminated and replaced by a unique weighted means. The New WA method can be considered as a generalization of the well established Hölder and Cèsaro means, used to sum divergent series [20, 21]. Numerous advantages of the new algorithm have been demonstrated. First of all, it was shown that its theoretical construction is straightforward, well defined and fully supported by a rigorous mathematical background. Secondly, it was demonstrated that, due to its more compact formulation, devoid of iterative and recursive steps, the New WA method is easier and more economical (in terms of basic operations) to implement, when compared to the classic WA method. Moreover, the new formulation is more robust than the classic one, as it provides a unique formulation, valid for both monotonic and oscillating functions. Finally, throughout numerous numerical examples it was also shown that the New WA outperforms, in terms of accuracy, the classic WA algorithm.

In Chapter 2, a novel technique for fast and accurate computation of SI tails via direct integration, based on DE-type quadrature formulas was also proposed. The method makes use of the quadrature formula based on Bessel function zeros and combines it with an appropriate variable transformation. More precisely, the selected variable transformation guarantees that the nodes of the quadrature approach double-exponentially to the zeros of the corresponding Bessel function, thus admitting the accurate evaluation of SI tails using moderate number of function evaluations. When compared to WA algorithms, the proposed method gives, on average, slightly lower accuracy, while being approximately 5 times more efficient in terms of computational cost.

Chapter 3 addresses the problem of efficient evaluation of semi-infinite range integrals involving products of Bessel functions of the first kind and an arbitrary order. Numerous practical problems in electromagnetics, acoustics, hydrodynamics and many other fields give rise to this type of integrals (see [22–25] among others). These integrals are notoriously difficult to evaluate, and typically no analytical solution is known. Their direct integration is unacceptably computationally expensive (due to irregularly oscillating and slowly converging integrands), or even impossible (in the case of divergent integrands). The algorithm proposed herein makes use of the New WA method (presented in detail in Chapter 2) for extrapolation on a sequence of partial sums obtained after applying integration-then-summation technique, and requires rewriting the product of N Bessel functions as the sum of 2^{N-1} asymptotically simply oscillating functions. Numerical results have been presented to demonstrate the superior performance of the method. Furthermore, since the proposed technique is justified by the asymptotic trigonometric behavior of Bessel functions, it was shown that the method can be straightforwardly generalized to infinite integrals involving also products of sine/cosine functions and Bessel functions of the second kind and an arbitrary order. The additional difficulty for the integrals containing Bessel function of the second kind (due to its singularity at the origin) was worked out as well. The proposed method remains valid even when the integrands are not converging, but are defined only in the sense of Abel's summability.

Finally, the optimization of planar multilayered antennas has been treated in Chapter 4, where the Particle Swarm Optimization (PSO) algorithm and its hybridization, called Tournament Selection Particle Swarm Optimization (TS-PSO) algorithm, have been introduced, implemented and compared. Our research was focused on exploring in detail the potentials of the PSO algorithm and on further improving its convergence. The PSO algorithm has several advantages when compared to other evolutionary algorithms: it is robust, easy to implement and has relatively fast convergence. Nevertheless, further improvement of its convergence properties is always welcome. More precisely, when used for the optimization of EM problems, reduction of the overall number of iterations (EM solver calls) is of paramount importance, since the EM simulation is usually the most time-consuming part of the optimization cycle. For that reason, the tournament selection, which has been very successfully used in Genetic

Algorithm (GA), has been incorporated in the classical PSO algorithm. For the purpose of comparing the performances of these two methods on planar multilayered problems, we have developed an interface between the optimizer and the robust in-house EM solver [9, 26], specially tailored to model multilayered structures of our interest. The optimization of three different structures has been considered: a microstrip antenna, an SSFIP antenna and a broadside-coupled filter. The obtained results show that the tournament selection significantly improves the convergence of the PSO algorithm.

5.2 Perspectives

This thesis has solved several problems in the efficient simulation and optimization of multilayered planar structures. However, there are always further possible improvements that can be carried out in addition to the developments presented herein. These and the new ideas that resulted from the work performed during this thesis are discussed in the following paragraphs.

This thesis has considered conventional layered media consisting of double positive (DPM) or right-handed (RHM) materials. However, there is an increasing interest of our community in layered media including metamaterials (MTMs), i.e., materials with negative magnetic permeability ($\mu < 0$) and/or dielectric permittivity ($\varepsilon < 0$). The MTM layers could represent a formidable challenge to numerical techniques currently being used in the context of SIs. Indeed, in addition to ordinary modes, which exist in the case of DPM, MTM multilayered structures support also evanescent surface (ES) and complex surface (CS) modes. Their existence must be taken into account when evaluating the SIs.

More precisely, the CS poles will not contribute to the SI if the integration is performed along the real-axis path. However, if the integration contour is deformed into the first quadrant of the complex spectral k_ρ -plane, the contribution of those CS poles lying between the integration contour and the real k_ρ -axis, must be taken into account. Clearly, this calls for the calculation of residues at captured poles. Furthermore, the SI tail might not be anymore singularity free (depending on the operation frequency, thicknesses and electrical characteristics of the substrates), due to the possible existence of ES poles. Obviously, when evaluating the SI tail, special care must be taken for the ES poles lying on the real axis. One possible way to tackle this problem is to simply deform the integration contour around ES poles (staying always in the first quadrant of the complex spectral k_ρ -plane). In this case the effect of the path deformation to the methods for evaluating the SI tails must be examined. Another alternative way would be to extract the ES poles from the spectral domain GFs and to add their contribution a posteriori, in spatial domain, with the help of suitable integral identities. In this case, the methods for evaluation of the SI tails, proposed in Chapter 2 of this thesis, can be straightforwardly applied to the remaining singularity-free tail, but a robust method for pole extraction is a critical point.

In Chapter 2 we have developed several very efficient methods for the numerical evaluation of SIs. It was shown that the real-axis integration of the first part of SIs combined with the pole extraction [19] and the DE quadrature significantly reduces the computational time, when compared to the traditional half-sine path integration. For the evaluation of the SI tails, two methods were presented: New WA method and the DE quadrature. Although these methods are very efficient, further improvement of their convergence characteristics is always welcome. For example, it was shown that the DE quadrature formulas for evaluation of SI tails are fivefold more efficient in terms of the computational time, when compared to the WA methods. However, the results obtained using the DE quadrature formulas, although very good, are still slightly less accurate than the ones obtained by using WA methods. Further improvement of the convergence properties/accuracy of the DE quadrature formulas could lead to a method yielding the accuracy of the WA algorithms, but with significant advantage in terms of the computational time. The possible way to address this problem has been suggested in [27], for the DE formulas targeting integrals with end-point singularities (which we have used in the evaluation of the first part of SIs). A similar approach for the convergence improvement of the DE quadratures targeting the SI tails is worth being tried.

The Particle Swarm Optimization algorithm has been introduced for the optimization of multilayered planar antennas. Moreover, by applying the tournament strategy, traditionally used in GA, to the PSO, we managed to further improve algorithm performance. However, it is well-known that the PSO algorithm, and generally all the evolutionary algorithms, have several heuristic parameters that directly influence their behavior. The literature offers some experimentally determined “default” values of these parameters, which provide very good results for a large variety of problems. However, typically these parameters are problem-dependent and defined by the user. Therefore, their proper choice depends on the user experience and the available information about the problem at hand. Fine tuning of these parameters can improve the algorithm performance. Also, it could happen that the user fails to provide the algorithm with the appropriate set of parameters, causing lower performance, or in extreme cases even failure of the optimization algorithm. In order to tackle this problem, a composite “self-learning” PSO algorithm, in which the choice of the heuristic PSO parameters will be replaced by an automatic algorithm, is very much desired. This would result in a much more robust tool without the need of tuning in advance the critical algorithm parameters. The composite PSO algorithm, in which the manipulation of the heuristic PSO parameters was assigned to double-evolutionary (DEV) algorithm has been already proposed in [28]. Essentially, the PSO algorithm is solving the optimization problem, while the DEV algorithm is running as a background procedure, tuning the heuristics of the PSO. The performance of this composite DEV-PSO method was tested on several mathematical functions, traditionally used as benchmark problems for optimization algorithms. The DEV-PSO algorithm was shown to surpass the success rates of the classical PSO, detecting the global minimum in all experiments (including those in which the classical PSO with the default values of heuristic parameters was performing poorly). Of course, the total number of function evaluations was

larger. However, the promise of having such a robust optimization algorithm, which is able always (after a finite number of iterations) to find the global minimum of a given problem, completely compensates this overload. It would be very interesting to test this new DEV-PSO algorithm in the context of optimization of EM problems. Also, in order to fully explore the possibilities of composite algorithms, other optimization methods are worth being tested in the role of the algorithm which is tuning PSO heuristic parameters. Finally, let us point out that this strategy is very interesting for optimization problems for which no *a priori* information is available (for example, in new areas of engineering, where we have not gathered enough experience), as it will most likely lead us, at the end of the day, to the solution that satisfies our requirements. Of course, for optimization problems about which, based on the past experience, we have enough *a priori* information in order to be able to start the search from a “good” starting point, gradient-based algorithms are a better choice, since they would certainly require less iterations.

Bibliography

- [1] M. I. Aksun and G. Dural, "Clarification of issues on the closed-form Green's functions in stratified media," *IEEE Trans. Antennas Propag.*, vol. 53, no. 11, pp. 3644–3653, Nov. 2005.
- [2] M. Yuan, T. K. Sarkar, and M. Salazar-Palma, "A direct discrete complex image method from the closed-form Green's functions in multilayered media," *IEEE Trans. Microw. Theory Tech.*, vol. 54, no. 3, pp. 1025–1032, Mar. 2006.
- [3] V. N. Kourkoulos and A. C. Cangellaris, "Accurate approximation of Green's functions in planar stratified media in terms of a finite sum of spherical and cylindrical waves," *IEEE Trans. Antennas Propag.*, vol. 54, no. 5, pp. 1568–1576, May 2006.
- [4] R. R. Boix, F. Mesa, and F. Medina, "Application of total least squares to the derivation of closed-form Green's functions for planar layered media," *IEEE Trans. Microw. Theory Tech.*, vol. 55, no. 2, pp. 268–280, Feb. 2007.
- [5] A. G. Polimeridis, T. V. Yioultsis, and T. D. Tsiboukis, "A robust method for the computation of Green's functions in stratified media," *IEEE Trans. Antennas Propag.*, vol. 55, no. 7, pp. 1963–1969, July 2007.
- [6] —, "Fast numerical computation of Green's functions for unbounded planar stratified media with a finite-difference technique and Gaussian spectral rules," *IEEE Trans. Microw. Theory Tech.*, vol. 55, no. 1, pp. 100–107, Jan. 2007.
- [7] A. G. Polimeridis and T. V. Yioultsis, "On the efficient computation of closed-form Green's functions in planar stratified media," *Int. J. RF Microw. Computer Aided Eng.*, vol. 18, no. 2, pp. 118–126, Mar. 2008.
- [8] K. A. Michalski, "Application of the complex image method to electromagnetic field computation in planar uniaxial multilayers," in *I Workshop on Integral Techniques for Electromagnetics (INTELECT)*, Lausanne, Switzerland, July 2007.
- [9] J. R. Mosig, "Integral equation techniques," in *Numerical Techniques for Microwave and Millimeter-Wave Passive Structures*, T. Itoh, Ed. New York: Wiley, 1989, ch. 3, pp. 133–213.
- [10] F. J. Demuyne, G. A. E. Vandenbosch, and A. R. V. de Capelle, "Analytical treatment of the Green's function singularities in a stratified dielectric medium," in *Proc. European Microwave Conference*, Madrid, Spain, Sept. 6–10, 1993, pp. 1000–1001.

-
- [11] F. J. Demuyneck and G. A. E. Vandenbosch, "The expansion wave concept - part I: efficient calculation of spatial Green's functions in a stratified dielectric medium," *IEEE Trans. Antennas Propag.*, vol. 46, no. 3, pp. 397–406, Mar. 1998.
- [12] N. Kinayman and M. I. Aksun, "Comparative study of acceleration techniques for integrals and series in electromagnetic problems," *Radio Science*, vol. 30, no. 6, pp. 1713–1722, Nov.–Dec. 1995.
- [13] K. A. Michalski, "Extrapolation methods for Sommerfeld integral tails," *IEEE Trans. Antennas Propag.*, vol. 46, no. 10, pp. 1405–1418, Oct. 1998.
- [14] T. Hasegawa and A. Sidi, "An automatic integration procedure for infinite range integrals involving oscillatory kernels," *Numerical Algorithms*, vol. 13, no. 1, pp. 1–19, Mar. 1996.
- [15] T. Ooura, "A continuous Euler transformation and its application to the Fourier transforms of a slowly decaying functions," *J. Comput. Appl. Math.*, vol. 130, no. 1–2, pp. 259–270, May 2001.
- [16] S. Singh and R. Singh, "Computation of Sommerfeld integrals using tanh transformation," *MOTL*, vol. 37, no. 3, pp. 177–180, Mar. 2003.
- [17] T. Ooura, "A generalization of the continuous Euler transformation and its application to numerical quadrature," *J. Comput. Appl. Math.*, vol. 157, no. 2, pp. 251–259, 2003.
- [18] M. Yuan and T. K. Sarkar, "Computation of the Sommerfeld integral tails using the matrix pencil method," *IEEE Trans. Antennas Propag.*, vol. 54, no. 4, pp. 1358–1362, Apr. 2006.
- [19] A. G. Polimeridis, T. V. Yioultsis, and T. D. Tsiboukis, "An efficient pole extraction technique for the calculation of Green's functions in stratified media using a sine transformation," *IEEE Trans. Antennas Propag.*, vol. 55, no. 1, pp. 227–229, Jan. 2007.
- [20] J. R. Mosig and R. Golubovic-Niciforovic, "Some new developments of the weighted averages algorithm," in *5th European Conference on Antennas and Propagation, EuCap 2011*, Rome, Italy, Apr. 11–15, 2011.
- [21] J. R. Mosig, "The weighted averages algorithm revisited," *IEEE Trans. Antennas Propag.*, submitted.
- [22] M. Ikonou, P. Köhler, and A. F. Jacob, "Computation of integrals over the half-line involving products of Bessel functions, with application to microwave transmission lines," *ZAMM -J. of Appl. Math. and Mech./ Zeitschrift für Angewandte Mathematik und Mechanik*, vol. 75, no. 11, pp. 917–926, Nov. 1995.
- [23] N. P. Singh and T. Mogi, "Electromagnetic response of a large circular loop source on a layered earth: a new computation method," *Pure App. Geophys.*, vol. 162, no. 1, pp. 181–200, 2005.

-
- [24] P. M. Morse and H. Feshbach, *Methods of theoretical physics: part II*. Minneapolis: Feshbach publishing, LLC, 1981.
- [25] A. M. J. Davis, “Drag modifications for a sphere in a rotational motion at small non-zero Reynolds and Taylor numbers: wake interference and possible Coriolis effects,” *J. Fluid Mech*, vol. 237, pp. 13–22, 1992.
- [26] A. A. Melcón, “Application of the integral equation technique to the analysis and synthesis of multilayered printed shielded microwave circuits and cavity backed antennas,” Ph.D. dissertation, Ecole Polytechnique Fédérale de Lausanne, Switzerland, 1998, Thèse No. 1901.
- [27] I. D. Koufogiannis, A. G. Polimeridis, M. Mattes, and J. R. Mosig, “A parametric study of the double exponential algorithm utilized in weakly singular integrals,” in *5th European Conference on Antennas and Propagation, EuCap 2011*, Rome, Italy, Apr. 11–15, 2011.
- [28] K. E. Parsopoulos and M. N. Vrahatis, “Recent approaches to global optimization problems through particle swarm optimization,” *Natural Computing*, vol. 1, no. 2–3, pp. 235–306, June 2002.

List of Acronyms

AM	Amplitude Modulation
BAN	Body Area Network
CAD	Computer Aided Design
CEM	Computational Electromagnetics
CFIE	Combined Field Integral Equations
CS	Complex Surface
CWA	Conventional Weighted Aggregation
DC	Direct Current
DE	Double Exponential
DEV	Differential Evolutionary
DNM	Double Negative Material
DPM	Double Positive Material
EFIE	Electric Field Integral Equation
EM	Electromagnetic
ENG	ϵ -negative
ES	Evanescent Surface
FDTD	Finite Difference Time Domain
FEM	Finite Element Method
GA	Genetic Algorithm
GCD	Greatest Common Divisor
GF	Green's Function
GPS	Global Positioning System

HED	Horizontal Electric Dipole
IE	Integral Equation
LHM	Left-Handed Material
MFIE	Magnetic Field Integral Equation
MIMO	Multiple Input Multiple Output
MNG	μ -negative
MoM	Method of Moments
MPIE	Mixed Potential Integral Equation
MTM	Metamaterials
NIM	Negative Index Material
OS	Ordinary Surface
PC	Personal Computer
PEC	Perfect Electric Conductor
PMC	Perfect Magnetic Conductor
PSO	Particle Swarm Optimization
RF-MEMS	Radio Frequency Micro Electro Mechanical Systems
RFID	Radio Frequency Identification
RHM	Right-Handed Material
SA	Simulated Annealing
SI	Sommerfeld Integral
SNM	Single Negative Material
SSFIP	Slot Strip Foam Inverted Antenna
SW	Surface Wave
SWP	Surface Wave Pole
TE	Transversal Electric
TM	Transversal Magnetic

TS-PSO	Tournament Selection Particle Swarm Optimization
UWB	Ultra Wide Band
VT	Variable Transformation
WA	Weighted Averages

List of Figures

2.1	Real-life multilayered working setups.	12
2.2	Possible integration paths for the computation of Sommerfeld integrals (choice $a = k(\sqrt{(\varepsilon_{r_i}\mu_{r_i})_{\max}} + 1)$ assures that there are no singularities for $k_\rho > a$). . . .	14
2.3	Generic stratified media showing a point source (level z') and a field observation point (level z) separated by a radial distance ρ . The medium can be terminated on the top and/or on the bottom by a perfect electric conductor (PEC), perfect magnetic conductor (PMC) and impedance plane.	15
2.4	Poles and branch point in complex k_ρ -plane for lossless grounded slab ($a = k\sqrt{(\varepsilon_{r_i}\mu_{r_i})_{\max}}$).	16
2.5	Deformed integration path for the computation of Sommerfeld integrals. . . .	19
2.6	Performance of the real-axis integration combined with the variable transformation (VT) (2.18) and the DE quadrature for different levels of quadrature M when evaluating the integral (2.37).	31
2.7	Performance of half-sine contour approach combined with the adaptive quadrature based on Patterson's formulas and the real-axis approach combined with the variable transformation (VT) (2.18)-(2.19) and with the DE quadrature formulas, for evaluation of the first part of the Sommerfeld identity (2.44), when $z = 0$	34
2.8	Performance of the half-sine contour approach combined with the adaptive quadrature based on Patterson's formulas and the real-axis approach combined with the variable transformation (VT) (2.18)-(2.19) and with the DE quadrature formulas, for evaluation of the first part of the Sommerfeld identity (2.44), when $z = 0$	36
2.9	The original spectral-domain component G_A^{xx} of the vector potential dyadic Green's function for the single-layer substrate of permittivity $\varepsilon_r = 4$ and thickness $d = \lambda$ at 8 GHz.	38
2.10	The modified spectral-domain component G_A^{xx} of the vector potential dyadic Green's function for the single-layer substrate of permittivity $\varepsilon_r = 4$ and thickness $d = \lambda$ at 8 GHz, obtained by annihilating the singular behavior in the proximity of surface-wave poles.	39
2.11	Performance of the real-axis and half-sine contour integration for component G_{xx}^A of the vector potential dyadic Green's function for a single-layer substrate: $\varepsilon_r = 4$, $d = \lambda$, $f = 8\text{GHz}$, backed by perfect electric conductor (PEC). Horizontal electric dipole (HED) is at the interface.	40

2.12	Magnitude of the component G_{xx}^A of the vector potential dyadic Green's function and surface-wave pole (SWP) contribution for a single-layer substrate: $\epsilon_r = 4$, $d = \lambda$, $f = 8\text{GHz}$, backed by perfect electric conductor (PEC). HED is at the interface.	41
2.13	Behavior of the DE transformation for different values of step size parameter h	53
2.14	Performance of DE formulas, New and Mosig-Michalski WA methods when applied to the Sommerfeld identity tail (2.110) for $z = 0$	56
2.15	Performance of DE formulas, New and Mosig-Michalski WA methods when applied to the ρ -derivative of the Sommerfeld identity tail (2.111) for $z = 0$	57
2.16	Performance of DE formulas, New and Mosig-Michalski WA methods when applied to the z -derivative of the Sommerfeld identity tail (2.112) for $z = 0$	57
2.17	Performance of DE formulas, New and Mosig-Michalski WA methods when applied to the second derivative of the Sommerfeld identity tail with respect to ρ and z (2.113) for $z = 0$	58
2.18	Number of significant digits for the SI tail (2.110) for a wide range of distances from the source.	59
2.19	Number of significant digits for the SI tail (2.111) for a wide range of distances from the source.	60
2.20	Number of significant digits for the SI tail (2.112) for a wide range of distances from the source.	61
2.21	Number of significant digits for the SI tail (2.113) for a wide range of distances from the source.	62
2.22	Relative number of integration points $N_{\text{DE}}/N_{\text{WA}}$ for the SI tail (2.110) for a wide range of distances from the source.	63
2.23	Relative number of integration points $N_{\text{DE}}/N_{\text{WA}}$ for the SI tail (2.111) for a wide range of distances from the source.	64
2.24	Relative number of integration points $N_{\text{DE}}/N_{\text{WA}}$ for the SI tail (2.112) for a wide range of distances from the source.	64
2.25	Relative number of integration points $N_{\text{DE}}/N_{\text{WA}}$ for the SI tail (2.113) for a wide range of distances from the source.	65
2.26	Spatial domain Green's function of three-layer geometry problem at 30 GHz.	67
2.27	Number of significant digits for three-layer geometry at 30 GHz.	68
3.1	Test functions Ex.1 (3.8) and Ex.2 (3.9): Behavior of the algorithm when equidistant break points separated by function's half-period (dashed lines) and by function's period (solid lines) are used as the upper limits of partial integrals.	80
3.2	Behavior of the integrand (—) and actual positions of the abscissas (\diamond).	81
3.3	Test function (3.8): behavior of h_1 and h_2	82
3.4	Test function (3.8): behavior of the three integrands, I_f , I_{h1} and I_{h2} , obtained by applying (3.17) and the abscissas $x_{1,i}$ and $x_{2,i}$ used as upper limits of the partial integrals.	85
3.5	Number of significant digits vs. number of partial integrals for Ex. 1 - Ex. 10.	87
3.6	Test functions Ex. 8 (3.30) and Ex. 10 (3.32).	88
3.7	Number of significant digits vs. number of partial integrals for Ex. 11 - Ex. 14.	92

3.8	Behavior of the integrand.	93
4.1	Flowchart describing the design procedure of an EM structure.	100
4.2	Updating the position of the particle.	103
4.3	Different boundary conditions used for particles trying to escape from the optimization space. (Full circles represent the particle in two consecutive iteration t and $t + 1$. With dotted circle, the intermediate position of the particle, when it hits one of the boundaries, is illustrated).	105
4.4	Flowchart depicting the PSO algorithm.	107
4.5	Two-dimensional Rastrigin function: 3-D view.	109
4.6	Two-dimensional Rastrigin function: alternating maxima and minima.	109
4.7	Swarm consisting of 15 particles in the process of searching for global minimum of the 2-D Rastrigin function.	110
4.8	Swarm consisting of 15 particles in the process of searching for global minimum of the 2-D Rastrigin function.	111
4.9	Binary tournament selection.	112
4.10	Microstrip antenna.	114
4.11	Microstrip antenna optimization problem: convergence of the algorithms.	115
4.12	SSFIP antenna.	116
4.13	SSFIP optimization problem: convergence of the algorithms.	118
4.14	The reflection coefficient s_{11} of the SSFIP antenna that satisfies our requirements.	118
4.15	Broadside coupled filter.	120
4.16	Broadside coupled filter optimization problem: convergence of the algorithms.	121
4.17	The reflection coefficient s_{11} of the optimized broadside coupled filter.	121

List of Tables

2.1	Spectral properties of complex modes on lossless DNG, ENG, MNG and DPS grounded slabs.	17
2.2	Average relative number of integration points needed for the evaluation of SI tails	66
4.1	Input and optimized parameters of the microstrip antenna optimization problem.	115
4.2	Input and optimized parameters of the SSFIP antenna optimization problem. .	117
4.3	Input and optimized parameters of the broadside coupled filter optimization problem.	120

Ružica Golubović Nićiforović

PERSONAL INFORMATION

Date of birth: 29.01.1983
Place of birth: Zemun, Belgrade, Serbia
Sex: female
Nationality: Serbian
email: ruzica.golubovic@epfl.ch

EDUCATION

Ecole Polytechnique Fédérale de Lausanne (EPFL), Lausanne, Switzerland **Laboratory of electromagnetics and Acoustics (LEMA)**

October 2007 - June 2011

Working towards the Ph.D. thesis entitled “*Challenges in Computational Electromagnetics: Analysis and optimization of planar multilayered structures*” under the supervision of Prof. Juan R. Mosig and in the frame of the European COST project on Antennas Action - ASSIST IC0603 (see <http://www.cost-ic0603>) within the two Working Groups:

- WG3 - New Frontiers in Antenna Theory & Design
- WG5 - EM Computational Models, Tools & Software for Antennas

University of Belgrade

Faculty of Electrical Engineering-Group of Telecommunications

September 2001 - October 2006

GPA 9.21/10.0

Diploma Thesis entitled “Particle Swarm Optimization Algorithms” marked 10.0/10.0

Fifth Belgrade’s Gymnasium

September 1997-July 2002

GPA 5.00/5.00

RESEARCH INTERESTS

- Computational electromagnetics with an emphasis on planar multilayered media
- Evolutionary optimization algorithms

TEACHING EXPERIENCE

- Proposed and supervised several student projects
- Teaching assistant for bachelor courses:
 - Laboratoires répartis
 - Electromagnetics 1
 - Electromagnetics 2

JOURNAL PUBLICATIONS

- R. Golubovic Niciforovic, A. G. Polimeridis and J. R. Mosig, “On the efficient real-axes evaluation of the Sommerfeld integrals,” *IEEE Transactions on Antennas and Propagation*, in preparation.
- R. Golubovic Niciforovic, A. G. Polimeridis and J. R. Mosig, “On the efficient evaluation of Sommerfeld integral tails,” *IEEE Transactions on Antennas and Propagation*, under review.
- R. Golubovic Niciforovic, A. G. Polimeridis and J. R. Mosig, “Evaluating semi-infinite range integrals involving products of Bessel functions using weighted averages method,” *IEEE Transactions on Antennas and Propagation*, under review.

R. Golubovic Niciforovic, A. G. Polimeridis and J. R. Mosig, "Fast computational of Sommerfeld integral tails via direct integration based on double exponential-type quadrature formulas," *IEEE Transactions on Antennas and Propagation*, Vol. 59, No. 2, pp. 694-699, Feb. 2011.

A. G. Polimeridis, R. Golubovic Niciforovic, and J. R. Mosig, "Acceleration of slowly convergent series via the generalized weighted-averages method," *Progress in Electromagnetics Research M*, Vol. 14, pp. 233-245, 2010.

B. Fuchs, R. Golubovic, A. K. Skriversvik and J. R. Mosig, "Spherical lens antenna designs with particle swarm optimization," *Microwave and Optical Technology Letters*, Vol. 52, No. 7, pp. 1655-1659, July 2010.

J. Peruisseau-Carrier, F. Bongard, R. Golubovic Niciforovic, R. Torres-Sanchez and J. R. Mosig, "Contributions to the modeling and design of reconfigurable reflecting cells embedding discrete control elements," *IEEE Transactions on Microwave Theory and Techniques*, Vol. 52, No. 7, pp. 1655-1659, July 2010.

R. M. Golubovic and D. I. Olcan, "Antenna Optimization Using Particle Swarm Optimization Algorithm," *Journal of Automatic Control, University of Belgrade*, Vol. 16, pp. 21-24, 2006, ISSN: 1450-9903.

CONFERENCE
PUBLICATIONS

R. Golubovic Niciforovic, A. G. Polimeridis and J. R. Mosig, "Double exponential quadrature formulas for the direct calculation of Sommerfeld integral tails," in *Proc. 5th European Conference on Antennas and Propagation, EuCAP*, Rome, Apr. 2011.

J. R. Mosig and R. Golubovic Niciforovic, "Some new developments of the Weighted averages algorithm," in *Proc. 5th European Conference on Antennas and Propagation, EuCAP*, Rome, Italy, Apr. 11-15, 2011.

R. Golubovic, A. Djordjevic, D. Olcan and J. R. Mosig, "Nonuniformly-wound helical antennas," in *Proc. 3rd European Conference on Antennas and Propagation, EuCAP*, Berlin, Germany, Mar. 23-27, 2009, pp. 3077 - 3080.

R. Golubovic, I. Stevanovic, D. Olcan and J. R. Mosig, "Can tournament selection improve performances of the classical particle swarm optimization algorithm?," in *Proc. 3rd European Conference on Antennas and Propagation, EuCAP*, Berlin, Germany, Mar. 23-27, 2009, pp. 506 - 509.

R. Golubovic, D. Olcan and J. R. Mosig, "Tournament selection particle swarm optimization algorithm applied to EM problems," in *Proc. IEEE European Electromagnetics conference*, Lausanne, Switzerland, July 21-25, 2008.

R. Golubovic, D. Olcan and B. Kolundzija, "Particle swarm optimization algorithm and its modifications applied to EM problems," in *Proc. IEEE TELSIKS 2007*, Niš, Serbia, Sept. 26-28, 2007.

R. Golubovic and D. Olcan, "Antenna optimization using the PSO algorithm," ("Optimizacija antena korišćenjem PSO algoritma,") in *Proc. ETRAN 2006*, Belgrade, Serbia, June 7-10, 2006.

D. Olcan, R. Golubovic and B. Kolundzija, "On the efficiency of particle swarm optimizer when applied to antenna optimization," in *IEEE-APS Proc.*, Albuquerque, NM, pp. 3297-3300, July 9-14, 2006, pp. 3297 - 3300.

D. Olcan and R. Golubovic, "Particle swarm optimization applied to EM problems," in *ACES Proc. 2006*, Miami, FL, Mar. 12-18, 2006, pp. 442-446.

WORKSHOP
PRESENTATIONS

R. Golubovic Niciforovic, A. G. Polimeridis and J. R. Mosig, "Numerical evaluation of the integrals involving products of Bessel functions of an arbitrary order," *COST-ASSIST workshop*, Les Diablerets, Switzerland, Mar. 2011.

R. Golubovic Niciforovic, A. G. Polimeridis and J. R. Mosig, "Study on the efficient computation of slowly-convergent infinite series and semi-infinite Fourier-type integrals," *COST-ASSIST workshop*, Lisbon, Feb. 2010.

R. Golubovic, I. Stevanovic, A. Djordjevic and J. R. Mosig, "On PSO algorithm and its application to EM problems," *COST-ASSIST workshop*, Dublin, Oct. 2008.